University of Bath

Alternative formats
If you require this document in an alternative format, please contact:
openaccess@bath.ac.uk

Alginate-based materials: Enhancing properties through multiphase formulation design and processing innovation

Fengwei Xie [a,*], Chengcheng Gao [b,c], Luc Avérous [b,*]

[a] Department of Chemical Engineering, University of Bath, Bath BA2 7AY, United Kingdom
[b] BioTeam/ICPEES-ECPM, UMR CNRS 7515, Université de Strasbourg, 25 rue Becquerel, Strasbourg Cedex 2, 67087, France
[c] College of Food Science and Engineering, Nanjing University of Finance and Economics, Nanjing 210023, China

ARTICLE INFO

ABSTRACT

Alginate, a polymer mainly derived from seaweed, has garnered significant attention owing to its renewability, biocompatibility, biodegradability, and exceptional gel formation characteristics, rendering it highly versatile for numerous applications. Recognizing the imperative for tailored bulk materials, this review scrutinizes the processing methodologies of alginate-based bulk materials and delineates strategies to improve their properties, encompassing ionic crosslinking, plasticization, and hybridization with other polymers and/or fillers. It explores noteworthy alginate-based blends with natural polymers like polysaccharides and proteins, alongside fossil-based polymers like poly(vinyl alcohol). It also examines alginate-based composites incorporating various nanofillers such as cellulose nanoparticles, graphene, and nanoclays. The processing techniques for these multiphase alginate-based systems encompass solution casting, coating, spinning, 3D printing, and thermo-mechanical processing. Strategies for crosslinking alginate, plasticizing it, and optimizing its interactions with other polymers/fillers are outlined, bearing repercussions on the resultant materials properties. This review emphasizes the structure–process–property relationships of these multiphase systems in bulk and highlights synergistic effects and potential impediments to property improvements. It surveys prospective applications for alginate-based multiphasic bulk materials, spanning membrane separation, controlled release, wound healing, tissue engineering, food packaging, and agricultural domains. Finally in this field, knowledge gaps have been identified and future research directions are suggested.

1. Introduction

Polysaccharides have commanded attention for centuries, offering a vast array of applications across various fields. Their distinctive attributes, including hydrophilic nature, thickening capabilities, adhesion, and binding properties, coupled with their cost-effectiveness, renewability, widespread availability, and biodegradability, position them as versatile contenders. Alginate is a prominent polysaccharide sourced from seaweed, extensively utilized. Since their initial extraction in 1881, alginates have found applications spanning diverse fields like food, pharmaceuticals, biomedicine, textile printing, and paper manufacturing [1]. Primarily harnessed in liquid or gel states, alginates' captivating thickening attributes and gel-forming prowess underpin their use across these applications [2]. Moreover, in recent years, with

alginate recognized as a prominent "blue carbon" source, coupled with its complete compostability, alginate-based bulk materials have garnered significant interest in both research and industry domains, driven by the aspiration to mitigate environmental repercussions. Over the past few years, a multitude of startups have emerged all over the world, specializing in seaweed-based packaging. These innovative companies produce a wide range of smart products, such as films, sauce sachets, edible liquid packaging, cardboard and paper coatings, retail bags, drinking straws, pipettes, cups, takeaway boxes, and vegan leather. Alginate, a key component of seaweed, serves as a pivotal ingredient in these sustainable packaging solutions.

In the present day, alginate stands as the fourth most utilized polysaccharide in the EU [3]. Nonetheless, the utilization of alginates in solid and bulk forms (like films, fibers, and processed solid parts) for packaging and other technical applications could be limited by their inferior mechanical properties and high susceptibility to water [2]. To address these concerns, different strategies can be used, including chemical derivatization and the development of multiphase systems like blends and (nano)composites through various processing methods. The latter proves to be a cost-effective and environmentally beneficial route for achieving desired properties to meet diverse requirements, as compared to the chemical alteration route.

Many reviews have been published on alginate, covering several topics such as extraction [4], chemical modification [5,6], various forms like microspheres/particles [7–10] and fibers [11,12], 3D printing [13], as well as its application in specific areas including wound dressing [14], drug delivery [7,9], tissue engineering [15–17], and environmental treatment [18,19]. While reviews on alginate blends and composites have been recently published [12,14,16,19,20], they have primarily focused on specific applications. Notably absent are reviews that focus on the design and processing of alginate-based multiphase materials customized for various applications such as packaging, cutlery, separation membranes, biomedical patches, scaffolds, as well as components for sensing, electronic and energy devices, which necessitates the creation of bulk materials. This forms the core objective of this review. The aim is to delve into the advancements in alginate-based multiphase systems encompassing blends and (nano)composites, with a particular emphasis on the associated processes and resulting enhancements in material properties. This comprehensive review could serve as a valuable resource for devising alginate-based multiphase systems that can deliver desired attributes. Ultimately, it sheds light on the potential of these materials for environmentally responsible applications.

2. Alginate

2.1. Alginate production

Alginate is mainly present within the cell walls of brown algae in the form of calcium, magnesium, and sodium salts of alginic acid, and it comprises up to 40 % of the dry matter of brown algae [21]. Sodium alginate is known for its stability, while alginic acid is considered less stable. Today, significant quantities of sodium alginate, calcium alginate, potassium alginate, and ammonium alginate are manufactured. Additionally, specialized varieties such as zinc alginate, copper alginate, sodium calcium alginate, ammonium calcium alginate, and propylene glycol alginate (PGA) serve specific purposes [22]. These commercial alginates are predominantly sourced from three brown algae: *Macrocystis*, *Laminaria*, and *Ascophyllum* [23], with an annual production of at least 30,000 metric tons [24,25].

Alginate extraction traditionally follows a multi-step process, starting with mechanical treatments to increase the surface area of the raw material. This is followed by acidification, using either HCl or CaCl$_2$, to remove counter ions and some impurities, resulting in insoluble alginate acid. Subsequently, alkaline extraction with NaOH or Na$_2$CO$_3$, along with solid-liquid separation through centrifugation or filtration, removes residual seaweed and produces soluble sodium alginate. The

subsequent stages include precipitation, drying, and grinding [4,25].

Alginate precipitation pathways can be categorized into three main routes:

(i) The alcohol precipitation: this route mainly with ethanol stands out as the predominant method for precipitating sodium alginate.
(ii) The calcium chloride route: this process is initiated with the formation of calcium alginate, followed by filtration, and washing with distilled water to eliminate surplus calcium. After this, an acid treatment, typically with HCl, is implemented to transform it into alginic acid.
(iii) The hydrochloric acid pathway: this last route yields alginic acid, which is then isolated through a flocculation-flotation process and/or centrifugation.

Alginic acid obtained from route (ii) and (iii) can be transformed into various commercial alginate forms through alkaline neutralization. Commonly utilized solutions for this purpose encompass Na$_2$CO$_3$, CaCO$_3$, K$_2$CO$_3$, MgCO$_3$, (NH$_4$)$_2$CO$_3$, or C$_3$H$_6$O, resulting in the production of sodium alginate, calcium alginate, potassium alginate, magnesium alginate, ammonium alginate, and PGA, respectively [4,25–27].

Novel extraction methods involve ultrasound, microwave, enzyme-assisted, and extrusion techniques, offering alternatives to conventional methods [4,25].

In addition, bacterial alginates can be generated as extracellular materials by bacteria like *Azotobacter vinelandii* and *Pseudomonas aeruginosa* [23,24]. Currently, they are not produced commercially.

2.2. Chemical structure and physicochemical properties of alginate

Alginate presents as a linear block polymer, comprising 1,4-linked β-D-mannuronate (M) and α-L-guluronate (G) (Fig. 1a). These two monomeric units can assemble into three block types: GG blocks, MM blocks, and alternating M and G units. Distinct blocks display varying degrees of softness: (i) GG blocks exhibit pronounced rigidity due to steric hindrance [28,29]; (ii) MM blocks create highly flexible structures [30], and (iii) MG blocks incorporate the most flexible components owing to equatorial-axial bonding [31,32]. The distribution and proportion of these three blocks fluctuate based on factors such as the source, geographical origin, degree of maturity, and harvesting time [33,34].

Commercial alginates exhibit molar masses spanning from 34 to 400 kDa, boasting viscosities in 1 % solutions that span 10–1000 mPa·s (degree of polymerization (DP) range of 100–1000 units), their values modulated through adjustments in extraction conditions [16,35].

Common alginates, including alginate salts (e.g., sodium, potassium, and ammonium alginates) and PGA, can be readily dissolved in water. The viscosity of alginate solutions increases with reducing pH, peaking around pH 3–3.5. This occurs as carboxylate groups in the alginate backbone become increasingly protonated, leading to the formation of higher hydrogen bonds contents [28]. Sodium alginate can also be rapidly dissolved in mixtures of water and hydrophilic organic solvents like ethanol, isopropanol, and acetone at optimal concentration (50–70 %) [36]. Moreover, tetrabutylammonium (TBA) salts of alginic acid can be dissolved in polar aprotic solvents containing tetrabutylammonium fluoride (TBAF) [37]. Among various alginates, sodium alginate has been predominantly utilized as the raw material for studies on alginate materials, as reviewed in this article.

Alginate exhibits distinctive colloidal properties, encompassing thickening, stabilization, suspension, film formation, gelation, and emulsion stabilization. These properties render it invaluable for various applications in the realms of food, food packaging, and biomedical fields such as wound healing, drug delivery, in vitro cell culture, and tissue engineering [28,38]. Films crafted from alginate demonstrate robustness and resistance to oil and grease [39]. However, like other polysaccharides, they exhibit poor water resistance owing to their inherent
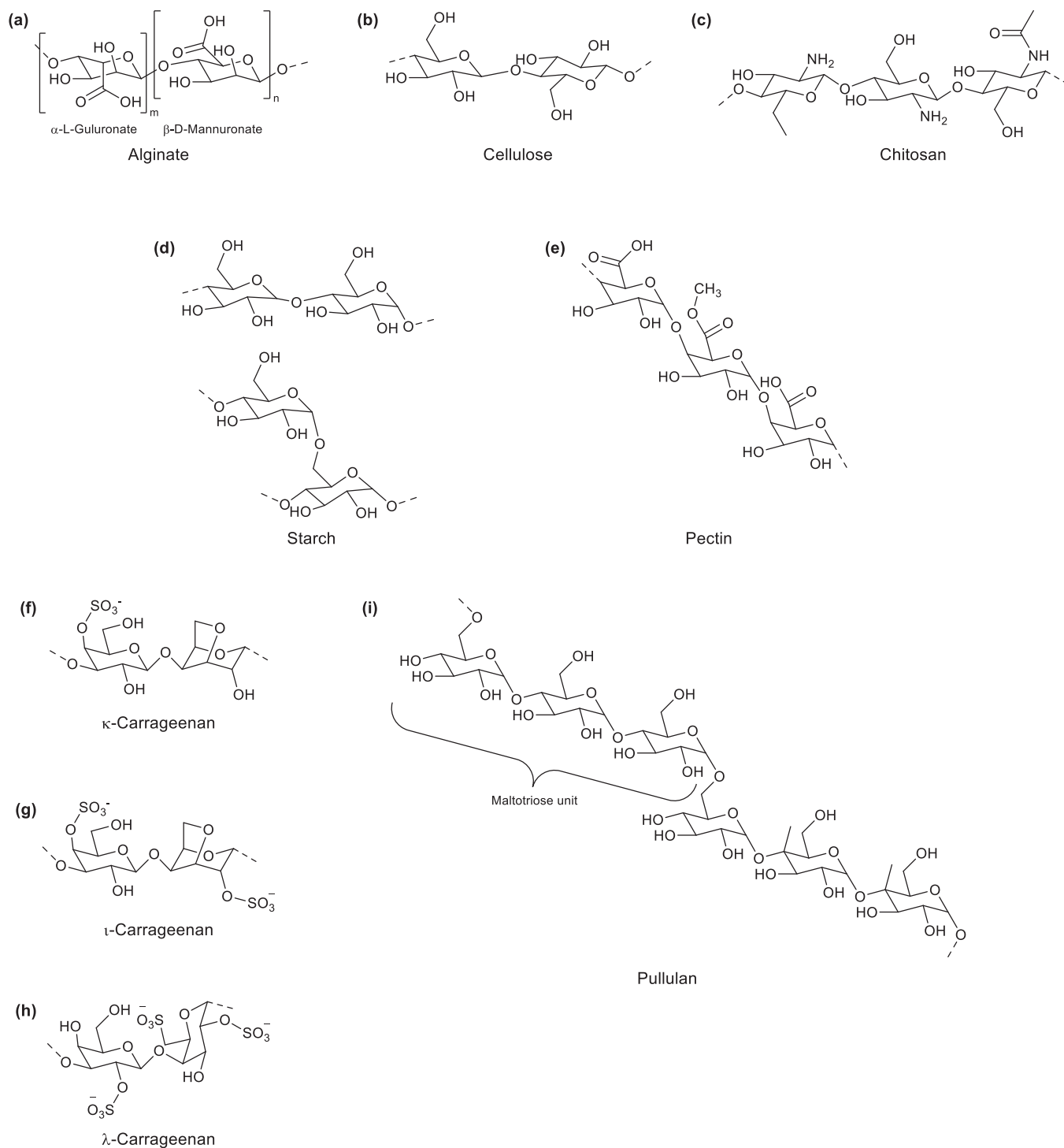
Fig. 1. Chemical structures of alginate and other polysaccharides for developing alginate-based blends.

hydrophilicity [40]. Consequently, alginate is often blended with other biopolymers or biobased polymers to enhance the mechanical properties of the films [38].

The gelation property of alginate primarily stems from its remarkable ability to bind divalent ions. Alginates exhibit varying affinities towards divalent ions, with the hierarchy being Pb > Cu > Cd > Ba > Sr > Ca > Co, Ni, Zn > Mn [41]. Among these, calcium (Ca^{2+}) stands out as the most frequently employed divalent ion for alginate gelation. Alginate can establish 3D crosslinked networks through electrostatic interaction, hydrogen bonding, and van der Waals forces, linking divalent ions like Ca^{2+} with the $-COO^-$, $-OH$, and $C-O-C$ groups in G blocks—a

model known as "egg box" (Fig. 2**a,b**). Ca^{2+} ions are believed to selectively bind to the G blocks of alginate chains [42,43]. This preference arises from the structural characteristics of the G blocks, which facilitate a high degree of coordination with divalent ions [28]. In addition to the principal formation of egg-box dimers at lower concentrations of Ca^{2+}, a lateral aggregation of the egg-box dimers at higher concentrations of Ca^{2+} (Fig. 2**c**) [44]. Additionally, research has shown that this junction zone aggregation occurs during dehydration and is largely reversible upon rehydration [45].

The concentration of polyvalent ions can affect the stability of the resulting crosslinks. It was shown that a low amount of Ca^{2+} leads to
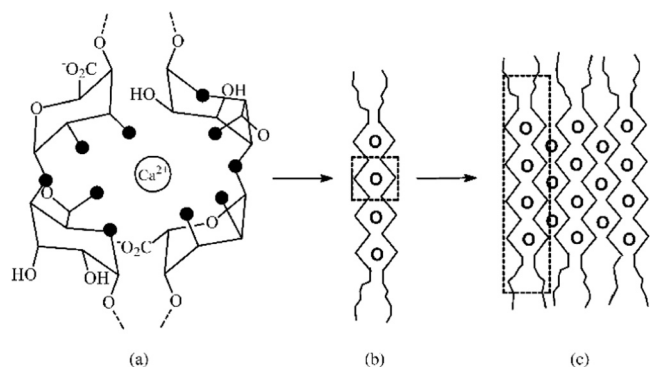
Fig. 2. Schematic representation of the hierarchical structure of egg-box junction zones in alginate/calcium gels: (a) Ca^{2+} coordination within a cavity formed by two guluronate sequences along alginate chains.; (b) Egg-box dimer, and (c) Lateral aggregation of egg-box multimers. Solid black circles indicate oxygen atoms potentially involved in Ca^{2+} coordination, while open circles represent Ca^{2+} ions. Reprinted from [44], with permission from ACS Publications, Copyright 2007.

temporary associations with alginate chains, while higher concentrations promote relatively permanent associations [46].

While CaCl$_2$ is commonly used to ionically crosslink alginate, its high solubility in water often results in rapid and uncontrolled gelation. One approach to mitigate this issue involves using a phosphate buffer, such as sodium hexametaphosphate (Na$_6$[(PO$_3$)$_6$]). The phosphate groups in the buffer compete with alginate's carboxylate groups ($-COO^-$) for Ca^{2+} ions, effectively slowing and controlling gelation. Additionally, calcium sulfate (CaSO$_4$) and calcium carbonate (CaCO$_3$), with their lower solubilities, can also prolong the working time of alginate gels by reducing the gelation rate. Moreover, At lower temperatures, the reactivity of Ca^{2+} decreases, leading to a slower rate of crosslinking [28].

The conversion of soluble alginate in salt form into insoluble alginic acid in free acid form under acidic conditions allows H^+ ions to interact with both the $-COO$ groups of the G and M blocks of alginate. This interaction forms an alginic acid gel, which also increases crosslinking density and thereby enhances film-forming properties [47].

2.3. Preparation of alginate-based bulk materials

This section explores techniques for fabricating alginate-based bulk materials, including films, coatings, tubes, and fibers. While traditional methods are elucidated, innovative approaches are also emphasized. Please note that the discussion does not encompass alginate-based particles or microemulsions.

2.3.1. Solution casting

Like for other polysaccharides, solution casting stands as the prevalent technique for the fabrication of alginate films, especially with extensive research studies on the laboratory scale. This is because alginate salts and PGA are soluble in water as discussed above. In this approach, alginate initially dissolves in water, forming a homogeneous solution, followed by casting in a mold or dish or on a substrate. Subsequently, the elimination of most of the solvent in the polymer solution through a drying process allows the polymer to solidify into a thin film. As a typical example, Santos et al. [48] used 1.5 % (w/v) sodium alginate solution obtained by mixing the polymer in water at 70 °C for 1 h and then dried the cast film from this solution at 40 °C for 24 h in an air circulation oven. This casting method resulted in transparent, glossy, flexible, soluble alginate films [49].

Alginate films can also be directly formed (without a drying process) by treating alginate solutions with Ca^{2+} to trigger the crosslinking of alginate. There are two primary methods for Ca^{2+} crosslinking of alginate materials: the "diffusion" method and the "internal setting" method

[5]. In the diffusion method, crosslinking ions diffuse into the alginate solution from an external reservoir. This process often results in gels with a crosslink density gradient across their thickness due to polymer chain diffusion during the action of Ca^{2+} ions, although this effect can be mitigated by the introduction of non-crosslinking salts like Na^+ and Mg^{2+} [50]. On the other hand, in the "internal setting" method, an ion source is embedded within the alginate solution. A controlled trigger, often pH or solubility of the ion source, initiates the release of crosslinking ions into the system, resulting in gels with uniform crosslinking throughout [5]. The ion source typically consists of insoluble calcium salts such as CaCO$_3$, and a change in pH caused by a slowly hydrolyzing lactone such as D-glucono-δ-lactone (GDL) triggers the release of Ca^{2+} ions internally, leading to gel formation [51–54].

To address the challenge of uneven crosslinking (gelation) arising from the rapid Ca^{2+} crosslinking of alginate via the external diffusion crosslinking approach, researchers have explored an alternative method: exposing a sodium alginate solution to an aerosolized spray of CaCl$_2$ solution [55,56]. This method has been shown to yield planar alginate hydrogels.

The properties of dried alginate films can be enhanced by further Ca^{2+} treatment. This can be achieved by immersion of dried sodium alginate films into a CaCl$_2$ solution [47,57–77], or spraying an aqueous solution of CaCl$_2$ onto dried sodium alginate films [78]. Crossingham et al. [58] showed that, in comparison to alginate film prepared using the diffusion method, a dried alginate film immersed in 0.34 M aqueous CaCl$_2$ exhibited a denser structure, higher mechanical strength, reduced rehydration in water and 0.1 M HCl, and lower in vitro diffusivity for a model drug, theophylline. Li et al. [79] discovered that incorporating ethanol into a CaCl$_2$ aqueous solution for crosslinking alginate enhanced the visual appearance, thickness, surface homogeneity, and mechanical properties of the films. These improvements were attributed to the reduced swelling degree of the films during the crosslinking process. However, the degree of Ca^{2+} crosslinking decreased when the ethanol content exceeded 30 % (v/v) [79].

Additionally, ultrasonic atomization has been demonstrated to treat dried alginate films with Ca^{2+} [80]. In this study, calcium gluconolactate served as the crosslinking agent, which is particularly advantageous for food packaging applications as CaCl$_2$ can impart a bitter taste whereas calcium gluconolactate is a commonly used food additive.

Notably, in some studies [61,78,81–83], a two-stage crosslinking approach was utilized. Initially, divalent ions were mixed into film-forming formulations for weak crosslinking of alginate in the first stage. Subsequently, the dried cast film was immersed in a more concentrated divalent ion solution for further crosslinking in the second stage.

Lyophilization serves as a valuable method for producing microporous materials based on alginate. It can be applied to CaCl$_2$-crosslinked alginate gels [84–86], or performed before CaCl$_2$-crosslinking [87–90]. Moreover, microporous structures can be induced through freeze-gelation. This process involves initially freezing an alginate solution to facilitate polymer/water phase separation, followed by immersing the frozen sample into a pre-cooled ethanol solution containing the optimal concentration of CaCl$_2$ at a subzero temperature. The samples are then washed and air-dried to complete the procedure [91].

2.3.2. Coating

Coating the surface of items, such as food items, can be easily accomplished by dipping the item into an alginate film-forming solution [92–94]. Subsequent air-drying allows the formation of a coating film on the item's surface [92]. Alternatively, after draining excess alginate solution, the item can be promptly immersed in a Ca^{2+} solution to initiate the crosslinking of the alginate [93–96].

In addition, the vacuum impregnation (VI) method has demonstrated the ability to create a thicker, more effective coating by efficiently incorporating the solution into porous solid matrices containing air, such as fruits and vegetables. VI coating process involves immersing the

item first into an alginate film-forming solution, followed by the application of vacuum. Subsequently, after restoring atmospheric pressure, the item is left to drain [94].

In addition to dipping, coatings can also be applied by spraying coating solutions onto targeted surfaces. A spray system enhances the liquid's surface area by forming droplets and dispersing them across the food surface via a series of nozzles. This technique offers several advantages, including uniform coating, precise thickness control, and the capability for multilayer applications, such as alternating sodium alginate and $CaCl_2$ solutions. Furthermore, spraying systems preserve the integrity of the coating solution, enable temperature control of the solution, and support the automation of continuous production. Key physical properties of the liquid, such as viscosity, density, and surface tension, play crucial roles in generating controlled droplets [97].

Various studies have highlighted the advantages of multi-layer coatings containing alginate and other polysaccharides when applied to fresh fruits and vegetables. These coatings demonstrate enhanced adhesion to the surfaces of freshly cut produce and offer improved functionality, including antimicrobial properties and water vapor barrier effects, resulting in extended shelf life [98–101]. This enhancement is achieved through layer-by-layer (LbL) techniques. For instance, pieces of fresh-cut watermelon or pineapple were sequentially dipped into various solutions, including a 2 wt% Ca^{2+} solution, a solution comprising 1 % sodium alginate plus a 2 wt% antimicrobial agent, a 2 wt% pectin solution, and finally, the Ca^{2+} solution again [99,100]. In another example, fresh-cut melon pieces were first immersed in a 1.5 % alginate solution, followed by immersion in a 5 wt% $CaCl_2$ solution to crosslink the alginate and rinsing with water; subsequently, the pieces
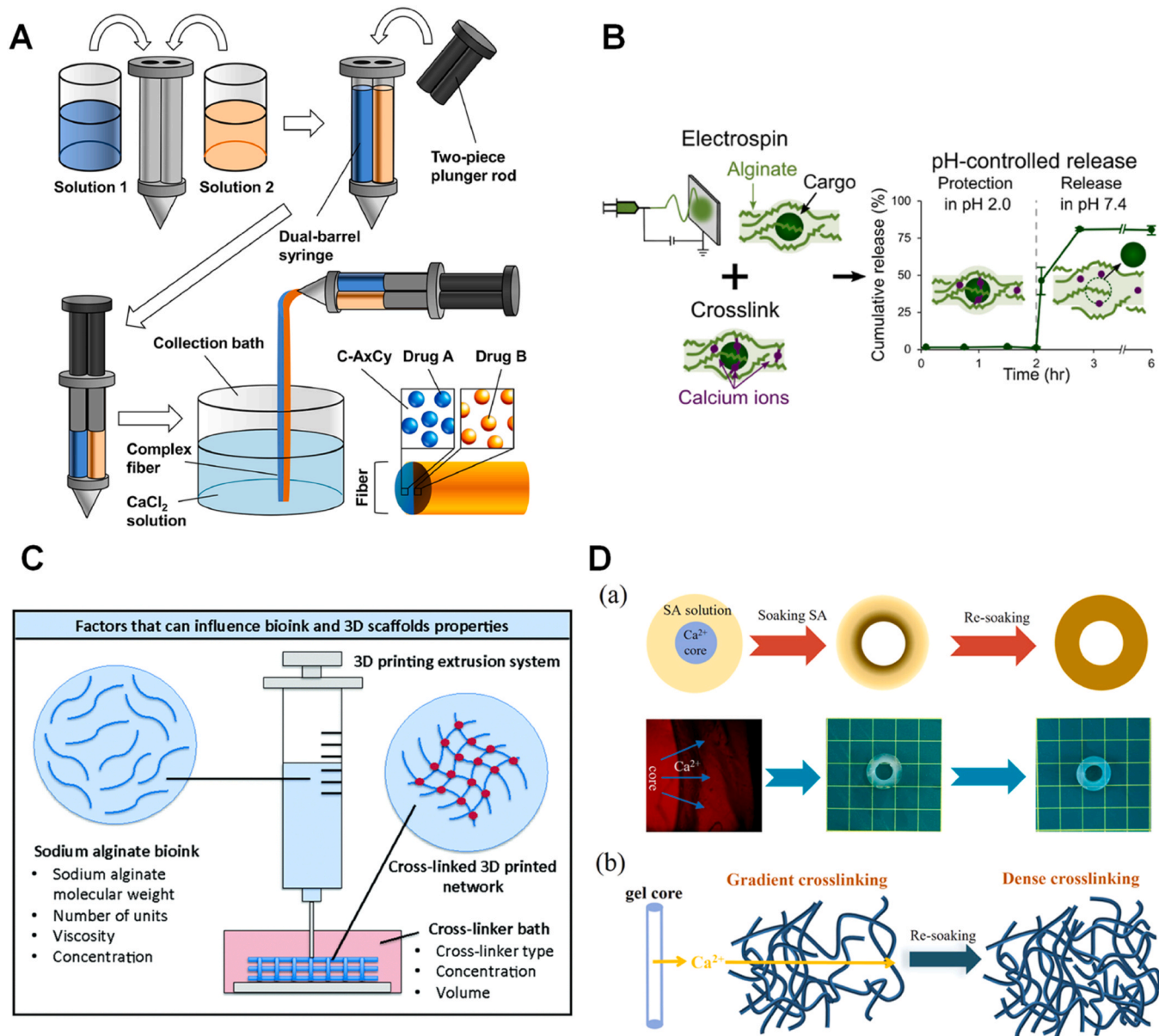
Fig. 3. Schematic illustrations of **(A)** the fabrication of Janus-morphological fibers using wet spinning; **(B)** the electrospinning of alginate in ethanol-free Ca^{2+} solutions, exhibiting pH-controlled release behavior. **(C)** a typical direct-ink-writing 3D printing principle for alginate-based inks relying on a Ca^{2+}-containing bath for post-extrusion crosslinking. **(D)** the directional diffusion assembly (DDA) method for seaweed-based straw fabrication. (a) Ca^{2+} diffusion and (b) change in crosslinking density during fabrication steps.
(a) **(A)** is reprinted from [108] with permission from Elsevier, Copyright 2021. (b) **(C)** is reprinted from [110] with permission from the Royal Society of Chemistry, Copyright 2020. (c) **(B)** is reprinted from [109] with permission from ACS Publications, Copyright 2023. (d) **(D)** is reprinted from [111] with permission from ACS Publications, Copyright 2023.

were immersed in a 1.5 wt% chitosan solution, and air-dried at room temperature [101]. In the latter scenario, polyelectrolyte complexation occurred between the layers of alginate and chitosan, which possess opposite charges. This process resolves the issue of alginate and chitosan mixture in solution, which often results in sedimentation rather than a homogeneous solution.

One of the main advantages of these coating techniques is that coating can be formed around complex-shaped or rough surfaces. In addition to dip coating and spray coating, other coating techniques include spin coating [56,102,103], blade coating [104], and slot die coating [105], all of which hold potential for fabricating alginate thin films. Blade coating and slot die coating offer the main advantage of producing films with highly defined thicknesses. After films are formed using these coating techniques, Ca^{2+}-treatment (e.g., by aerosol spray [56] or by immersion into a Ca^{2+} solution [103]) can be similarly applied, as previously discussed in **Section 2.3.1** .

2.3.3. Spinning

Wet spinning, a textile manufacturing process, offers a method for producing alginate fibers by leveraging alginate's ability to crosslink with Ca^{2+}. This technique involves dissolving alginate in a solvent, typically water, to create a spinning solution with appropriate properties, including viscosity, coagulation/precipitation, and stretchability. The solution is forced through a spinneret—a nozzle with minuscule holes—into a coagulation bath containing Ca^{2+}. In this case, the alginate crosslinks with Ca^{2+} and precipitates into solid fibers, which are collected onto a reel. It may be necessary to wash the obtained fibers with deionized water to remove any residual coagulant. As a typical example, in a study by Zheng et al. [106], a spinning dope of 2.5 wt% sodium alginate and a 5 wt% $CaCl_2$ solution were utilized. Wang et al. [107] fabricated fibers by extruding a 5 wt% mixture of alginate and starch at room temperature. The extruded solution was then directed into a coagulating bath consisting of an aqueous solution containing 10 wt% $CaCl_2$ and ethanol, ultimately resulting in the formation of fibers. Lai et al. [108] illustrated a method based on wet spinning for fabricating Janus-morphological alginate-based fibers (Fig. 3**A**). Carboxymethyl cellulose (CMC) sodium was employed as a polymeric modifier to adjust the properties of each fiber compartment. The syringe pump was employed to drive the two-piece plunger rod, with a rubber piston attached to the end of each piece, facilitating the ejection of solutions from the dual-barrel syringe into a collection bath containing a 10 % (w/v) solution of $CaCl_2$.

Electrospinning is a method to produce mats from microfibers based on polymers. However, creating a pure alginate electrospun nanofiber membrane presents challenges due to the high surface tension, high electrical conductivity, and absence of chain entanglements in alginate when in an aqueous solution. For electrospinning of alginate, polyethylene glycol (PEG) is usually used as a co-spinning agent [112,113], which can be subsequently removed by rinsing with hot ethanol [112, 113] or $CaCl_2$ solution [114]. Mokhena et al. [114] suggested that even in this way, nanofibers could not be obtained at low alginate content ranging from 20 to 60 v/v%. Dodero et al. [113] successfully demonstrated electrospinning from an aqueous solution of sodium alginate, PEG (7:3 w/w), and ZnO nanoparticles. They suggested that for electrospinning, alginates with a low molar mass and high M/G ratio, or alginates with a medium molar mass and low M/G ratio, should be preferred when combined with ZnO nanoparticles. In another study, Dodero et al. [112] additionally used Triton as a surfactant to increase the alginate/PEG solution electrospinnability. Additionally, blending alginate with other polymers such as polyvinyl alcohol (PVA) has been acknowledged as a viable approach to enhance the electrospinnability of alginate [115].

Electrospun alginate nanofibers can then be crosslinked by immersion in a solution of divalent ions (e.g., $SrCl_2$), before rinsing with water and drying [112,113].

It is noteworthy that while ethanol can aid in maintaining the

structure of fibers in the crosslinking solution, its use may not be suitable for certain applications, especially biomedical ones. Taking this into consideration, Diep and Schiffman [109] effectively produced ethanol-free alginate-based nanofibers via electrospinning and subsequent crosslinking using either a Ca^{2+}/glycerol solution or pH-optimized solutions containing Ca^{2+} (Fig. 3**B**). These crosslinked fibers exhibited stability in water and acidic buffers while swelling in phosphate-buffered saline (PBS), rendering them valuable for pH-controlled release applications.

2.3.4. 3D printing

Alginate has emerged as a widely used polymer for formulating 3D printing inks. The 3D printing of alginate hydrogels can be achieved through two main methods: direct-ink-writing (DIW) 3D printing and inkjet 3D printing [116,117].

In DIW, alginate hydrogels with appropriate viscoelastic properties are extruded into a predetermined structure. This can be achieved by incorporating a low content of Ca^{2+} into the alginate-based ink formulation, thereby inducing partial crosslinking of the alginate [118–120]. It is crucial that the alginate hydrogels set instantly after extrusion to maintain the integrity of the printed structures. Typically, this setting process is facilitated by printing the hydrogels into a supporting bath containing Ca^{2+} ions [116,117] (Fig. 3**C**). Using aerosol spraying of $CaCl_2$ solution to crosslink alginate hydrogels during printing has also been reported [121]. Alternatively, the printed structures must be promptly submerged in a $CaCl_2$ solution for additional crosslinking for achieving adequate solidification [118,119,122–128].

In inkjet 3D printing, the print head, capable of horizontal movement, jets alginate-based inks into a bath containing a $CaCl_2$ solution to ionically crosslink the alginate while simultaneously forming the printed structure on a vertically movable platform. Alternatively, alginate can serve as a supporting liquid into which a $CaCl_2$ solution is jetted to crosslink the alginate. Both methods enable the creation of highly intricate structures [116,117].

2.3.5. Directional diffusion assembly

Liu et al. (2023) [111] recently introduced a novel directional diffusion assembly (DDA) method for directly fabricating hollow tubes from seaweed-based materials, presenting an alternative to the traditional rolling-up technique (Fig. 3**D**). In this method, a preformed agar core, enriched with Ca^{2+}, is submerged into an alginate solution. This results in the directional diffusion of Ca^{2+} ions from the core into the surrounding dissolved alginate phase, thereby forming a tube. The core can then be easily removed due to its thermo-reversibility. Subsequently, the hollow tube can undergo further crosslinking, particularly on the external side, by immersing it in a Ca^{2+} solution. Upon drying at 60 °C and 80 % relative humidity (RH), the resulting hollow tube exhibits excellent hygrostability, even when exposed to hot water up to 85 °C, and boasts impressive mechanical properties. This method offers several advantages: (1) It enables the fabrication of articles with intricate shapes, depending on the sacrificial core's shape; (2) Its flexibility and versatility are demonstrated by adjusting various parameters such as raw materials, crosslinker and substrate concentrations, and diffusion duration; (3) The tubes produced using this method demonstrate superior mechanical and thermal properties compared to prevalent counterparts made of polylactic acid (PLA) and paper; (4) Importantly, this technique can be extended beyond alginate to materials like κ-carrageenan (dissolved and crosslinked at 70 °C) and low-acetyl gellan gum (crosslinked using K^+/Ca^{2+}), showcasing its broad applicability.

2.3.6. Thermomechanical processing

Thermomechanical processing, utilizing traditional plastic processing techniques, has emerged as a recent innovation for processing alginate into a plastic-like material [129–132]. Like many other polysaccharides featuring extremely dense hydrogen bonding, alginate's theoretical melting temperature surpasses its degradation point, making

direct thermal processing impossible. Therefore, the thermomechanical processing of alginate necessitates the addition of small molecules such as water and polyols (typically glycerol), acting as plasticizers. These agents disrupt alginate's inherent hydrogen bonds and supramolecular structures. While water serves as an efficient plasticizer, its volatility poses processing challenges and destabilizes material properties. Hence, non-volatile plasticizers like glycerol become necessary. In this thermomechanical approach, the initial step involves premixing raw alginate with water and other plasticizers. Allowing the premixed material time to equilibrate facilitates the diffusion of small molecules into alginate. Subsequently, the resulting blends are introduced into a thermomechanical setup such as an internal mixer. Through the application of thermomechanical forces, native alginate particles transition into a "molten" state. These plasticized materials, exhibiting thermoplastic-like traits, are amenable to processes like compression molding, allowing the creation of items such as sheets. This method enables the creation of innovative materials with regulated properties, achieved through blending with various (biobased or fossil) polymers, as well as the incorporation of (nano)fillers as reinforcements to engineer (nano)composites.

The tensile properties of different polyol-plasticized alginates obtained by thermomechanical mixing and solution casting were compared (see Table 1) [131]. With identical compositions, samples produced via solvent casting exhibited greater Young's modulus (YM) and tensile strength (TS) compared to those processed by thermomechanical mixing. Elongation at break (EB) showed an opposing trend, particularly pronounced in samples containing reduced plasticizer content. The observed disparities between solution casting and thermomechanical processing could stem from variations in alginate chain packing during film formation and the thickness of films crafted through distinct methods. On a broader note, plasticized samples yielded by both techniques showcased commendable mechanical attributes.

2.4. Factors affecting the properties of alginate-based bulk materials

Existing literature underscores that a multitude of factors—ranging from the source and chemical composition of alginate, to its molar mass, plasticizer nature and concentration, alongside processing parameters—exert influence over the attributes and performance of alginate-based materials. How the key properties of alginate-based materials are affected by different factors are summarized in Table 2 and discussed below.

2.4.1. Crosslinking

As previously discussed in **Section 2.2**, crosslinking by divalent ions typically as Ca^{2+} is an important feature of alginate, which is predominantly utilized for enhancing alginate material properties (e.g., water resistance, barrier properties, and mechanical attributes) [52,59,63,69, 78,133]. Also, crosslinked alginate has demonstrated a greater capacity

to retain entrapped ingredients (e.g., drugs) that require controlled or slow release [46]. Russo et al. [134] suggested that crosslinking with Ca^{2+} of alginate films in a swollen state reduces both the glass transition temperature (T_g) and the β-relaxation temperature, presumably attributed to the expansion of free volume during the crosslinking process. Notably, this phenomenon contrasts with the effect of increasing guluronic moiety content, which typically promotes chain-to-chain interactions, resulting in an elevation of T_g.

Rhim [2] conducted a comparative study on alginate films using two Ca^{2+} treatment methods: direct mixing of $CaCl_2$ (1–3 wt% of alginate) into the film-forming solution and immersion of the cast film into a $CaCl_2$ solution (0.1–0.5 w/v% concentrations). The immersion method notably increased TS, and decreased EB, water vapor permeability (WVP), water solubility, water swelling, and thickness, whereas the mixing method did not produce such effects. This shows that compared to the mixing method, immersion of prepared alginate films could be a more effective way to achieve a crosslinked structure and thus enhance film properties.

Presumably, higher ion concentration and longer crosslinking duration lead to increased crosslink density, until reaching a maximum level. Hence, the properties of crosslinked alginate should be impacted by ion concentration and crosslinking duration. For instance, Costa et al. [63] reported that dried cast alginate films crosslinked with higher $CaCl_2$ concentrations (1–1.5% w/v) exhibited greater TS and lower EB, as well as reduced water solubility and swelling. Besides, Zactiti and Kieckbusch [78] observed that dried alginate films subjected to 2nd-stage crosslinking using $CaCl_2$ solutions with concentrations from 2 or 7% presented a drastic decrease in water solubility, higher TS, lower EB, as well as a slower release of potassium sorbate as an antimicrobial agent. In another study [52], an increase in the degree of crosslinking (by $CaCO_3$ at up to 0.03% (w/w) based on alginate, with 5.4 g of GDL per gram of $CaCO_3$) produced alginate films that were significantly thicker and stronger but less elastic than those non-crosslinked films. WVP of the films decreased significantly only with the highest level of crosslinking [52]. According to Liling et al. [62], increasing Ca^{2+} ion concentration initially boosted the TS and EB of alginate films until reaching a peak at a concentration of 2% (w/v), after which they decreased. Meanwhile, WVP and light transmittance gradually decreased. As for crosslinking time, WVP increased gradually, EB initially rose and then stabilized after 2 min of crosslinking, while TS and light transmittance remained nearly constant. The alginate film crosslinked in 2% (w/v) $CaCl_2$ for 2 min exhibited overall optimal performance. These results suggest that the effects of ion concentration and crosslinking duration on alginate material properties may not always follow straightforward patterns.

Likely, variations in alginate material properties could also be influenced by uneven crosslinking, which, in turn, can be markedly influenced by the rate of reaction. A slower crosslinking rate tends to result in a more uniform structure and enhanced mechanical properties.

Table 1

Tensile properties of plasticized alginate, obtained by thermomechanical mixing and solution casting (AW: alginate; AG: alginate/glycerol; AS: alginate/sorbitol). Reprinted from [131] with permission from Elsevier, Copyright 2016.

Samples (w/w)	Thermomechanical mixing			Solution casting		
	Modulus (MPa)	Tensile strength (MPa)	Elongation (%)	Modulus (MPa)	Tensile strength (MPa)	Elongation (%)
Neat AW	1989±106	52±3	11±2	3050±109	63±4	9±0
AG20/80	250±14	17±1	37±4	813±41	25±2	12±2
AG25/75	40±1	10±2	47±4	345±29	15±6	17±1
AG30/70	17±3	7±1	54±4	116±11	13±2	32±3
AG40/60	4±1	5±0	74±4	34±0	4±0	60±0
AG50/50	3±1	2±0	60±4	2±1	2±0	105±3
AS20/80	801±5	31±3	16±2	1534±105	45±4	9±1
AS25/75	333±21	23±2	29±2	1102±47	36±3	9±1
AS30/70	110±37	13±0	37±1	718±52	31±1	13±1
AS40/60	5±1	6±0	61±4	30±3	7±1	34±3
AS50/50	3±1	3±0	73±4	3±1	3±1	61±1

Table 2
Key properties of alginate-based materials as affected by different factors.

Property/Parameter	Evolution	Main Factor	References
Thickness	Increase	Crosslinking	[52]
		Clitoria ternatea extract	[48]
		Grapefruit seed extract	[377]
		Cottonseed protein hydrolysates	[152]
	Decrease	Crosslinking	[2]
T_g	Increase	Plasticizer PEG	[164]
	Decrease	Crosslinking	[134]
		Higher M/G ratio	[142]
		Plasticizer glycerol	[142]
Thermal stability (TGA)	Increase	Plasticizer PEG	[164]
		Essential oils	[72]
		Castor oil	[57]
		Aloe vera extract	[72,378]
		Peanut red skin extract	[74]
	Decrease	Pterostilbene	[157]
Thermal stability (DSC)	Increase	*Clitoria ternatea* extract	[48]
	Decrease	Pterostilbene	[157]
Tensile strength	Increase	Crosslinking	[2,52,59,62–64, 69,78,133]
		Higher *M*	[35]
		Essential oils	[72]
		Castor oil	[57]
		Clitoria ternatea extract	[48]
		Aloe vera extract	[72,378]
		Peanut red skin extract	[74]
		Plasma activated water	[159]
	Decrease	Higher M/G ratio	[63]
		Plasticizer glycerol	[60,81]
		Plasticizer sorbitol	[30,60]
		Plasticizer fructose	[60]
		Plasticizer PEG	[60,147]
		Essential oils	[40,52,165,166]
		Citric acid	[159]
		Natamycin	[66]
		Pterostilbene	[157]
Young's modulus / elastic modulus	Increase	Crosslinking	[59,64,69]
		Citric acid	[159]
		Castor oil	[57]
		Plasma activated water	[159]
	Decrease	Plasticizer glycerol	[147]
		Plasticizer PEG	[147]
		Essential oils	[166]
		Grapefruit seed extract	[377]
Elongation at break	Increase	Crosslinking	[62,133]
		Higher M/G ratio	[43]
		Plasticizer glycerol	[60,81]
		Plasticizer sorbitol	[30,60]
		Plasticizer fructose	[60]
		Plasticizer PEG	[147]
		Essential oils	[40,52,72,165, 166]
		Castor oil	[57]
		Natamycin	[66]
		Aloe vera extract	[72,378]
		Peanut red skin extract	[74]
		Grapefruit seed extract	[377]
		Citric acid	[159]
		Plasma activated water	[159]

Table 2 (*continued*)

Property/Parameter	Evolution	Main Factor	References
	Decrease	Crosslinking	[2,52,59,62,63, 69,78,133]
		Plasticizer PEG	[60]
		Pterostilbene	[157]
		Clitoria ternatea extract	[48]
Water solubility or swelling	Increase	Plasticizer glycerol	[81]
		Clitoria ternatea extract	[48]
	Decrease	Crosslinking	[2,63,69,78,82]
		Plasticizer glycerol	[147]
		Plasticizer PEG	[147]
		Pterostilbene	[157]
Water contact angle	Increase	Sulfur nanoparticles	[73]
		Pterostilbene	[157]
		Peanut red skin extract	[74]
	Decrease	Grapefruit seed extract	[377]
Oxygen barrier	Increase	Plasticizer glycerol	[30]
	Decrease	Crosslinking	[30,133]
Water vapor barrier	Increase	Crosslinking	[2,52,62,69,133]
		Decreasing M/G ratio	[60]
		Plasticizer sorbitol	[60]
		Plasticizer fructose	[60]
		Vegetable oils	[96]
		Essential oils	[52]
		Castor oil	[57]
		Citric acid	[159]
		Plasma activated water	[159]
		Aloe vera extract	[72,378]
		Peanut red skin extract	[74]
		Pterostilbene	[157]
	Decrease	Plasticizer glycerol	[30]
		Plasticizer PEG	[60]
		Essential oils	[72,165]
		Natamycin	[66,83]
		Clitoria ternatea extract	[48]
		Sugarcane vinasse	[69]
		Cottonseed protein hydrolysates	[152]
Transparency (light transmittance)	Increase	Crosslinking	[62]
	Decrease	Crosslinking	[82]
		Sugarcane vinasse	[69]
		Clitoria ternatea extract	[48]
		Aloe vera extract	[378]
		Cottonseed protein hydrolysates	[152]
UV shielding	Increase	Essential oils	[72]
		Aloe vera extract	[72]
		Beet root extract	[162]
		grapefruit seed extract	[377]
Release rate	Decrease	Crosslinking	[78]

To reduce the crosslinking rate, various approaches can be employed, including utilizing sparingly soluble salts like $CaSO_4$ or $CaCO_3$, employing phosphate-based buffers instead of $CaCl_2$, and lowering the reaction temperature [28]. Drury et al. [64] suggested that lower temperatures reduced the diffusion rate of Ca^{2+} ions, which led to slower crosslinking, a more ordered network structure, and hence enhanced tensile properties.

Jang et al. [54] observed that employing higher concentrations of $CaCO_3$/GDL for crosslinking resulted in smaller pore sizes and increased compressive modulus, as well as storage and loss moduli. Kuo and Ma [135] produced alginate hydrogel scaffolds with uniform structures

using CaCO$_3$/GDL and CaSO$_4$/CaCO$_3$/GDL. They illustrated that controlling the gelation rate was achievable, with enhancement observed through increased total Ca^{2+} content, a higher proportion of CaSO$_4$, elevated temperature, and decreased alginate concentration. Slower gelation yielded hydrogels characterized by uniformity and enhanced mechanical strength. Meanwhile, the compressive modulus and strength were increased with alginate concentration, total Ca^{2+} content, and the molar mass and G content of the alginate.

In a study [133] to examine the effects of different calcium salts (CaCl$_2$ + ethylenediaminetetraacetic acid (EDTA), CaHPO$_4$, and CaCO$_3$) on internally crosslinked alginate films, it was found that Ca^{2+}-induced crosslinking significantly enhanced the TS and EB of cast alginate films. Optimal concentrations of Ca^{2+} for this purpose ranged 1.0–1.5 wt% of alginate. Besides, Ca^{2+}-induced crosslinking led to reductions in oxygen permeability (OP) and WVP, with the lowest permeabilities observed at Ca^{2+} concentrations based on alginate of 1 wt% for CaHPO$_4$, 1.2 wt% for CaCl$_2$, and 2.7 wt% for CaCO$_3$, suggesting an highest effect of CaHPO$_4$.

The dynamic ionic bonding established between Ca^{2+} and the carboxyl group of alginate bestows alginate materials with additional properties, including self-healing and adhesion [136].

Ca^{2+} usually leads to overall excellent material properties. For instance, Liling et al. [62] showed that, while Ca^{2+}, Zn^{2+}, and Mn^{2+} could all increase the TS and light transmission and decrease the WVP of dried cast alginate films, the film crosslinked using Ca^{2+} solution exhibited the greatest TS, EB, and light transmission. Bierhalz et al. [61] demonstrated that 2nd-stage crosslinking of dried cast alginate films with Ca^{2+} yielded favorable properties, including higher TS and lower opacity, OP, and WVP. Nonetheless, it also resulted in unfavorable higher water solubility and water uptake compared to crosslinking with Ba^{2+}. However, Gao et al. [137] demonstrated that an alginate hydrogel membrane crosslinked in a CaCl$_2$/BaCl$_2$ mixture solution exhibited a more stable structure, enhanced mechanical properties, and improved salt tolerance compared to a Ca^{2+}-crosslinked alginate hydrogel membrane. In biomedical applications, utilizing BaCl$_2$ for crosslinking sodium alginate may elicit a less fibrotic reaction compared to CaCl$_2$-crosslinked alginate [138].

In addition to ionic crosslinking, which is the primary focus of this review, alginate hydrogels can be formed using various other crosslinking strategies. These alternative approaches have been discussed elsewhere [139,140].

2.4.2. Alginate chemical composition

The M/G ratio stands as a pivotal determinant impacting the attributes of alginate-based materials. As previously discussed in **Section 2.2**, M blocks and MG blocks are conformationally more flexible than G blocks. In line with this, films made of alginate containing a higher ratio of MM and MG blocks exhibited increased stretchability [43,141]. Besides, alginate featuring elevated M and/or MG block content demonstrates reduced T_g compared to those with higher G block content [142]. Nonetheless, alginate with a high content of M blocks presented greater resistance to plasticization compared to its counterpart rich in G blocks [141]. The buckled and folded configuration of G blocks enables effective entrapment of plasticizers.

As previously discussed in **Section 2.2**, Ca^{2+} ions primarily bind selectively to the G blocks of alginate chains. Consequently, alginates with higher G content demonstrate enhanced crosslinking potential with divalent ions compared to those with a higher M content. Consistent with this, Olivas and Barbosa-Cánovas [60] found that alginate films with a high G ratio fostered the formation of extensive 3D networks, resulting in reduced WVP. Costa et al. [63] proposed that elevated levels of M residues lead to the production of fragile and flexible films, whereas higher G residue contents result in stronger films, with these properties being significantly influenced by the concentration of CaCl$_2$. For alginate films with high M block content, a saturation point in crosslinking was reached, whereas higher concentrations of CaCl$_2$ were required to achieve similar properties for films with high G block content [63]. Similarly, Drury et al. [64] suggested that high-guluronate-content alginates crosslinked by CaSO$_4$ yielded stronger, more ductile hydrogels than high-mannuronate-content ones.

A study by Lee et al. [59] demonstrated that alginate films with higher G block content, crosslinked with Ca^{2+}, contained a greater proportion of Ca^{2+}, yet exhibited a lower percentage change in TS and YM. This suggests that the GG blocks were arranged in a more rigid manner, limiting the movement of polymer chains during crosslinking. Conversely, polymer chains comprising a higher proportion of MM and MG blocks displayed greater flexibility and mobility during crosslinking, allowing for chain alignment and the formation of a stronger matrix, as indicated by the significant percentage change in tensile properties [59]. These findings suggest that the tensile properties of the matrix are influenced by both the extent of crosslinking and the flexibility and mobility of polymer chains, with the latter factor being of greater importance [59].

De'Nobili et al. [142] assessed the effectiveness of Ca^{2+}-crosslinked alginate films with varying M/G composition and glycerol content in preserving L-(+)-ascorbic acid (AA) (also known as vitamin C, renowned for its antimicrobial, antioxidant, and immune system maintenance properties) from hydrolysis. The capability of AA preservation, evaluated through vacuum storage at 25 °C, decreased only with increasing RH levels when alginates consisted mainly of GG blocks. Conversely, when higher proportions of MM or alternating GM/MG flexible blocks were present, AA preservation decreased with both increasing RH and glycerol levels. This phenomenon is likely due to the reduced ability of the latter alginate block compositions (MM or GM+MG) to immobilize water in the network, as they cannot form Ca^{2+}-mediated junction zones where water molecules are highly retained. Additionally, AA preservation was studied under air storage conditions, revealing that both GG- and GM + MG-enriched alginate networks generally preserved AA from oxidation, even under less favorable RH and glycerol levels [142].

2.4.3. Alginate molar mass

Molar mass significantly influences the attributes of alginate-based materials. Typically, higher molar mass leads to increased mechanical strength owing to enhanced interchain bonding [35]. However, molar mass variations was shown to have minimal impact on water uptake and WVP [143].

Alginates with comparable M/G ratios but varying molar masses showed significant differences in the tensile properties of the crosslinked alginate films. Higher-molar mass-alginates demonstrated greater percentage increases in both TS and YM, although the percentage increase in YM plateaued at higher molar masses. Additionally, lower-molar-mass alginates exhibited smaller differences in EB before and after crosslinking, indicating the formation of a more flexible alginate matrix in these cases [59].

2.4.4. Effect of plasticizers

Plasticizers possess certain characteristics, including low molar mass and high polarity, which enable them to interact with natural polymers and disrupt interchain hydrogen bonding to improve chains mobility. They are incorporated into polymers to mitigate brittleness, enhance flow and flexibility, and bolster toughness and strength in films. In the realm of coatings, plasticizers play a crucial role in enhancing resistance, reducing flaking and cracking, improving flexibility, toughness and processability. However, a drawback of plasticizers is their tendency to elevate film permeability to oxygen, moisture, aroma, and oils by diminishing intermolecular attractions along the polymer chains [144]. As in the case of other polysaccharides such as starch, various plasticizers have been tested with alginate, including water as a volatile compound [145], as well as non-volatile plasticizers such as glycerol [2, 30,40,47,48,52,57,60–63,68,69,72,73,81,82,92,131,132,141, 146–153], sorbitol [30,60,75,76,85,131,154–162], fructose [60], polyglycerol [163], and PEG [60,147,155]. The effects of these plasticizers

on alginate film properties were not consistently reported (as seen in Table 2), potentially influenced by factors such as plasticizer content, alginate chain composition, and whether alginate was crosslinked or not.

Jost et al. [30] conducted a comparison between glycerol and sorbitol as plasticizers on cast alginate films (without ionic crosslinking). They observed that both plasticizers reduced porosity in alginate films. Interestingly, films containing 30 % glycerol exhibited nearly identical TS and EB as films with 50 % sorbitol. This suggests that glycerol, with its lower molar mass, is more effectively integrated into the alginate network, consequently increasing free volume, compared to sorbitol. Furthermore, while the addition of glycerol resulted in increased OP and WVP, the inclusion of sorbitol did not impact these barrier properties. The effect of sorbitol was attributed to its good steric fit within the alginate network, which preserved the barrier properties, as well as enhanced networking of hydroxyl groups within the alginate network, leading to fewer bonding points for water vapor. Pongjanyakul and Puttipipatkhachorn [147] found that in cast alginate/magnesium aluminum silicate (MAS) films (without ionic crosslinking), glycerol imparted greater flexibility compared to PEG-400. Additionally, they observed that the WVP of the films decreased with increasing plasticizer content within the range of 10–30 % (w/w). Swamy et al. [164] reported that cast alginate films (without ionic crosslinking) incorporated with a higher content of PEG-6000 exhibited an increase in T_g, which was ascribed to chain entanglement. PEG incorporation also enhanced thermal stability as shown by thermogravimetric analysis (TGA).

Olivas and Barbosa-Cánovas [60] compared various plasticizers, including fructose, glycerol, sorbitol, and PEG-8000, for dried cast alginate films crosslinked with $CaCl_2$. Their findings revealed that PEG-8000 resulted in lower TS and EB, whereas glycerol exhibited the highest values among all the plasticizers tested. Surprisingly, there was no significant difference in WVP between the alginate film without plasticizer and that plasticized with glycerol. However, films plasticized with fructose and sorbitol demonstrated the lowest WVP, while those plasticized with PEG-8000 exhibited the highest.

It is noteworthy that in the above studies, PEG was incompatible with alginate and led to phase separation in the films [60,164].

Da Silva et al. [81] fabricated alginate/low-methoxy pectin films through a two-step Ca^{2+}-crosslinking process and investigated the impact of glycerol concentration (ranging from 1 % to 15 % w/v) during the final reticulation step on the characteristics of the resulting films. Elevating the glycerol concentration in the crosslinking solution increased the film solubility in water, moisture content, volumetric swelling, and flexibility while decreasing TS. Optimal mechanical resistance and flexibility, coupled with low solubility and swelling in water, were achieved with glycerol concentrations ranging from 5 % to 10 %. Conversely, concentrations below 3 % glycerol yielded brittle films, while phase separation was observed on the film surface at glycerol concentrations exceeding 12 %.

It is noteworthy that a high content of guluronate residues, combined with a high molar mass, represents an optimal compromise for achieving desirable microstructural properties that enable glycerol molecules to become entangled within specific binding sites of the alginate polymeric network. Conversely, lower molar mass and a higher proportion of mannuronate residues result in a flexible, linear three-dimensional arrangement that interacts minimally with the introduced plasticizer. From this, the utilization of alginates with high guluronate content may be more favorable concerning mechanical behavior and the ability to adjust them with glycerol [141].

2.4.5. Effect of other additives

Additional ingredients, particularly those serving functional purposes, are commonly integrated into material formulations. These ingredients can also affect the properties of alginate materials as plasticizers. For instance, in Ca^{2+}-crosslinked alginate coatings, the inclusion of sunflower oil notably enhanced water vapor resistance

(WVR), increasing it from 15.70 s/cm to 19.2 s/cm [96]. In addition, incorporating higher levels of antimicrobial agents such as essential oils, potassium sorbate, or natamycin into alginate films was observed to augment thickness, reduce TS, and initially boost EB [40,52,66,165, 166]. However, varying effects on WVP were documented, with increases by garlic oil and natamycin noted in some studies [66,83,165] and decreases by oregano oil (OO) in others [52]. Da Silva et al. [83] observed that the addition of potassium sorbate resulted in alginate films becoming opaque, and brittle, and developing a whitish precipitate on their surface, rendering them unsuitable for practical applications. Santos et al. [48] showed that the inclusion of *Clitoria ternatea* extract in alginate films led to enhanced TS and reduced EB, accompanied by increases in thickness, WVP, water solubility, and opacity.

The incorporation of sugar vinasse, an underutilized biomass, into alginate materials was observed to decrease the transparency and increase the WVP of the films. However, its impact on the mechanical properties of the films was minimal [69].

Additional details regarding the effects of various ingredients on the material properties of alginate are outlined in Table 2.

2.4.6. Effect of processing parameters

Processing parameters, including alginate concentration and temperature, can impact the processability and properties of alginate films. Alginate concentration in solutions influences the characteristics of the final alginate-based materials, especially chain network structure and rheological properties [167]. It has been suggested that the optimal working concentration range falls between 1–2 % (w/w), as determined by viscosity, mechanical properties, and water resistance [168]. The temperature of alginate solutions impacts both the viscosity of the solution and the molar mass of alginate. Depolymerization occurred at temperatures exceeding 50 °C for prolonged periods. Raising the temperature results in a gradual decrease in viscosity, typically at a rate of approximately 2.5 % per degree Celsius [35]. The addition of NaCl or $CaCl_2$ to alginate solutions was found to increase the solution viscosity [104]. Additionally, temperature influences the crosslinking rate. As previously discussed in Section 2.4.1, lower temperatures may diminish crosslinker reactivity, slowing down crosslinking and fostering the creation of a more comprehensive and uniform 3D structure, ultimately enhancing mechanical properties [28].

Ashikin et al. [145] demonstrated that the plasticity of alginate films can be adjusted by varying drying temperature (ranging from 40 to 80 °C), alginate solution concentration (2 or 4 %), and the choice of alginate composition (guluronate-rich or mannuronate-rich). Specifically, film plasticity was promoted by using lower alginate solution concentration, mannuronate-rich alginate as the raw material, and drying temperatures of either 40 or 80 °C. A lower drying temperature mitigated heat-induced polymer chain interactions, while at a high drying temperature of 80 °C, film plasticity was significantly enhanced through air bubble formation and reduced alginate molar mass within the film.

2.4.7. Effect of relative humidity and aging time

RH and aging duration exert substantial effects on properties, as alginate can absorb or release moisture while in equilibrium with the environment. Like other polysaccharides, higher RH results in increased water content in alginate-based materials. It would be reasonable to assume that this increase weakens chain interactions due to the plasticization effect of water, consequently leading to reduced T_g, TS, and YM, while EB tends to increase. However, RH and plasticizer could have some interplay to influence the material's ability to absorb/desorb moisture during conditioning and the overall plasticization effect, consequently impacting material properties. According to Olivas & Barbosa-Cánovas [60], Ca^{2+}-crosslinked dried cast alginate films with plasticizer exhibited an enhanced capacity to adsorb water during conditions (at 58–98 % RH) compared to that without plasticizer. At 58 % RH, the incorporation of plasticizer did not increase EB. As RH

increased, TS decreased, and EB increased for all films irrespective of plasticizer inclusion. But this effect was more pronounced in plasticizer-containing films, which exhibited lower TS at all RH levels. At 78 % and 98% RH, glycerol, sorbitol, and fructose showed a significant increase in EB compared to PEG-8000 and no plasticizer.

3. Alginate-based blends

Native alginate, like many polysaccharides, exhibits drawbacks such as subpar mechanical properties and high water sensitivity, constraining its utility in environmental applications. Combining it with other, especially natural, polymers offers an easy, cost-effective means of enhancing alginate's performance.

The primary method for preparing alginate-based blends involves the direct mixing of various polymer solutions, followed by homogenization and casting [169]. The properties of these blends are heavily reliant on the attributes of each component, their compatibility, and the resultant phase morphology [170].

Below, various blends incorporating alginate and either biobased or fossil-based polymers are discussed in detail.

3.1. Alginate-polysaccharides blends

Due to their renewability, biodegradability, and excellent compatibility with alginate, assorted polysaccharides have been employed in the formulation of alginate-based blends. These endeavors aim to enhance the mechanical, barrier, and mass transfer properties of the blends. For example, mixing alginate with other polymers, such as neutral gums, pectin, and chitosan, has been discovered as a solution to the issue of drug leaching [46]. These polysaccharides can be readily processed, leveraging their solubility in certain solvents, intrinsic gelation properties, or enhanced processability achieved through chemical modification.

3.1.1. Alginate–cellulose blends

Cellulose stands as the most abundant carbohydrate polymer worldwide, sourced from various plant-based materials such as wood, cotton, hemp, algae, tunicates, and certain bacteria. This linear polysaccharide comprises D-glucose units connected by β-(1,4)-glycosidic bonds (Fig. 1**b**). Native cellulose remains insoluble in water and common organic solvents due to its chain rigidity and the numerous intra- and intermolecular hydrogen bonds [171]. However, cellulose can be dissolved in certain solvents, such as phosphoric acid-based solvents, LiCl-based solvents, ionic liquids (ILs), and NaOH-water-based solvents [172,173].

Most studies on alginate/cellulose blends have been conducted using NaOH-water-based solvents. Zhang et al. [174] prepared alginate/cellulose membranes by casting mixtures of cellulose NaOH/urea aqueous solution and alginate aqueous solution. These membranes exhibited a degree of miscibility. Micro- or macrophase separations became evident when the cellulose/alginate ratio was below or above 1:1.5, respectively. Due to cellulose's greater rigidity and thermal properties compared to pure alginate, the alginate/cellulose blend membranes demonstrated improvements in these properties relative to neat alginate [175,176]. The incorporation of Ca^{2+} further enhanced the mechanical properties of the blended membranes [177]. Similar results were reported by Phisalaphong et al. [178] who employed a NaOH/urea aqueous solution to dissolve bacterial cellulose (BC), which was then blended with an alginate aqueous solution before casting. The resulting films displayed superior TS, EB, and improved water resistance compared to films composed solely of alginate.

In contrast to pure cellulose, cellulose derivatives have garnered significantly more interest in blending with hydrophilic polymers like alginate due to their exceptional solubility and processability. Among these derivatives, CMC and hydroxyethyl cellulose (HEC) have emerged as the most frequently employed choices for crafting alginate-based

blends. Both derivatives have demonstrated excellent compatibility with alginate [155,179,180]. Kalyani et al. [181] produced membranes comprising alginate and HEC, utilizing ionic crosslinking for separating water-organic mixtures. These membranes exhibited reduced swelling capacity. Similar results were also obtained by Naidu et al. [180]. Russo et al. [182] reported that HEC was softer than alginate chains. Consequently, the inclusion of HEC led to reductions in YM and TS, along with an increase in EB (Fig. 4). Moreover, the introduction of plasticizers contributed to a further reduction in material stiffness, while the crosslinking reaction notably enhanced TS. In their investigations, these blends also demonstrated higher degradation temperatures compared to pure alginate. The incorporation of CMC into the alginate matrix similarly resulted in improved mechanical and thermal properties relative to neat alginate [183].

3.1.2. Alginate–starch blends

Native starch granules are primarily derived from cereal seeds (e.g., corn and wheat) and tuberous roots (e.g., potato and cassava) and exhibit multi-scale three-dimensional structures. Starch comprises two α-D-glucopyranose homopolymers, namely, amylose and amylopectin (Fig. 1**d**). Amylose represents a linear biopolymer composed of D-glucose units primarily linked by α-(1,4) bonds, while amylopectin is a highly branched carbohydrate with approximately 95 % α-(1,4) linkages and about 5 % β-(1,4) linkages [184]. The ratio of amylose to amylopectin varies considerably depending on the botanical source and significantly influences the structure and properties of starch [185–189].

Wet and melt processing have been used to prepare alginate/starch blends [190]. In wet processing, starch and alginate are separately dissolved in an ample quantity of water. Subsequently, both solutions are mixed, and a casting step follows. In the studies focusing on melt processing, alginate has been primarily investigated as a plasticizer, with a maximum loading level of 20 wt%. Although infrequently documented, two distinct melt processing approaches exist. The one-step process involves incorporating starch with alginate as a plasticizer directly into a thermomechanical setup, such as an extruder [191,192]. Conversely, the two-step method begins by dissolving alginate in water; subsequently, the alginate solution is mixed with starch granules, and the water is removed through drying; the resulting mixtures are then subjected to thermomechanical kneading [193].

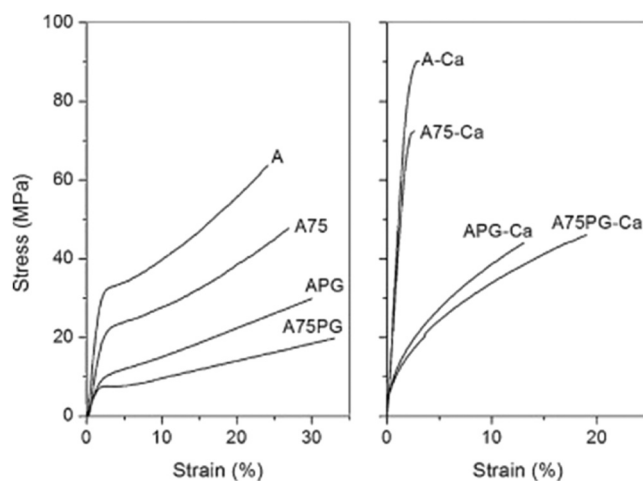It was demonstrated that alginate and starch displayed excellent

Fig. 4. Stress-strain curves of alginate (A), alginate/hydroxyethyl cellulose 3/1 (A75), alginate/polyglycerol 3/1 (APG), alginate/hydroxyethyl cellulose/polyglycerol 3/1/1 (A75PG). Samples on the left plot were not crosslinked while those on the right (with codes followed by "-Ca") were crosslinked by $CaCl_2$ by the immersion method. Reprinted from [182] with permission from Elsevier, Copyright 2010.

compatibility through the analysis of crystallinity, morphology, and the T_g of alginate/starch blends prepared via casting [107]. Nevertheless, phase separation arises during one-step melt processing [192]. Lopez et al. [191] discovered that incorporating alginate into a starch matrix could lower the T_g of the starch phase, attributed to its plasticizing effect. Using a two-step melt, Souza and Andrade [193] observed that the presence of alginate elevated the T_g of the starch-rich phase, likely due to the recrystallization of starch induced by the low alginate content. Furthermore, they noted that the inclusion of alginate substantially enhanced the TS and EB of alginate/starch films. However, Cordoba et al. [192] reported a contrasting result with a reduction in TS and YM, along with an increase in EB in the case of one-step mixing. These discrepancies in mechanical properties could be attributed to the distinct processing strategy employed. One-step melting processing appeared to lead to weak interactions between alginate and starch, resulting in diminished TS.

Lozano-Vazquez et al. [194] used native starch granules (without gelatinization) to reinforce alginate. Starch granules were uniformly distributed in the alginate matrix, exhibiting excellent interfacial compatibility with the alginate matrix. The authors proposed that starch and alginate demonstrated strong compatibility owing to their similar chemical characteristics. Their mixture exhibited superior mechanical strength compared to pure alginate. Incorporating a higher amount of starch led to denser and more convoluted structures, thereby enhancing barrier properties.

Edible films were prepared from a mixture of partially hydrolyzed sago starch and alginate. Lemongrass oil (LGO) (0.1–0.4%, v/w) and glycerol (0 and 20 wt%) were incorporated in the films to act as a natural antimicrobial agent and a plasticizer, respectively. The zone of inhibition was increased significantly ($P < 0.05$) by the addition of LGO at all levels in the presence and absence of glycerol. This indicated that the film containing LGO was effective against *Escherichia coli* O157:H7 at all levels. Without glycerol, the TS of the film decreased as the LGO content increased, but there was no significant ($P > 0.05$) difference in EB. The EB and WVP values for film with 20 % glycerol were found to be increased significantly with increasing LGO content. The added LGO did not have any interaction with the functional groups of films as shown by Fourier-transform infrared (FTIR) [40].

3.1.3. Alginate–chitosan blends

Chitosan, a cationic polysaccharide composed of D-glucosamine and *N*-acetyl-D-glucosamine linked by α-(1,4)-glycosidic bonds (Fig. 1c), is derived from the controlled *N*-deacetylation of chitin. Chitosan readily dissolves in water under mildly acidic conditions. This is because of the protonation of the amine groups of chitosan at low pH, resulting in a positively charged state and rendering chitosan a water-soluble cationic polyelectrolyte [195]. Moreover, chitosan possesses inherent antimicrobial behavior [196]. Therefore, incorporating chitosan into alginate materials can impart some antimicrobial properties to the resulting systems.

When combined, chitosan and alginate can create polyelectrolyte complexes (PECs) via interactions between the positively charged amino groups of chitosan and the negatively charged carboxylic acid groups of alginate [197,198]. In general, the formation of PECs typically results in enhanced mechanical strength, improved water resistance, and reduced swelling behavior due to the dense and robust ionic interactions [199].

Many factors, such as pH values, the ratio between both biopolymers, the chemical structures of the biopolymers, their molar masses, the order of mixing, and the solvent system, have been identified as influencing the extent and characteristics of chitosan/alginate PECs [46, 200]. The formation of the PECs can occur at pH values ranging between the pKa of chitosan and that of alginate. Agostini de Moraes et al. [201] showed that the fully protonated amino groups of chitosan readily interacted with the fully deprotonated carboxyl groups of alginate. Yan et al. [202] found that low-molar-mass chitosan displayed a greater binding potential with alginate because of its increased chain mobility,

making it more prone to conformational changes compared to high-molar-mass chitosan. As a result, low-molar-mass chitosan produced fibrous coacervates with alginate that were finely dispersed throughout the blend films. In contrast, medium- and high-molar-mass chitosans formed clumpy coacervates, resulting in heterogeneous films [202]. Gaserod et al. [203] also found that the binding extent between alginate and chitosan improved when the number-average molar mass (M_n) of chitosan was below 20,000 Da. Furthermore, the binding degree increased as the fraction of *N*-acetylation decreased and the pH was raised within the range of 4–6. Becherán-Marón et al. [204] investigated the composition of the alginate/chitosan PECs. They determined that the complex's composition was unaffected by the molar mass of chitosan and the composition of alginate. Saether et al. [205] studied the impact of the mixing order on the average size of the complex using dynamic light scattering (DLS). They observed that when alginate content was in excess, the size of the complex prepared by adding alginate solution into chitosan solution was larger than the one obtained by adding chitosan solution into alginate solution. Conversely, when chitosan was in excess, adding alginate solution into the chitosan solution led to the formation of smaller-size PECs. Kulig et al. [206] investigated the impact of the ratio between the biopolymers on the properties of alginate/chitosan complexes. They observed that the number of aggregated particles reached its maximum value when the ratio was equimolar. Additionally, the roughness of the complex film increased, and water solubility decreased with an increase in chitosan content.

It is important to note that while un-complexed alginate and chitosan in solution form a flexible matrix upon solvent evaporation, an excessive extent of polyelectrolyte complexation between chitosan and alginate may lead to a lack of connection between complexes, making the blend susceptible to tearing [207]. In general, the kinetics of ionic crosslinking are rapid and result in the formation of a heterogeneous structure, which limits their ability to create homogeneous films [208]. To address the limitation of the direct mixing method for polyelectrolytes, an alternative approach known as the semi-dissolution/acidification/sol-gel transition (SD-A-SGT) method was introduced. In this technique, chitosan powder is initially evenly dispersed in an alginate solution, resulting in a semi-dissolved slurry mixture. Upon exposure to a gaseous acidic atmosphere, chitosan dissolves and interacts with alginate, forming a uniformly structured composite hydrogel [209–211]. Some mixed organic solvents, such as acetone with water, slow down the complexation process and facilitate the formation of more uniform films [212]. Modified water-soluble chitosan, such as hydroxyethylacryl chitosan, whose reacted amine group is no longer positively charged, has also been employed as a replacement for neat chitosan [213].

Xie's group [130] uncovered nanoscale phase separation in 1:1 (w/w) chitosan-alginate blends prepared via thermomechanical processing, as observed through scanning transmission electron microscopy (STEM). This phase separation was notably affected by the choice of plasticizer. Glycerol, as a plasticizer, enhanced miscibility, evident in the blurred boundary between the chitosan and alginate phases, while an IL, 1-ethyl-3-methylimidazolium acetate ([C$_2$mim][OAc]), accentuated phase separation.

As previously shown, LbL assembly has gained significant attention as a method for preparing alginate/chitosan films, coatings, and membranes for food packaging and permeation applications [201,214–218]. A chitosan solution is cast or sprayed onto a dried alginate film or coating, or a dried alginate film is immersed in a chitosan solution, and the complex forms at the interface between both polysaccharides [205, 219].

Crosslinking is typically performed to enhance the mechanical properties and water resistance of polymer materials. Reddy et al. [216] fabricated alginate/chitosan membranes with double crosslinking using both CaCl$_2$ and maleic anhydride. The crosslinked membrane was found to exhibit greater thermal stability than the uncrosslinked membrane. Manabe et al. [220] observed similar trends when utilizing CaCl$_2$ and glutaraldehyde (GA) for crosslinking alginate/chitosan multilayer films.

3.1.4. Alginate–pullulan blends

Pullulan is a non-ionic exopolysaccharide consisting of maltotriose units (three glucose units linked by α-(1,4)-glycosidic linkage) connected by α-(1,6)-glycosidic bonds (Fig. 1**i**). Pullulan exhibits a more flexible backbone than alginate, attributed to its flexible α-(1,6)-glycosidic bonds [221] and an amorphous structure due to the non-uniform segmental mobility of chains [167,222–224]. Pullulan possesses favorable film- and fiber-forming properties [223].

Alginate and pullulan exhibit miscibility in both solution and films across the entire composition range, as shown by Prasad et al. [225]. Xiao et al. [226] found that the addition of pullulan increased the EB and decreased the TS of alginate-based films, although this trend was influenced by RH. When the water activity exceeded a certain threshold, the interaction between polymer chains weakened due to the high water content, leading to decreased EB. However, the addition of pullulan enhanced the water resistance of pure alginate because pullulan has lower water sensitivity due to the absence of carboxylic acid groups in contrast to alginate [226,227].

3.1.5. Alginate–pectin blends

Pectin is primarily commercially extracted from apple pomace and citrus peels [228–230]. Pectin is an anionic polysaccharide composed of poly(D-galacturonic acid) bonded via α-(1,4)-glycosidic linkage, which constitutes the smooth region of pectin. The more complex structures of rhamnogalacturonan I and II are found to form the hairy regions of pectin [231,232]. Pectin can be classified into high- and low-methoxy pectin based on the degree of esterification with methanol [233].

Low-methoxy pectin forms a 3D network with divalent cations in an "egg-box" structure at a pH of around 3.5, similar to alginate gelation, but the binding sites are different [234]. Alginate binds with calcium ions in a blockwise form, whereas pectin binds randomly with calcium ions. Furthermore, the structure of alginate is less affected by the presence of Ca^{2+} compared to pectin [235].

Alginate and pectin gelation depends on their chemical attributes like GulA/GalA ratio, molar mass, the length and distribution of Ca-binding blocks, the degree of methoxylation, acetylation, and amidation. External factors such as polymer and Ca^{2+} concentrations, Ca^{2+} addition methods, pH, temperature, ion strength, and co-solutes also influence gelation. These factors affect alginate and pectin differently due to their distinct structures (e.g., the linear chain structure of alginate but the branched chain structure of pectin), resulting in varying gelation mechanisms, such as egg-box structure (shifted egg-box for pectin), egg-box dimer growth mode ("zipping" for alginate and "dotting" for pectin), and crosslink morphology (rod-like for alginate and both rod- and point-like for pectin) [236].

In most cases, alginate/pectin blends exhibit intermediate values between the properties of each component. Krause Bierhalz et al. [237] studied the properties of solvent-cast alginate/pectin blend films for food packaging. They noted that alginate/pectin blends showed greater swelling and prolonged dissolution times compared to pure alginate. Nevertheless, augmenting the pectin content resulted in a decrease in the mechanical properties including TS and YM of the blends [81,143, 238]. Da Silva et al. [81] observed that alginate/pectin blend films crosslinked with Ca^{2+} exhibited increased WVP in comparison to crosslinked alginate films alone. This higher WVP can be attributed to the reduced organization of the crosslinked pectin network, primarily due to its branch structure and its random binding with Ca^{2+}. In some instances, antagonistic effects may arise, leading to inferior properties in the blends compared to each individual biopolymer. For instance, Gohil [235] discovered that blends with a high pectin content exhibited reduced mechanical properties compared to each individual biopolymer. This was attributed to the low compatibility and the disruption of the non-continuous pectin network caused by the inclusion of alginate.

Nonetheless, alginate/pectin blends have the potential to display a noteworthy improvement in certain properties. The occurrence of this synergistic effect hinges on numerous factors, including the ratio of alginate to pectin, the chemical structure of both polysaccharides, and their overall compatibility. In the research conducted by Walkenström et al. [239], an exploration into the characteristics of blends comprising various alginates and pectins revealed a substantial synergistic effect in blends using alginate rich in guluronate content and pectin with high degrees of esterification. Notably, this synergy was most pronounced in terms of mechanical properties, leading to the highest YM. This phenomenon can be attributed to the formation of denser networks of pectin characterized by high degrees of esterification. Gohil [235] compared the impact of $CaCl_2$ treatment on sodium alginate/pectin blends with varying ratios. Their findings (Fig. 5) indicated a synergy in mechanical properties for both untreated and $CaCl_2$-treated blends. Notably, untreated blends exhibited this synergy in mechanical properties up to a pectin content of 40%, while $CaCl_2$-crosslinked blends displayed the same effect with pectin concentrations below 20%. The reduced range of pectin composition in the crosslinked blends was attributed to the decreased crystallinity and increased chain mobility of pectin. Additionally, their research revealed a similar trend in the WVP of these blends. Galus and Lenart [240] similarly observed enhanced EB due to a synergistic effect within alginate/pectin blend films. However, this increase in TS was only noticeable in blends with a high pectin content and did not manifest in the WVP across all samples.

3.1.6. Alginate–carrageenan blends

Carrageenan is a linear anionic sulfated polysaccharide primarily derived from red seaweeds. Commercially, there are three main types of carrageenan, distinguished by the number and position of ionic sulfate groups: κ-, λ-, and ι-carrageenans, respectively [241,242] (Fig. 1**f,g,h**). κ-Carrageenan and ι-carrageenan adopt a random coil structure at elevated temperatures (above 80 °C), which transitions into a double-helix structure upon cooling. This double-helix arrangement further aggregates, forming a three-dimensional network at lower temperatures when suitable cations like Na^+, K^+, Ca^{2+}, and Mg^{2+} are present [241,243]. Among these carrageenans, κ-carrageenan is the most prevalent and exhibits the highest strength [146,244].

Xu et al. [245] showed miscibility between alginate and carrageenan up to a carrageenan content of 20 wt%, while phase separation occurred when the carrageenan content exceeded 30 wt%. Paula et al. [146] characterized blends comprising alginate, κ-carrageenan, and ι-carrageenan. Through FTIR spectra analysis, they did not observe significant interactions between alginate and carrageenan. All three components exhibited independent effects on the physical properties of the film-based blends. The order of TS and EB values was as follows: κ-carrageenan > alginate > ι-carrageenan, while the sequence for WVP and opacity was ι-carrageenan > alginate > κ-carrageenan. Both alginate/κ-carrageenan and alginate/ι-carrageenan blend films displayed intermediate physical properties compared to those of each individual component. It is important to highlight that κ-carrageenan is generally more hydrophilic than alginate due to its sulfate groups [245]. However, in their research, κ-carrageenan exhibited lower WVP than alginate, potentially attributed to the creation of a more condensed structure, leading to reduced water diffusivity.

Blends incorporating crosslinked alginate and carrageenan can exhibit a noteworthy synergistic effect in certain properties. Paşcalău et al. [82] compared the properties of neat alginate, neat κ-carrageenan, and their blends without crosslinking, with partial crosslinking, or with full crosslinking treatments. Their findings revealed that all the blends displayed enhanced mechanical properties and water resistance (reduced water swelling) when contrasted with those of pure alginate and κ-carrageenan. Notably, compared to non-crosslinked blends, partially and fully crosslinked ones exhibited more uniform network structures, demonstrating better mechanical properties and reduced water swelling.
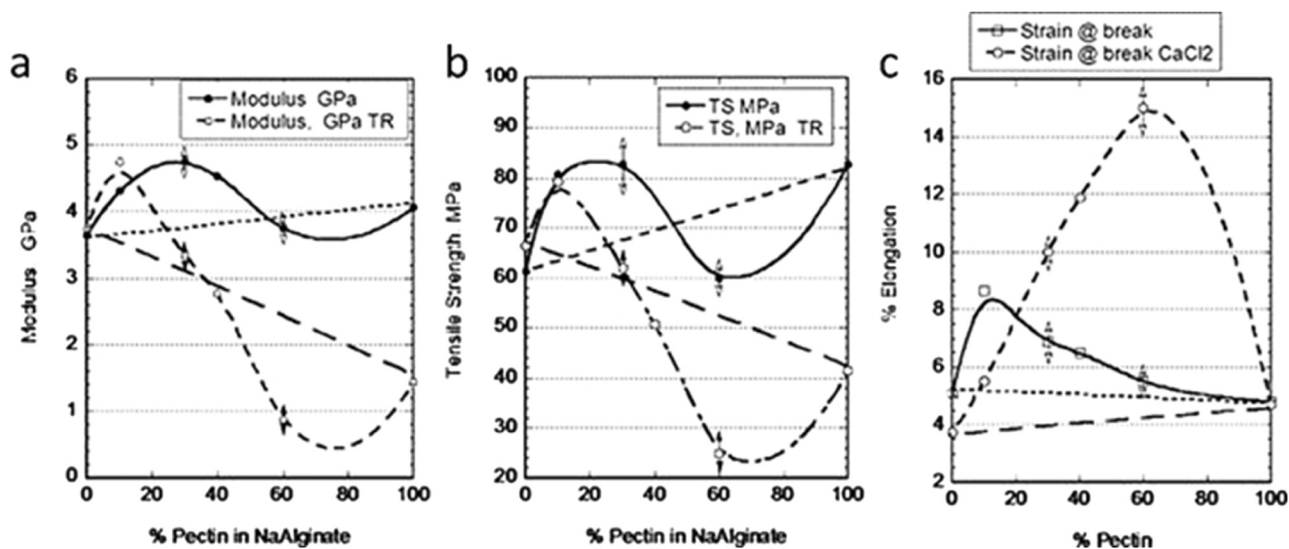
Fig. 5. Uniaxial tensile tests. Variation of Young's modulus (a), tensile strength (b), and elongation (c) of films as a function of pectin content in sodium alginate for CaCl$_2$-treated (TR) and untreated blends. Double arrows indicate standard deviation. Reprinted from [235] with permission from Wiley, Copyright 2010.

3.2. Alginate–protein blends

Due to their structures and the inherent properties of the amino acids involved, protein-based films typically outperform polysaccharide-

based films in terms of water resistance, mechanical strength, and barriers against oxygen and carbon dioxide [246,247]. Furthermore, proteins have garnered significant attention as packaging materials owing to their abundant availability, biodegradability, and commendable
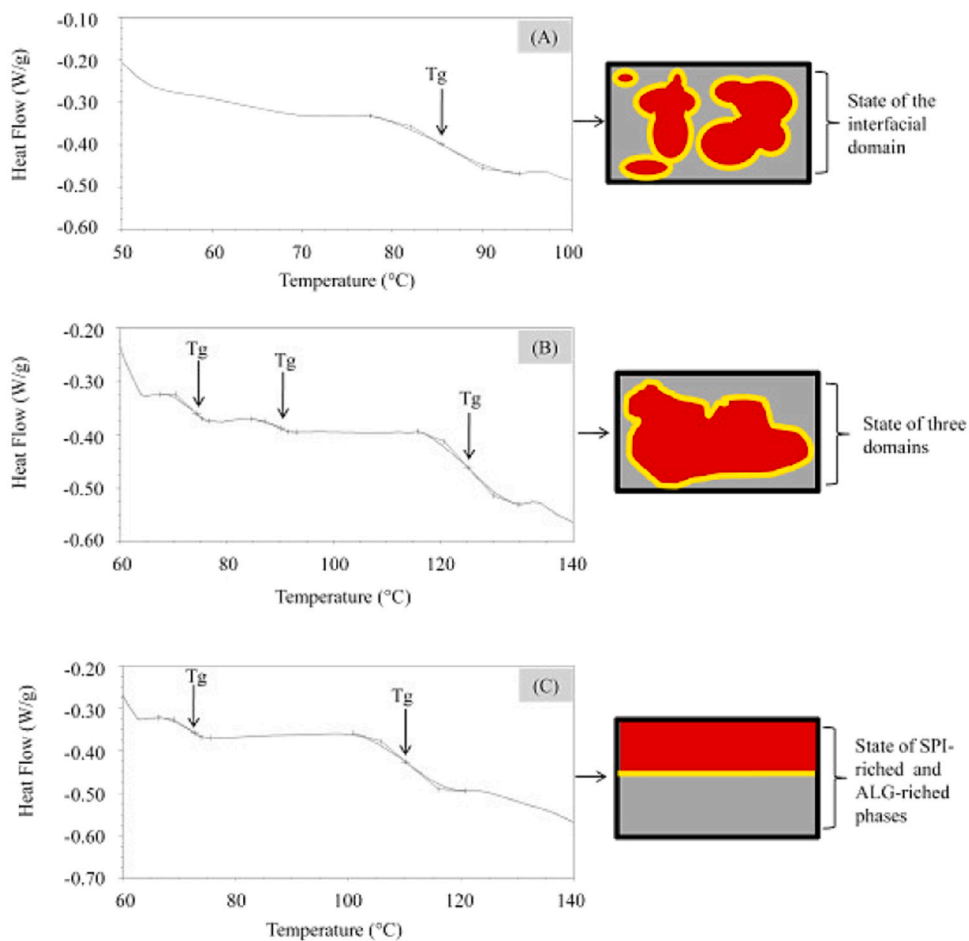

Fig. 6. DSC thermograms and schematic representation of the phase-separated soy protein isolate/alginate (10:1) blend systems: (A) original material after homogenization; (B) material with 30 min deposition after homogenization; (C) complete phase-separation, after centrifugation. Reprinted from [170] with permission from Elsevier, Copyright 2015.

barrier properties.

Given these diverse advantages, blend films comprising proteins and polysaccharides, like alginate, have garnered considerable attention for use in food packaging applications. Alginate and proteins can interact to create complexes through hydrogen bonds, electrostatic forces, and/or hydrophobic interactions [248,249]. To create films, the native structure of globular proteins like soy protein isolate (SPI) and whey protein isolate (WPI) must first undergo denaturation, typically induced by pH adjustments, electrical or mechanical forces, or heat. During the drying process, the unfolded protein chains become interconnected within the film through the formation of hydrogen, ionic, hydrophobic, and covalent bonds [247,250].

The properties of alginate/protein blends are influenced by many factors, encompassing the (macro)molecular characteristics of alginates and proteins (e.g., chemical structure, amino acid type, molar mass, conformation, and charge density), the protein/alginate ratio, phase morphology, and interactions between alginate and protein [251]. The interactions between alginate and protein have been widely studied in liquid systems [252]. Proteins and alginate exhibit thermodynamic incompatibility at pH levels exceeding the protein isoelectric point (pI) and/or under high ionic strength beyond a specific protein/alginate ratio in solution. Additionally, they can form either soluble or insoluble weak intermolecular complexes when their surfaces bear opposite charges, facilitated by hydrogen bonds, electrostatic forces, and/or hydrophobic interactions [248,249].

Nevertheless, research into the correlation between alginate–protein interactions in liquid and the resulting properties of alginate/protein materials in solid form remains limited. Pan et al. [170] studied the relationship between the extent of phase separation, processing conditions, and the formulation of SPI and alginate blends, using differential scanning calorimetry (DSC) analysis. As depicted in Fig. 6, the blend with an SPI/alginate ratio of 10:1, following homogenization and without deposition, exhibited a single T_g, indicating the absence of phase separation. In contrast, the same blend, after 30 min of homogenization and deposition, displayed some degree of phase separation, evident from the presence of three T_g values corresponding to the protein-rich phase, the interface, and the alginate-rich phase, respectively. Upon centrifugation, a complete phase separation state was observed, with the blend showing two T_g values representing the protein-rich and alginate-rich phases, respectively. It is noteworthy that the interactions were also influenced by the formulation of SPI/alginate blends, as the blend with an SPI/alginate ratio of 20:1, after 30 min of homogenization and deposition, did not exhibit phase separation, unlike the blend with an SPI/alginate ratio of 10:1.

3.2.1. Effect of protein type and alginate composition

While the impact of protein type and alginate structure on the properties of alginate/protein blends in the solid state is rarely documented, several studies [251–253] have explored how various proteins and alginates influence interactions between alginate and protein in solution.

In general, flexible proteins like caseins or gelatin tend to establish more robust connections with polysaccharides compared to globular proteins [253,254]. For instance, due to its flexible random coil conformation, the positively charged groups of gelatin have the capacity to establish a greater number of contacts with the negatively charged groups of alginate in a solution [255]. Harper et al. [256] showed that gelatin exhibited greater compatibility with alginate compared to SPI or WPI. The robust interactions between alginate and gelatin chains led to a more condensed structure in alginate/gelatin blends. However, they observed that blends consisting of gelatin/alginate, WPI/alginate, or SPI/alginate displayed reduced TS in comparison to pure alginate, primarily due to the disruption of the alginate structure within these blends caused by the incorporation of these proteins.

The M/G ratio of alginate also plays a role in its interactions with proteins. Earlier research has indicated that alginate with a higher ratio

of flexible MG blocks exhibited greater miscibility with gelatin [257].

3.2.2. Effect of pH and ionic strength

Both pH and ionic strength can influence the extent of globular protein unfolding and, consequently, impact the interactions between alginate and protein. It has been documented that proteins are unable to unfold and create films around the pI [258]. Under varying pH or ionic strength conditions, alginate and proteins may either form protein–alginate complexes or exhibit self-association behaviors. When the pH falls just below the protein's pI, the protein and alginate carry opposite charges, with the protein being positively charged and the alginate negatively charged. This charge difference can lead to the formation of either soluble or insoluble complexes through electrostatic forces [253,259]. When the pH surpasses the pI and/or when the ionic strength is significantly elevated, a thermodynamic incompatibility arises between the protein and the alginate, resulting in weak interactions and macro-phase separation [252,255,260–263]. Yang et al. [248] noted that pH can also alter the types of hydrogen bonds and impact the bonding strength between alginate and protein. Dong et al. [67] observed that films derived from alginate/gelatin blends exhibited a denser structure at pH 3.6 due to the nearly equal quantities of $-COO^-$ and $-NH_3^+$ groups. However, this equilibrium could be disrupted at high or low pH levels.

3.2.3. Effect of protein and alginate contents

The protein and alginate contents exert a significant influence on miscibility. When protein and alginate concentrations are equal, it can lead to the formation of protein-rich and alginate-rich phases characterized by high interfacial tension and poor adhesion, ultimately resulting in unfavorable film properties. Furthermore, when one biopolymer's concentration is excessively low, the synergistic effects between protein and alginate become notably limited [259]. It is important to highlight that the phase state is the result of multiple factors, including pH and ionic strength. Consequently, achieving consistent results in optimizing the protein/alginate content ratio can be challenging. Klemmer et al. [264] found that the optimum protein/alginate ratios were between 4:1–8:1 for the formation of protein-alginate complexes. Dong et al. [67] found that the alginate/gelatin blends with 50 wt% gelatin exhibited the maximum value of TS and EB. Zheng et al. [265] showed that a SPI/ alginate weight ratio of 1:1 presented the highest miscibility. Gupta and Nayak [266] explored the compatibility between alginate and keratin through X-ray diffraction (XRD) and scanning electron microscopy (SEM). Their findings indicated that the blend with an alginate/keratin ratio of 80:20 achieved the highest level of compatibility, with all blends displaying intermediate properties relative to both biopolymers. Furthermore, blends with an alginate/keratin ratio of 90:10 exhibited the highest TS and EB.

3.2.4. Effect of processing temperature

Moreover, suitable temperatures can facilitate protein unfolding by fostering the formation of disulfide bonds between protein chains, thereby enhancing protein's mechanical properties. Temperature adjustments can also enhance the interaction between protein and alginate, consequently improving the mechanical properties of the respective blends [259,267].

3.3. Blends between alginate and fossil-based polymers

Fossil-based polymers have also been extensively employed in the development of biodegradable blends with polysaccharides such as starch or cellulose [268–270]. There is a scarcity of reports on blends involving alginate and fossil-based polymers, primarily due to their different processing methods employed. Traditionally, alginate-based materials have been predominantly fabricated using wet processing techniques. Consequently, only water-soluble fossil-based polymers, such as certain polyurethanes [271] and PVA, have been employed to

obtain alginate-based blend materials.

Alginate/PVA blends are primarily obtained through solution casting. Although both alginate- and PVA-based materials can be processed via melt processing, there is currently no literature reporting the preparation of alginate/PVA blends using melt processing. Notably, PVA and alginate exhibit good miscibility at specific ratios, facilitated by the formation of robust hydrogen bonds [272].

The incorporation of PVA into alginate systems has the potential to enhance the flexibility and water resistance of alginate-based blend films [273–275]. In general, blends dominated by PVA exhibit flexible characteristics, whereas those dominated by alginate display rigid and brittle attributes. Russo et al. [182] fabricated biodegradable blend films intended for agricultural applications, comprising alginate, PVA, and glycerol, using solvent casting. They conducted tensile tests on blends with varying components and proportions, as illustrated in Fig. 7. Their findings indicated that pure alginate films were excessively brittle, while PVA films were overly flexible. Only the blend films incorporating all three components (alginate, PVA, and glycerol) demonstrated a satisfactory balance of rigidity and deformability, boasting an EB of 43% and a TS of 44 MPa. It was also noted that the addition of PVA extended the biodegradation time of the blends because PVA exhibits low water sensitivity and is less susceptible to microbial degradation compared to polysaccharides like alginate [276,277]. Nevertheless, the blends exhibited noticeable degradation after being buried in garden soil for six weeks.

Crosslinking is typically employed to enhance the mechanical, thermal properties, and water resistance of alginate/PVA blends. Hua et al. [278] engineered membranes using alginate and PVA with an interpenetrating network (IPN) structure, as illustrated in Fig. 8. Alginate and PVA established a 3D network in the presence of Ca^{2+} and through the repetition of freeze-thaw treatment. Elevating the crosslink density, achieved by methods such as increasing the number of freeze-thaw cycles, had the potential to enhance the TS and EB of the blend membranes [279].

Crosslinking can also be accomplished through chemical reactions. Various crosslinking agents, including maleic acid and GA, have been explored in the context of alginate/PVA systems [280–282]. Kulkarni et al. [282] employed GA as a crosslinking agent to hybridize alginate and PVA. The resulting films demonstrated superior TS and thermal stability when compared to alginate or PVA on their own. Sheela et al. [283] utilized UV irradiation to treat alginate/PVA films, inducing an esterification reaction between alginate and PVA. UV-treated films exhibited enhanced TS, stiffness, T_g, and thermal stability in comparison to untreated films. Prolonged treatment time further improved the

mechanical and thermal properties. Amri et al. [284] directly synthesized alginate/PVA copolymers through esterification reactions, resulting in alginate/PVA films with higher TS than pure alginate.

4. Alginate-based composites

To enhance the performance of alginate-based materials, facilitate the development of composites, and unlock new applications, various micro- and nano-fillers have been introduced into alginate matrices, leading to various alginate-based nanocomposites. These nanocomposites are discussed in this section.

4.1. Alginate–cellulose nanoparticles composites

Cellulose nanoparticles can be extracted from various cellulose sources, such as wood, plants, tunicates, algae, or bacterial systems, using mechanical processing, acid treatment, or enzymatic hydrolysis [285]. Differences in the cellulose source, as well as the type and intensity of the extraction process, yield various types of particles with distinct lengths, widths, crystallinities, and morphologies, leading to diverse properties. Typically, cellulose nanoparticles exhibit high crystallinity, a high aspect ratio, and a hydrophilic surface due to the abundant hydroxyl groups on their surface. This hydrophilic surface is highly compatible with other hydrophilic biopolymers [285–289]. Cellulose nanoparticles have been widely investigated in combination with various polysaccharides [77,151,160,162,290–295], including alginate, as discussed below.

4.1.1. Processing route

Solvent casting assisted with ultrasonication and homogenization treatment is primarily employed to produce homogeneous alginate/cellulose nanoparticles nanocomposites [296]. A unique preparation method has been devised for BC-based composites. Kanjanamosit et al. [297,298] initially introduced alginate into the culture medium of cellulose-producing bacteria (*Acetobacter xylimun*). Subsequently, they washed the alginate/cellulose pellicle to eliminate the bacteria and other media components, resulting in the formation of alginate/BC films.

4.1.2. Effect of cellulose nanoparticles addition

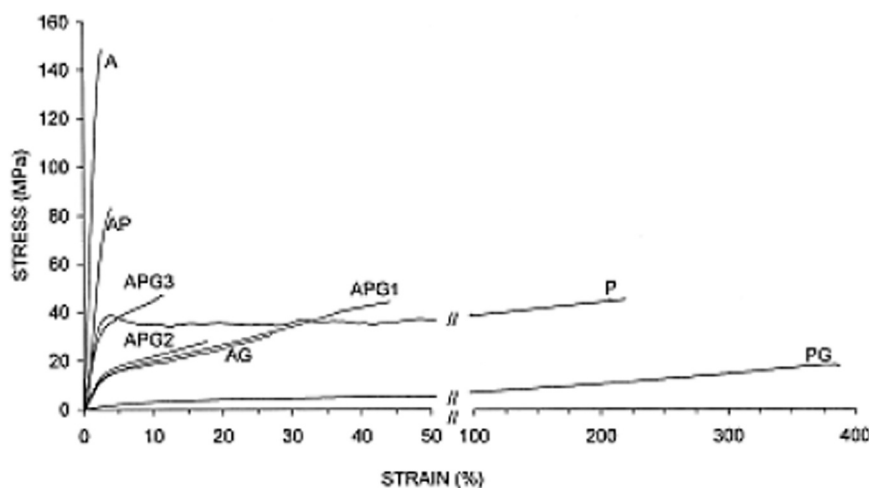The addition of cellulose nanoparticles could improve many properties including:

Fig. 7. Stress-strain curves for alginate (A), PVA (P), alginate/PVA 50:50 (AP), alginate/glycerol 50:50 (AG), PVA/glycerol 50:50 (PG), alginate/PVA/glycerol 33:33:33 (APG1), alginate/PVA/glycerol 50:17:33 (APG2), and alginate/PVA/glycerol 50:33:17 (APG3). Reprinted from [276] with permission from Wiley, Copyright 2005.
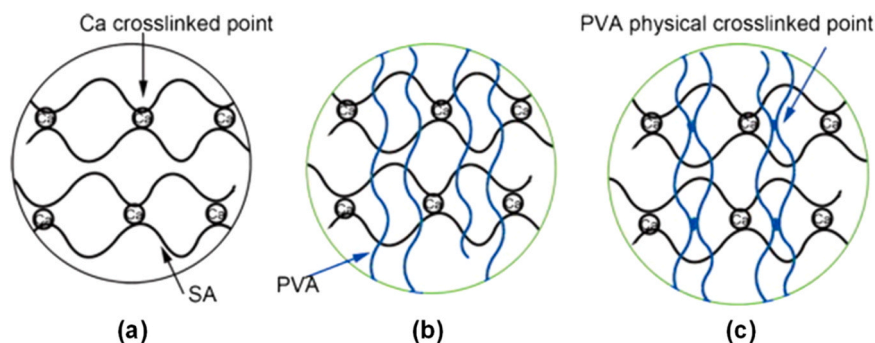
Fig. 8. Schematic illustration of polymer chain networks of different hydrogels based on polyvinyl alcohol (PVA) and sodium alginate (SA): (a) SA crosslinked by Ca^{2+}; (b) 3:1 (w/w) PVA/SA crosslinked by Ca^{2+}; (c) 3:1 (w/w) PVA/SA crosslinked by Ca^{2+} and treated by freeze-thawing. Reproduced from [278] with permission from Elsevier, Copyright 2010.

a) an increase in mechanical properties (TS and YM) in the case of a homogeneous distribution of cellulose nanoparticles in an alginate matrix, with the formation of tight cellulose nanoparticle–alginate hydrogen bonds allowing efficient matrix–filler stress transfer, high stiffness of cellulose nanoparticles, restricted alginate chain motion caused by the strong matrix–filler interactions, and/or the formation of cellulose nanoparticles networks [299–301];

b) a decrease in water sensitivity (e.g., water solubility, moisture content, and WVP) related to the increased tortuous pathways [302], strong hydrogen bonds between alginate and cellulose nanoparticles, or the high crystallinity of cellulose nanoparticles [301,303–305];

c) an increase in T_g attributed to decreased alginate chain mobility caused by the strong alginate–cellulose nanoparticles interactions;

d) an increase in thermal stability due to the strong alginate–cellulose nanoparticles interactions or the increased tortuous pathways hindering gas diffusion [306]; and

e) an increase in degradation rate linked to the homogeneous cellulose nanoparticles dispersion in the matrix or the strong alginate–cellulose nanoparticles interactions [307].

It is important to note that excessive loading of cellulose nanoparticles can lead to negative outcomes due to uneven distribution of cellulose nanoparticles and its agglomeration [77,302,307,308]. Deepa et al. [307] also observed decreased mechanical properties in composites with a low amount of cellulose nanofibrils, which resulted from the disruption of the organization of alginate chains, leading to different failure strains at the matrix-filler interfaces.

4.1.3. Effect of cellulose nanoparticle type

Cellulose nanoparticles from different plants [77,302,304,308,309] and BC [310] have been utilized as reinforcements to produce alginate-based composites. Sirviö et al. [77] discovered that nanofibrillated cellulose had a greater reinforcing effect on the alginate matrix compared to microfibrillated cellulose. They also noted that adding modified nanofibrillated cellulose with anionic dicarboxylic acid groups led to reduced mechanical properties in alginate due to poor interactions. However, when these alginate/anionic dicarboxylic acid cellulose blends underwent crosslinking treatment, they exhibited a remarkable increase in mechanical strength.

4.2. Alginate–nanoclay composites

Nanoclays have found extensive use in the development of nanocomposites based on polysaccharides, including alginate-based nanobiocomposites. This is due to their high aspect ratio, widespread availability, cost-effectiveness, versatility, eco-friendliness, and low toxicity [291,311–313]. Nanoclays can be classified into layered or fibrous structures with great differences in morphology, charge density, and cationic exchange capacity [314–317]. Montmorillonite (MMT),

hectorite, and saponite are the most common layered clays. Sepiolite and palygorskite are the most used fibrous clays [316,317]. Layered clays, the primary type of nanoclays used in nanocomposite production, can create three distinct structures within a polymer matrix: tactoids, intercalation, and exfoliation. The formation of these structures is highly influenced by factors such as clay content and type, organo-modification, and processing conditions [291,304,318]. Alboofetileh et al. [304,319] investigated the properties of alginate/MMT nanocomposites with various formulations using solution casting and observed a well-established exfoliated structure at low loading levels (1–3 wt% of MMT). Moreover, laponite, a synthetic layered clay showing high biocompatibility and blotting clotting ability has also been commonly used as a nanofiller for alginate, especially for biomedical applications [320].

4.2.1. Processing route

Solution casting is the primary method for preparing alginate/nanoclay nanocomposites because it allows for the easy dispersion of hydrophilic nanoclay particles into an alginate solution [304,321,322]. Homogenization and ultrasound treatment can be employed to enhance the distribution and the degree of nanoclay dispersion [304]. To date, there have been no reports in the literature of a melt-based process to produce these nanocomposites.

4.2.2. Effect of nanoclay addition

The inclusion of nanoclay could improve the mechanical properties, thermal stability, and barrier properties [304,314,315]. Improvements have been reported in different material properties, such as:

a) YM due to the strong alginate–silicate layers interactions, the high aspect ratio, or the high extent of exfoliation [314],

b) thermal stability as a result of a more tortuous pathways for gas diffusion, the strong nanofiller-matrix interactions, or the higher thermal nanoclay stability [323],

c) water resistance (water sorption and WVP) because of the increase of tortuous pathways, the homogeneous dispersion of silicate layers in the alginate matrix, or strong alginate–clay interactions, which reduce the number of available free hydroxyl groups leading to a decrease of the potential binding sites for water molecules [147, 324–326].

Typically, the mechanical, thermal, and barrier properties improve with an increase in clay content up to a certain threshold. However, a high loading level of clay can result in reduced TS and increased WVP due to limited dispersion and partial agglomeration of clay within the matrix [327]. In some instances, void formation can be observed because alginate is unable to bind all particles at high particle content [147,321,328].

In addition to the properties mentioned above, Chen et al. [329]

demonstrated that the incorporation of MMT enhanced the flame retardancy of alginate-based nanocomposites due to heat and mass transport barriers. Bhat and Aminabhavi [330] discovered that the addition of MMT increased the selectivity in water and organic solvent systems of alginate-based composites due to microscale effects and the formation of a larger surface area. Nanoclay can increase the EB of alginate-based materials, resulting from the formation of dangling chains and conformational effects at the silicate–matrix interface in the case of platelet exfoliation [331].

4.2.3. Factors influencing alginate/nanoclay composite properties

Various factors, such as the alginate chemical structure [325], alginate content [304,321], clay type [318,332,333], calcium content [319], film thickness [326], the incorporation of plasticizers [147], the alginate/clay ratio [304,334], and the processing conditions, have been found to impact the structure and properties of alginate/clay nanocomposites.

Alginate with a high G block content exhibited higher crystallinity when combined with layered clay compared to alginate with a high M block content. This is responsible for the lower water uptake of alginate/clay nanocomposites in an acidic medium. However, the M/G ratio of alginate showed no obvious influence on the interlayer spacing of layered clays [325].

Many types of nanoclays and organo-modifications have been used to fabricate alginate-based nanocomposites. Abou Taleb et al. [335] successfully prepared the nanocomposites based on organomodified montmorillonite (OMMT). The organomodification brings a larger interlayer spacing and higher compatibility with the matrix. They observed that the OMMT within the polysaccharide matrix exhibited an intercalated structure and demonstrated improved thermal stability and water resistance. Tezcan et al. [318] found that alginate was unable to penetrate the silicate layer of pure MMT due to the repulsive forces between the carboxylic groups of alginate and the negatively charged clay surfaces. In contrast, they observed an expansion of the interlayer spacing in OMMT samples created using different cationic surfactants within the nanocomposites, resulting in enhanced thermal decomposition temperatures. Benli et al. [322] proposed a model for nanocomposites created using sodium alginate and calcium bentonite, wherein the Ca^{2+} ions within the clay partially crosslinked with alginate molecules, forming an "egg-box" structure, and the crosslinked alginate was intercalated between the silicate layers.

Fibrous clays, such as sepiolite and palygorskite, have also been added into alginate [316,317,333]. Fibrous clays have a high specific surface area (around 320 and 150 m^2/g for sepiolite and palygorskite, respectively) and a high density of hydroxyl groups on their external surfaces, benefiting the formation of strong interactions with the alginate matrix [336]. Compared to palygorskite, sepiolite was found to show a higher reinforcement in mechanical properties [316].

In addition to increasing the flexibility of alginate as previously mentioned, plasticizers can also enhance dispersion and increase the interlayer spacing of silicate layers. Pongjanyakule et al. [147] found that glycerol and PEG-400 were inserted between silicate layers and also increased the interlayer spacing according to the plasticizer content. Compared to PEG-400, glycerol resulted in a larger interlayer spacing of nanoclay and lower crystallinity of the plasticized alginate.

4.3. Alginate–graphene composites

Graphene and graphene oxide (GO) have found extensive use in nanocomposite fabrication due to their high aspect ratio, and excellent mechanical and thermal properties. However, because of its hydrophobic nature, graphene struggles to disperse homogeneously in water, posing challenges for nanocomposite preparation. In contrast, hydrophilic GO can be uniformly dispersed in water and forms strong interactions with water-dispersible or water-soluble polymers like starch [291], chitosan [129,294,337,338], and alginate [339].

In general, introducing GO into the alginate matrix results in nanocomposites exhibiting enhanced mechanical, thermal, and electrical properties [340,341]. These enhancements can be attributed to the same phenomena observed in alginate/layered clay nanocomposites. However, the incorporation of GO nanosheets also increases the water permeability of composite materials [342]. This can be attributed to the formation of continuous and interconnected water channels, which are composed of the free volume cavities around alginate–GO interfaces, structural defects of GO nanosheets, and edge-to-edge slits between GO nanosheets [343]. Zhao et al. [103] introduced zwitterionic GOs into an alginate membrane. The composite membrane exhibited increased water permeation and enhanced capacity for water/alcohol separation, attributed to the zwitterionic GO providing more electrostatic interaction sites for water molecules.

Xie et al. [129] found that the influence of GO and reduced GO (rGO) on the thermomechanically processed 1:1 (wt/wt) chitosan/alginate matrix depends on the plasticizer used (glycerol or [C2mim][OAc]). In the glycerol-plasticized matrix, GO and rGO increased chitosan crystallinity and ductility. For the [C2mim][OAc]-plasticized matrix, GO countered the IL-induced weakening of polysaccharide interactions, improving mechanical properties and reducing surface hydrophilicity; rGO had a lesser effect in promoting chitosan–alginate interactions and even increased surface hydrophilicity. Irrespective of plasticizer type, the inclusion of rGO reduced the biopolymers' crystallinity and enhanced ionic conductivity. This study highlights how 2D carbon materials affect polysaccharides and GO's efficacy in mitigating the IL cation's negative effect on the polyelectrolyte complexation in polysaccharide materials.

Zheng et al. [344] investigated the microstructure and properties of alginate/GO films crosslinked using various multivalent metal ions (Fe^{3+}, Ca^{2+}, and Ba^{2+}). They observed that the presence of metal ions further increased the interlayer spacing of GO due to the incorporation of crosslinked alginate chains into the interlayer space. Among these ions, the addition of Fe^{3+} resulted in alginate/GO composite films with the highest interlayer spacing, TS, and YM, surpassing those with Ca^{2+} and Ba^{2+}. Additionally, Vilcinskas et al. [339] noted that the orientation of GO nanosheets was influenced by the type of metal ion used.

New processing techniques have also been reported to further enhance the mechanical properties of alginate/GO nanocomposites. Chen et al. [345] devised a novel artificial nacre-like composite paper using vacuum-assisted flocculation of an alginate/GO solution. The outcomes demonstrated that the mechanical properties of the alginate/GO composite paper far exceeded those of numerous previously reported alginate-based nanocomposites. Hu et al. [346] introduced a continuous wet-spinning method for the production of alginate/GO composite films. These films displayed exceptional mechanical properties in uniaxial tensile tests.

4.4. Alginate-based composites included with other fillers

Shi et al. [347] introduced graphitic carbon nitride (g-C$_3$N$_4$) nanoparticles to enhance the thermal stability of alginate. The resulting composite, with a filler loading of 6 wt%, exhibited a substantial increase of 118 °C in the degradation temperature as determined by TGA. An even greater enhancement in thermal stability was observed for the composite containing both g-C$_3$N$_4$ and MMT, indicating a synergistic effect [348].

Silicon dioxide (SiO_2) has garnered attention for its use in alginate-based composites due to its large surface area and numerous hydroxyl groups on its surface. Yang et al. [349] created crosslinked alginate/nano-SiO_2 films through in-situ synthesis of nano-SiO_2. They observed that the SiO_2 dispersed uniformly within the alginate matrix. The formation of Si—O—C bonds between alginate and SiO_2 was confirmed via FTIR analysis. The results demonstrated that the presence of SiO_2 improved the transparency, thermal stability, TS, and EB of the composite.

Other fillers, including metals and metal oxides, hydroxyapatite (HA), and bioglass, have also been utilized in the fabrication of alginate-based materials [107,194,350–353]. The utilization of HA and bioglass to create alginate-based composites for biomedical applications, such as tissue engineering for bone regeneration and drug release, has been extensively detailed in a prior review [16].

5. Applications of alginate-based multiphase bulk material systems

In this section, prominent applications of alginate-based bulk materials, demonstrated in the literature, are discussed.

5.1. Membranes separation and filtration

Alginate has shown promise as a suitable material for separation membranes in processes involving liquid mixtures containing water, especially aqueous–organic mixtures, owing to its hydrophilic nature and high water permselective characteristic.

Agostini de Moraes et al. [354] demonstrated that alginate membranes have the capability to adsorb herbicides, namely diquat and difenzoquat. The adsorption efficiency for diquat reached about 95%, while for difenzoquat it was approximately 62%, after 120 min at a concentration of 50 μM. Huang et al. [70] observed that among different divalent ions (Ca^{2+}, Zn^{2+}, Mn^{2+}, Co^{2+}, Fe^{2+}, and Al^{3+}), the use of Ca^{2+} to crosslinking alginate resulted in membranes with superior pervaporation performance for ethanol and isopropanol dehydration in terms of both flux and separation factor. Liu et al. [355] demonstrated that compared to alginate membranes crosslinked solely by $CaCl_2$, those crosslinked by both $AlCl_3$ and $CaCl_2$ exhibited significantly improved adsorption performance for fluoroquinolones (antibiotics), along with high stability. The maximum adsorption capacity of levofloxacin and ciprofloxacin using the Al^{3+}/Ca^{2+}-crosslinked alginate membrane was 836.31 mg·g^{-1} and 858.94 mg·g^{-1}, respectively. Li et al. [356] observed that a porous alginate membrane, fabricated through freeze-drying and Ca^{2+}-crosslinking, exhibited significant efficacy in removing methylene blue from water, achieving a removal percentage of 84.6% and a maximum adsorption capacity of 3506.4 mg/g. Gao et al. [137] demonstrated that the flux of a Ba^{2+}/Ca^{2+}-crosslinked alginate hydrogel membrane for a mixed solution of methyl blue and NaCl reached 43.5 L·m^{-2}·h^{-1}, significantly higher than that of the Ca^{2+}-crosslinked alginate membrane. Moreover, the Ba^{2+}/Ca^{2+}-crosslinked alginate membrane exhibited higher dye rejection (>99.6%) and lower salt rejection (<8.2%). Additionally, alginate membranes crosslinked with phosphoric acid demonstrated pervaporation separation capability for ethanol/water mixtures, achieving the highest separation selectivity of 2182 with a flux of 35 g·m^{-2}·h^{-1} [357].

Despite the above-mentioned studies, pure alginate membranes may experience significant swelling and reduced selectivity when applied in liquid mixtures. There has been a focus on optimizing the balance between swelling ability and selectivity for these applications [358]. In this context, incorporating hydrophilic porous particles, such as GO (including its reduced and modified forms) [103,343,359–361], carbon nanotubes (CNTs) [362], active carbon [363,364], palygorskite [365], clinoptilolite [366], Preyssler heteropolyacid nanoparticles [367], and metal-organic frameworks (MoF) [368], as well as hydrophilic polymers, such as polyvinylpyrrolidone (PVP) [369], PVA [370], PEG [370], and cellulose [177], have been examined.

As an example of alginate incorporating carbonaceous materials, Cao et al. [343] showcased Ca^{2+}-crosslinked dried cast alginate/rGO membranes that possessed brick-and-mortar morphology, increased free volume, enhanced swelling resistance, and mechanical stability. The hybrid membrane exhibited improved separation performance for ethanol/water mixtures with increased separation factor (1566) and an unusual change of permeation flux (1699 g/(m²·h)) at 1.6 wt% rGO content. For the same purpose, Zhao et al. [103] reported a permeation

flux of 2140 g·m^{-2}·h^{-1} and separation factor of 1370 demonstrated by Ca^{2+}-crosslinked dried cast alginate membranes incorporating 2.5 wt% zwitterionic GO. Similarly for ethanol dehydration, Xing et al. [365] demonstrated the optimal performance of alginate/palygorskite composite membranes. Using the hybrid membrane with 2 wt% of palygorskite nanorods, a permeate flux of 1356 g·m^{-2}·h^{-1} and a separation factor of 2030 for the dehydration of a 90/10 (w/w) ethanol/water feed were achieved.

In a study by Yu et al. [361], composite nanofiltration membranes with an ordered layered "brick-and-mortar" structure formed by GO and alginate crosslinked with Ca^{2+} were fabricated on a hydrophilic polyvinylidene fluoride (PVDF) substrate via vacuum filtration. These membranes showed outstanding water permeability and excellent separation capabilities for various dyes such as methyl blue, congo red, crystal violet, and direct red 80. Moreover, they demonstrated high stability in water, as well as in strong acid and alkali solutions [361]. In another study, the capabilities of Ca^{2+}-crosslinked alginate/GO hydrogel membranes for Cr(III) and Pb(II) separation were showcased, with the maximum adsorption capacity being 118.6 and 327.9 mg/g, respectively [359]. Ugur Nigiz [360] showcased the outstanding performance of alginate membranes filled with GO for pervaporation desalination. The highest rejection rate reached 99.95%, with a flux of 3.46 kg·m^{-2}·h^{-1} achieved at 40°C using 1 wt% of GO-filled alginate membrane.

Jie et al. [362] developed an alginate/multi-walled carbon nanotubes (MWCNT) nano-filtration membrane using the diffusion Ca^{2+}-crosslinking method with PEG-400 as the pore-forming agent. The composite membrane exhibited a high TS (1.83 MPa), satisfactory antifouling properties, and the ability to reject 98.62% of Congo red even after saturated adsorption.

Also, a Ca^{2+}-crosslinked alginate/activated carbon membrane demonstrated the ability to absorb methylene blue, with an absorption capacity of 666 mg/g [363]; with sodium benzyl dodecyl sulfate (SBDS)-treated MMT included in the formulation, a higher absorption capacity of 1429 mg/g was achieved [364].

Moreover, alginate/Preyssler heteropolyacid nanoparticle membranes [367] and Ca^{2+}-crosslinked alginate/MoF [368] have been investigated for isopropanol/water separation. Crosslinked alginate/clinoptilolite composite membranes were devised for dimethylformamide/water separation [366]. Ca^{2+}-crosslinked alginate/PVP membranes were developed for acetone/water separation [369].

GA-crosslinked alginate/PVA/PEG were investigated for acetic acid/water and isopropanol/water separation [370].

Li et al. [254] assessed the effectiveness of alginate/gelatin PEC membranes for propylene dehydration. Dehumidification tests revealed that as the gelation content increased, both water vapor permeance and water/propylene selectivity rose simultaneously due to improved water sorption capability and reduced free volume cavity size. At a gelatin content of 60 wt%, the PEC membrane displayed the highest permeance, along with an infinite permselectivity, surpassing the performance of pure alginate and gelatin membranes. The phenomenon could be attributed to the interplay between sorption and diffusion processes.

A membrane composed of electrospun alginate nanofibers coated with cellulose nanowhiskers (CNWs) demonstrated enhanced filtration efficiency. It effectively retained Cu and TiO_2 nanoparticles, separated oil from an oil/water emulsion, and removed chromium ions from an aqueous solution [114].

The separation capabilities of alginate-based membranes can be extended to fuel cell applications. Alginate can enhance fuel cell performance by improving proton conductivity and membrane durability and reducing fuel crossover and electro-osmotic drag [371]. In this domain, Smitha et al. [372] investigated the viability of using polyion complex (PIC) membranes made by blending chitosan (84% deacetylated) and sodium alginate for direct methanol fuel cells (DMFCs). The membranes showed low methanol permeability, excellent mechanical properties, and relatively high proton conductivity along with

cost-effectiveness, suitable for DMFC applications. Pasini Cabello et al. [149] explored electrolyte membranes based on alginate incorporating carrageenan for DMFCs. The films underwent chemical crosslinking by GA followed by sulfonation to increase ionic groups. Increasing carrageenan content from 0% to 20% led to an increase in methanol permeability and enhanced proton conductivity, despite decreased mechanical stability. Shaari and Kamarudin [154] observed that a GA-crosslinked alginate-based composite membrane incorporating alumina exhibited superior results in water uptake, ion exchange capacity, methanol permeability, proton conductivity, and oxidative stability compared to the pure alginate membrane, demonstrating the potential for DMFC applications.

Similarly, the application of alginate membranes with ionic selectivity (high proton conductivity and low quinone permeability) to the construction of quinone-based aqueous redox flow batteries was also demonstrated [373].

Wang et al. [374] presented an alginate/$Ti_3C_2T_x$ membrane showcasing remarkable selectivity for H^+ and Fe^{2+} ions. This study introduced a method of stabilizing the $Ti_3C_2T_x$ laminar structure using alginate hydrogel pillars while adjusting ion selectivity. The ultrathin Mn–alginate pillared membrane, with matched *d*-spacing, demonstrated 100% rejection of Na_2SO_4 coupled with high water permeability.

This application of membranes for protein purification demands stringent requirements for disinfection resistance, low protein adsorption, antifouling properties, and the preservation of protein structure. Gao et al. [375] showcased alginate/TiO_2 hydrogel membranes, prepared via ionic crosslinking, exhibiting outstanding rejection of bovine serum albumin (BSA) and antifouling characteristics. These membranes demonstrated resilience to chlorine, allowing for disinfection or cleaning with sodium hypochlorite. Furthermore, the alginate/TiO_2 membrane loaded with polyhydroxybutyrate (PHB) nanofibers maintained high flux and BSA rejection, while exhibiting excellent antifouling properties. Remarkably, the membrane's separation process preserved the secondary structure of BSA.

The filtration and separation studies utilizing alginate-based membranes discussed above highlight the significant potential of such membranes in various fields, including chemical/environmental engineering, water treatment, biomedical, and energy applications.

5.2. Entrapment and controlled release of bioactive and antimicrobial agents

Ca^{2+}-crosslinking produces compact alginate networks with decreased water resistance and permeability, making them ideal for entrapping small molecules like antimicrobial agents, bioactive compounds, antioxidants, therapeutic agents, and nutrients. These networks facilitate gradual and controlled release of the entrapped molecules, making Ca^{2+}-crosslinked alginate materials beneficial for various uses including nutritional supplementation, food preservation, therapeutics, and biomedical applications.

5.2.1. For drug delivery

In clinical applications, where the controlled release of povidone-iodine (PVPI) as an antiseptic agent into open wounds is crucial to prevent the absorption of toxic iodine doses by the wound, Liakos et al. [148] investigated the controlled release performance of alginate films containing PVPI. Their results revealed highly effective antibacterial and antifungal activity against *E. coli* bacteria and *Candida albicans* fungi within 48 h. Similar results were obtained in other studies [85]. Crossingham et al. [58] emphasized that compared to Ca^{2+}-crosslinked alginate films prepared by the diffusion method, those prepared by the immersion method exhibited significantly lower permeability to theophylline, used as a model drug. This difference was particularly notable when the films were rehydrated in water and 0.1 M HCl, showing 90 times and 5 times differences, respectively. Dong et al. [67] examined the release kinetics of Ca^{2+}-crosslinked alginate/gelatin films

for ciprofloxacin as a model drug. Their findings indicated that the drug release rate decreased with increasing gelatin content in the film and higher drug loading. Moreover, drug release at pH 7.4 surpassed that at lower pH, a trend accelerated by higher ionic strength. Furthermore, the drug release percentage within 24 h decreased from 100% to 52% with increasing crosslinking duration till 30 min.

Shi et al. [376] introduced a hydrophobically modified biomineralized alginate membrane for smart drug release. This membrane was prepared by first casting a dried membrane containing alginate, poly(*N*-isopropylacrylamide) (PNIPAAm) (a thermally responsive component), sodium palmitate (a hydrophobic component), indomethacin (a model drug), and Na_2HPO_4. Subsequently, this membrane was immersed into a coagulation fluid containing chitosan and $CaCl_2$. The resulting membranes featured a biomineralized component ($CaHPO_4$) formed through the interaction between Ca^{2+} and HPO_4^{2-}, along with polyelectrolyte complexation between chitosan and alginate. Their findings demonstrated that the controlled deposition of inorganic minerals and hydrophobic components within porous organic polymeric matrices effectively restricted the permeation of the encapsulated drug.

Alginate materials have the potential to offer protection for the bioactive ingredients they contain. For example, De'Nobili et al. [142] illustrated that Ca^{2+}-crosslinked alginate films, primarily composed of GG blocks, effectively preserved AA against hydrolysis under both vacuum and air conditions. This preservation capacity remained robust even amidst decreasing RH and glycerol levels.

Other than films, alginate materials in the form of fibers have also been studied for the controlled release of drugs. For instance, Wang et al. [107] fabricated alginate/starch fibers incorporating salicylic acid as a model drug via wet spinning. Their findings indicated that increasing the starch content in the formulation, enhancing drug loading, and adjusting the pH from 1 to 7.4 led to a higher release of salicylic acid. Lai et al. [108] demonstrated that in Janus-morphological alginate fibers, adjusting the concentration of CMC sodium in each fiber compartment allowed for adjustment of physical properties and thus precise customization of the release profiles of model drugs such as malachite green and minocycline hydrochloride (Fig. 3A).

5.2.2. For antimicrobial active food packaging

Antimicrobial active food packaging development typically involves encapsulating plant-derived essential oils [40,52,72,95,165] and some vegetable oils [57,72,165], known for their antimicrobial properties, within packaging films to enable controlled release. For instance, Maizura et al. [40] produced edible films using a blend of partially hydrolyzed sago starch and alginate, incorporating LGO (0.1–0.4%, v/w) and glycerol (0–20%, w/w). Regardless of glycerol and LGO levels, all films containing LGO were effective against *E. coli* O157:H7. Benavides et al. [52] demonstrated that alginate films prepared via internal gelation with $CaCO_3$/GDL and containing OO exhibited superior efficacy against Gram-positive bacteria such as *Staphylococcus aureus* and *Listeria monocytogenes* compared to Gram-negative bacteria like *E. coli* and *Salmonella enteritidis*. A minimum OO concentration of 1.0% was required for antibacterial effectiveness. Furthermore, alginate films incorporating garlic oil displayed antibacterial activity against *S. aureus* and *Bacillus cereus* [165]. Similarly, Abdel Aziz and Salama [72] demonstrated the efficacy of garlic oil-containing alginate films against *S. aureus* (Gram-positive bacteria), *E. coli* (Gram-negative bacteria), and *Syncephalastrum racemosum* (Fungi). Rojas-Graü et al. [166] assessed the antimicrobial properties of alginate/apple puree edible films containing essential oils/oil compounds against the foodborne pathogen *E. coli* O157:H7. Their findings ranked the antimicrobial activities as follows: carvacrol > OO > citral > LGO > cinnamaldehyde > cinnamon oil. In a related study, the same research group [95] examined the impact of incorporating LGO, OO, and vanillin into Ca^{2+}-crosslinked alginate/apple puree edible coatings on the shelf-life of fresh-cut 'Fuji' apples. Their results demonstrated that all antimicrobial coatings significantly suppressed the growth of psychrophilic aerobes, yeasts, and molds on

the coated apples. LGO (1.0 and 1.5% w/w) and OO-containing coatings (0.5% w/w) displayed the strongest antimicrobial activity against *Listeria innocua* inoculated into apple pieces before coating.

Zactiti and Kieckbusch [78] demonstrated the potential of alginate films prepared through a two-step Ca^{2+}-crosslinking process for the controlled release of potassium sorbate. They observed a decrease in the potassium sorbate permeability constant as the concentration of the crosslinking solution increased. However, da Silva et al. [83] found that Ca^{2+}-crosslinked alginate films containing practical levels of potassium sorbate (17 wt% based on alginate) did not exhibit inhibition zones against *Debaromyces hansenii*, *Penicillium commune*, and *Penicillium roqueforti* in the agar diffusion test without altering the film's physical properties. Instead, they observed Ca^{2+}-crosslinked alginate films containing natamycin (as low as 0.5 wt% based on alginate) and alginate/chitosan films containing natamycin (as low as 1 wt% based on the total polysaccharides) effectively inhibited the growth of these microorganisms. Bierhalz et al. [61] investigated the release pattern and antimicrobial properties of natamycin-containing alginate films prepared by a two-step crosslinking process using Ca^{2+} and Ba^{2+} ions. Their findings revealed that the selection of ions during the initial stage affected both the rate at which natamycin was released and its effectiveness in inhibiting microbial growth against four common cheese contaminants: *Aspergillus niger*, *P. roqueforti*, *Penicillium chrysogenum*, and *Penicillium crustosum*. Particularly, films crosslinked with Ba^{2+} followed by Ca^{2+} displayed the lowest natamycin diffusion coefficient and resulted in the smallest inhibition zones against the tested microorganisms.

A Ca^{2+}-crosslinked alginate coating infused with nisin and EDTA, employed as antimicrobial packaging, significantly diminished the chemical spoilage of refrigerated (4 ± 1 °C) northern snakehead (*Channa argus*) fillets [93]. Additionally, alginate films incorporating *Cryptococcus laurentii* as a yeast antagonist were found to effectively inhibit mold growth and preserve the quality of strawberries [65].

5.2.3. For broader antimicrobial purposes

Enhancing controlled release performance can involve loading antimicrobial agents into nanoparticles, such as nanoclays, before incorporating them into biopolymers. For instance, studies have shown that alginate films incorporating salicylic acid-loaded halloysite exhibited controlled release behavior for this antimicrobial agent [161]. Additionally, it was shown that microencapsulation of carvacrol by β-cyclodextrin before loading it into alginate films enhances controlled release performance for carvacrol, as well as its antifungal and antioxidant efficacy [76].

Eghbalifam et al. [272] showcased that PVA/alginate films embedded with in-situ synthesized silver nanoparticles, synthesized in situ through the reduction of silver nitrate under gamma irradiation, demonstrated controlled release of the nanoparticles. Moreover, they found that the release rate in lukewarm water escalated with higher gamma doses. These composite films displayed potent antibacterial properties against *S. aureus* (Gram-positive bacteria) and *E. coli* (Gram-negative bacteria) even at minimal concentrations of silver nanoparticles. Similarly, antimicrobial results have been reported by others [377,378]. Abdel Aziz et al. [378] additionally demonstrated the antimicrobial activity of ZnO-nanoparticles-containing alginate-based films against *S. racemosum* (Fungi).

Besides their applications in food, alginate materials encapsulating antimicrobial agents are also crucial in biomedical contexts. For example, Cleetus et al. [118] formulated alginate hydrogel with incorporated ZnO nanoparticles, which exhibited a photoinduced bactericidal effect against *Staphylococcus epidermidis*. Additionally, these materials were effective for humidity retention and did not adversely affect the cell viability of STO fibroblasts.

Antibacterial fibers hold significant promise for various applications such as medical dressings, surgical sutures, and masks, sparking considerable interest in developing durable, high-performance

antibacterial textiles. In this context, Zheng et al. [106] presented a novel approach to creating antibacterial fibers through the wet spinning process. These fibers, a blend of zeolitic imidazolate framework-8 (ZIF-8) and alginate, displayed remarkable antibacterial efficacy, surpassing many other fiber types enhanced with inorganic nanoparticles. Additionally, they exhibited high TS and durability. The exceptional antibacterial performance of the fibers was attributed to the production of reactive oxygen species from ZIF-8 and the swelling of alginate.

5.3. Biomedical applications

Alginate offers numerous appealing characteristics, including biocompatibility, low toxicity, and cost-effectiveness, along with its gelation properties, making it well-suited for biomedical applications. Its hydrogels, with their network structure, can deliver bioactive agents such as small chemical drugs and proteins. Additionally, alginate exhibits structural similarities to the extracellular matrices (ECMs) of living tissues, thereby facilitating various applications in wound healing and cell transplantation [28]. While **Section 5.2** already covers much about the entrapment and delivery of bioactive agents, the following discussion will focus specifically on wound healing and tissue engineering using alginate-based bulk materials.

5.3.1. Wound healing

Alginate-based materials have long been utilized for wound healing purposes, primarily due to their moisture-retention capacity and their ability to enhance cell proliferation and adhesion [379]. The beneficial effects of alginate on wound healing may involve biological mechanisms linked to the expression of transforming growth factor-β1, fibronectin, vascular endothelial growth factor (VEGF), and collagen-I [380]. However, Doyle et al. [381] proposed that calcium alginate may enhance certain cellular aspects of normal wound healing while influencing others differently. Specifically, their findings indicated that calcium alginate promoted the proliferation of fibroblasts while reducing the proliferation of microvascular endothelial cells (HMEC) and keratinocytes. Besides, calcium alginate was found to decrease fibroblast motility without affecting keratinocyte motility. Moreover, the impact of calcium alginate on cell proliferation and migration could be mediated by the release of Ca^{2+} ions.

Recent studies on alginate for wound healing have increasingly concentrated on incorporating bioactive ingredients, including drugs [84,382,383], enzymes [384,385], and cells [87]. These investigations aim to deliver these components in a controlled manner to augment the wound-healing process.

For instance, Bagher et al. [85] illustrated that sodium alginate/PVPI films could mitigate the inflammatory response in human foreskin fibroblasts following lipopolysaccharide (LPS) stimulation, as well as in rodents with induced wounds. Rats treated with the film exhibited significantly accelerated wound closure compared to untreated counterparts, achieving complete closure within 12 days. Zheng et al. [84] developed a hydrogel dressing based on Zn^{2+}-crosslinked alginate incorporating cannabidiol for wound management. In vitro experiments demonstrated the hydrogel's favorable biocompatibility, antibacterial properties, and angiogenesis promotion. Additionally, it effectively scavenged 2,2-diphenyl-1-picrylhydrazyl (DPPH) free radicals, reducing inflammatory responses. In vivo studies revealed the hydrogel's efficacy in controlling inflammation, promoting collagen deposition and granulation tissue formation, and fostering blood vessel formation, thereby expediting the wound healing process. Recognizing hydrogen sulfide (H_2S) as a crucial gasotransmitter pivotal for angiogenesis and wound healing, Zhao et al. [88] engineered a sodium alginate-based sponge incorporating JK-1, a pH-dependent H_2S donor. This sponge gradually released H_2S under acidic conditions by absorbing wound exudate. In vitro cell studies demonstrated the sponge's cytocompatibility and its ability to enhance fibroblast proliferation and migration. In vivo experiments further showcased the sponge's efficacy in improving wound

healing through enhanced granulation tissue formation, re-epithelialization, collagen deposition, and angiogenesis. Zhang et al. [385] engineered a pH-sensitive porous cryogel containing citric acid (CA) and vancomycin. The vancomycin-loaded gel demonstrated potent antibacterial activity in mildly acidic conditions, with the combination of CA and vancomycin exhibiting a synergistic therapeutic effect against acute infections. Additionally, the drug-loaded hydrogel displayed favorable coagulation properties, strong platelet adhesion, high fluid absorption capacity, and maintained a suitable fluid balance on the wound bed. Wang et al. [383] devised a hydrogel comprising alginate and platelet-rich plasma (PRP), in which the addition of thrombin/FeCl$_3$ solution induced plasma coagulation and fibrin network formation, while alginate was crosslinked by Fe^{3+}. This dual-network structure encapsulated amoxicillin. The hydrogel, cultured in a phosphate buffer solution, exhibited detectable levels of epidermal growth factor (EGF) and VEGF, indicating potential for cell proliferation and vascular regeneration. In vivo trials conducted with rats underscored the hydrogel's effectiveness in promoting wound closure.

Theocharidis et al. [87] showcased the effectiveness of a calcium-crosslinked alginate dressing in locally delivering primary macrophages and their secretome to diabetic wounds. This dressing, characterized by a porous structure, facilitated uniform cell loading, extended cell survival, and sustained cell release for up to 16 days post-injury. Application of all macrophage subtypes and their secretome using this dressing significantly expedited wound healing in wounds of db/db mice compared to the control group.

Combinations of alginate with other biopolymers, such as chitosan [71,85,86,386], gelatin [91], and hyaluronan [387] have been formulated to enhance wound healing effects. This is due to the rapid degradation and high-swelling profiles of alginate hydrogels, as well as their lack of cell-binding sites [388].

For example, Caetano et al. [71] discovered that a Ca^{2+}-crosslinked dried cast chitosan/alginate membrane effectively regulated the inflammatory phase and promoted fibroplasia and collagenesis, thus accelerating wound healing in experimental cutaneous wounds in rats, compared to the control group treated solely with saline. In two separate studies, alginate/chitosan porous gels, prepared by crosslinking with CaCl$_2$ and GA followed by lyophilization, were used to load hesperidin [85] and α-tocopherol (vitamin E) [86], respectively. The time-kill assay demonstrated the antibacterial properties of the hesperidin-loaded gel, while the MTT assay revealed its positive effect on cell proliferation, with no observed toxicity on cells [85]. In vivo results indicated that both hesperidin- and vitamin E-loaded gels exhibited superior wound closure compared to gauze-treated wounds (the control group) [85,86]. Wang et al. [386] reported on flexible cast chitosan/alginate PEC films crosslinked with CaCl$_2$ for wound healing purposes. In vitro studies demonstrated that these films and their aqueous extracts were non-toxic to mouse and human fibroblast cells. Compared to conventional gauze dressing, the films accelerated the healing of incision wounds in a rat model and induced active inflammation in the dermis. In contrast to the aforementioned studies involving mixtures of alginate and chitosan, Zhao et al. [389] developed a wound dressing in the form of chitosan-coated calcium alginate. In vitro and in vivo experiments revealed that the composite film exhibited good moisturizing and antibacterial properties with no cytotoxicity. It was capable of inhibiting inflammation by reducing IL-6 and promoting angiogenesis by increasing VEGF, resulting in enhanced wound healing compared to alginate film.

Afjoul et al. [91] revealed that for alginate/gelatin porous scaffolds, a higher gelatin content led to increased biodegradation and enhanced cell proliferation and viability. In vivo results demonstrated the biocompatibility of the blend scaffold and its positive contribution to the wound-healing process in rats. Catanzano et al. [387] observed that an alginate/hyaluronan hydrogel significantly enhanced gap closure in a scratch assay at both early (1 day) and late (5 days) stages compared to an alginate-only hydrogel. In vivo wound healing experiments conducted on a rat model of excised wounds indicated that after 5 days, the alginate/hyaluronan hydrogel significantly promoted wound closure compared to the alginate-only hydrogel.

Alginate has also been combined with synthetic polymers for wound-healing applications. For instance, Golafshan et al. [320] developed Ca^{2+}-crosslinked alginate/PVA/laponite hydrogels for wound healing, demonstrating excellent biocompatibility against MG63 and fibroblast cells. Remarkably, fibroblast proliferation significantly increased on the composite alginate/PVA hydrogel with 0.5 wt% laponite compared to those without. Additionally, the hydrogels promoted hemostasis, which could be beneficial in wound dressing. Abbasi et al. [382] devised a novel thermosensitive hydrogel membrane comprising PVA, sodium alginate, pluronic F-127 (a thermo-responsive polymer), and poloxamer 407 (surfactant) for accelerated wound healing. This membrane, incorporating amikacin, exhibited sustained release of this antimicrobial agent, resulting in a significantly larger zone of inhibition against *S. aureus* and *P. aeruginosa*. Excisional animal models demonstrated significantly higher wound healing efficacy of the hydrogel membranes, characterized by faster wound closure, increased re-epithelialization, and enhanced granulation tissue formation compared to positive and negative control groups.

5.3.2. Bone tissue engineering

Early studies exploring the use of alginate as guided bone regeneration (GBR) membranes, formed on bone defect surfaces through crosslinking sodium alginate with CaCl$_2$ solution, indicated their potential to restore bone defects to nearly original conditions, albeit with delayed healing and absence of inflammatory response surrounding the alginate membrane [390,391]. However, for bulk materials such as hydrogels or porous cryogels applied to treatment sites, the material characteristics play a crucial role in bone regeneration efficacy, with porosity being particularly significant. Research showed that smaller pore structures in alginate hydrogels significantly increased the generation rate of glycosaminoglycans (GAGs) and collagens in human chondrocytes [54]. Additionally, to create a porous structure, Valente et al. [392] fabricated alginate microparticles and microfibers through CaCl$_2$ crosslinking in an alginate solution, subsequently aggregating these into bulk scaffolds within a mold. The biocompatibility of these scaffolds was confirmed through observed cell adhesion and proliferation after 5 days of seeding, alongside non-radioactive assays.

In bone tissue engineering, the intrinsic characteristics of alginate, such as M/G content and molar mass, can significantly influence the efficacy of resulting materials. Wang et al. [393] proposed the potential of Ca^{2+}-crosslinked alginate as a substrate for rat marrow cell proliferation and as 3D degradable scaffolds. They found that a high-purity, high-G-type alginate hydrogel retained 27% of its initial strength after 12 days in culture, with comparable levels of proliferation observed on this material and tissue culture plastic. Dodero et al. [112] found that for electrospun alginate nanofibers, longer chains and a higher concentration of guluronic moieties resulted in a pronounced polyelectrolyte nature, which led to higher cell adhesion efficiency (compared to seeded cells, 15–36%) as tested using osteoblast cell lines. In comparison, lower adhesion of 5–25% was observed with a neutral nature of alginate nanofibers. However, fibroblasts and keratinocytes, primary cell lines in skin, did not exhibit preferences for the three tested mats with varying polyelectrolyte nature in terms of cell seeding percentages, ranging 30–40% and 10–20%, respectively.

As the reasons already discussed in the realm of wound healing, it is common practice to formulate alginate with other biopolymer matrices (e.g., chitosan [89,90], gelatin [120,122,123,125], collagen [124], agarose [124], decellularized extracellular matrix (dECM) [121], and nanofillers (e.g., cellulose nanofibrils/nanocrystals [119,125], mesoporous silica nanoparticles (MSNs) [90], carbon nanofibers [123], HA [128,394], and polydopamine nanoparticles (PDANPs) [119]) to enhance structural properties and performance in bone tissue engineering.

For instance, Li et al. [89] observed that bone-forming osteoblasts readily adhered to a porous chitosan/alginate scaffold, exhibited robust proliferation, and deposited a calcified matrix. Additionally, in vivo findings demonstrated that the chitosan/alginate scaffolds facilitated rapid vascularization and deposition of connective tissue and calcified matrix throughout the scaffold structure. Similarly, Yousefiasl et al. [90] noted that alginate/chitosan porous composite scaffolds incorporating MSNs exhibited favorable swelling behavior, enhanced mechanical strength, and significantly improved biomineralization properties without compromising porosity or inducing cytotoxic effects, compared to alginate/chitosan scaffolds without MSNs. Notably, the alginate/chitosan scaffold with 30 wt% MSNs exhibited substantially increased cell viability compared to the control, suggesting its potential for bone tissue regeneration.

Recent studies have delved into the 3D printability of alginate gelatin hydrogels and the structure and properties of the resulting printed constructs, with 3D bioprinting emerging as a promising approach in tissue engineering. For example, Chawla et al. [122] observed that when printing cell-laden 3D scaffolds for bone tissue engineering, both 20 and 25% infill within alginate/gelatin scaffolds resulted in increased viability and proliferation of osteoblasts (MG63) cells. Kreller et al. [120] explored 3D printing as a method to mimic the inherent hierarchical structure of natural articular cartilage using alginate di-aldehyde (ADA)/gelatin hydrogel as an ink. Pre-treating gelatin with heat (80 °C for 3 h) altered the mechanical and rheological properties of ADA/gelatin, which enabled the printing of intricate hierarchical structures, achieving scaffold heights exceeding 1 cm, with elastic moduli approximately ~5 kPa. Dutta et al. [125] developed 3D-printed hybrid hydrogel scaffolds composed of alginate, gelatin, and cellulose nanocrystals (CNCs), which exhibited superior mechanical strength compared to pure polymer scaffolds. The 1% CNC/alginate/gelatin scaffold showed enhanced cell proliferation and improved mineralization compared to the control, indicating its potential for osteogenesis. Furthermore, rapid bone regeneration was observed in the rat CCD-1 defects model following transplantation of the composite scaffolds after three weeks, suggesting their enhanced capacity for bone regeneration.

Yang et al. [124] employed bioinks containing alginate mixed with either collagen type I (SA/COL) or agarose (SA/AG), along with chondrocytes, for 3D printing of in vitro cartilage tissue. Among the three alginate-based scaffolds, SA/COL notably enhanced cell adhesion, accelerated proliferation, and upregulated the expression of cartilage-specific genes such as Acan, Col2al, and Sox9 compared to the other groups, demonstrating potential in cartilage tissue engineering. Lee et al. [121] found that adding methacrylated (Ma)-dECM to an alginate-based bioink improved printability for creating 3D cell-laden structures and enhanced cell viability in the printed constructs. Additionally, the biologically enriched microenvironment of the alginate-based cell-laden structures, formed using this approach, notably affected the osteogenic differentiation of human adipose-derived stem cells within the bioink.

Im et al. [119] formulated alginate/tempo-oxidized cellulose nanofibrils (TOCNF) hydrogel bioinks without or with PDANPs, all suitable for 3D printing. In vitro investigations of 3D-printed osteoblast-laden scaffolds demonstrated that the bioink incorporating 0.5% PDANPs significantly promoted osteogenesis.

HA, the primary mineral component of bones, is naturally compatible with human tissues and exhibits bioactive properties, capable of stimulating bone growth. Furthermore, incorporating polymers with HA may enhance mechanical properties [395]. Benedini et al. [394] synthesized Ca^{2+}-crosslinked alginate/nano-HA composite materials with ciprofloxacin loaded in either alginate or nano-HA, demonstrating their efficacy in promoting bone regeneration. These composites exhibited controlled release of ciprofloxacin, and antibacterial activity against the three main strains causing osteomyelitis, with the nano-HA-loaded alginate material showing superior performance compared to the

alginate-loaded composite. Both composites demonstrated bioactivity, evidenced by the growth of biogenic HA, high biocompatibility, and cell viability with *Calvaria* rat osteoblasts, indicating their potential for use as bone filler antibiotic devices. In another work [128], alginate/HA aerogel scaffolds for bone regeneration were prepared through 3D-printing of hydrogels followed by supercritical CO_2 drying. The resulting aerogel scaffolds exhibited high porosity, biocompatibility, and printing fidelity, enabling the attachment and proliferation of mesenchymal stem cells (MSCs). These aerogels also enhanced fibroblast migration toward the damaged area, suggesting their efficacy in bone regeneration.

5.3.3. Other tissues engineering

Incorporating electrically conductive materials into alginate hydrogels can render the resulting scaffolds electroactive, presenting potential for various biomedical applications related to tissue regeneration. These applications include skeletal muscle tissue engineering, as well as cardiac and neuronal tissue engineering [123,396]. In this context, Serafin et al. [123] developed printable alginate/gelatin/carbon nanofibers hydrogel inks, which were utilized to print electroconductive 3D scaffolds. In vitro studies demonstrated enhanced cellular proliferation with the used of these scaffolds compared to controls. Similarly, Aparicio-Collado et al. [396] developed Ca^{2+}-crosslinked alginate/polycaprolactone (PCL)/rGO composites to address drawbacks associated with alginate, such as low cell adhesion and weak structural stability. Moreover, the inclusion of reduced rGO nanosheets increased the electrical conductivity of the hydrogels, achieving values within the range of muscle tissue. In vitro cultures with C2C12 murine myoblasts demonstrated that the conductive nanohybrid hydrogels were not cytotoxic and significantly enhanced myoblast adhesion and myogenic differentiation.

More studies have investigated the potential of 3D printing for tissue engineering applications. Kakarla et al. [127] demonstrated that incorporating boron nitride nanotubes (BNNTs) into a gelatin/alginate formulation for 3D printing resulted in reduced strand thicknesses, increased printing accuracy (>90%), and lower swelling rates, along with higher compressive stress load of the printed constructs. These improvements are beneficial for fabricating tissue engineering constructs. However, it was observed that increased doping of BNNTs led to a slight rise in toxicity, as indicated by cell viability tests using human embryonic kidney cells (HEK293T).

Kang et al. [126] presented the 3D printing of a gelatin/alginate composite hydrogel to fabricate a multilayer composite scaffold containing essential cell types precisely distributed in three dimensions, mimicking the hair follicle microenvironment in the body. In vivo experiments demonstrated that the multilayer scaffold exhibited favorable cytocompatibility and enhanced proliferation ability of dermal papilla cells (DPCs) by 1.2-fold. Notably, hair follicles were regenerated in the appropriate orientation in vivo.

5.4. Food packaging and drinking straws

Alginate holds great promise in the field of food packaging, particularly in the realm of edible films and coatings. Its popularity in these applications stems from its exceptional ability to form films, its effective barrier properties against O_2 and CO_2, and its suitability for consumption. For example, Puscaselu et al. [49] illustrated that cast agar/alginate films supplemented with *Stevia rebaudiana* possessed excellent attributes for powder-type packaging. These films exhibited high solubility, uniformity, well-defined edges, moderate roughness, as well as good strength and elasticity, and could manage high-humidity environments or products containing photodegradable compounds.

When creating edible films and coatings, ensuring a pleasant taste is crucial. While Ca^{2+} crosslinking is commonly employed for producing alginate materials, the use of $CaCl_2$ can introduce a bitter flavor. To mitigate this issue, calcium gluconolactate, a widely used food additive, can serve as a crosslinking agent for alginate [80].

As discussed to some extent in **Section 5.1** , alginate-based films have demonstrated the ability to encapsulate various antimicrobial compounds, including essential oils [40,52,95,166], some vegetable oils like castor oil [57] and garlic oil [72,165], cinnamic acid [156], salicylic acid [161], carvacrol [76], beetroot extract [162], grapefruit seed extract [377], potassium sorbate [61,78,83], nisin/EDTA [93], natamycin [61,66,83,397], *C. laurentii* (yeast antagonist) [65], silver nanoparticles [272], sulfur nanoparticles [73], sulfur quantum dots (SQDs) [398], and CuO nanoparticles [151]. Additionally, they can also incorporate antioxidants/anti-browning agents such as AA [142,399], CA [399], cysteine [95,96,399], glutathione [96]), cinnamic acid [156], pterostilbene [157], carvacrol [76], SQDs [398], CuO nanoparticles [151], and graphitic carbon nitride (g-C_3N_4) nanoparticles [75]. Moreover, studies have shown that plant extracts like *Aloe vera* [72,378] and peanut red skin extract [74], cottonseed protein hydrolysates [152], and garlic (*Allium sativum*) cloves-derived carbon dots [153] exhibited both antibacterial and antioxidant effects. The antibacterial and antioxidant properties make alginate films useful for active food packaging, effectively extending shelf-life.

Rojas-Graü et al. [95] compared the effects of alginate/apple puree edible coatings incorporating different essential oils, including LGO, OO, and vanillin. While all these coatings demonstrated strong capabilities in inhibiting the growth of psychrophilic aerobes, yeasts, and molds, the LGO-containing coating resulted in significant texture softening, possibly due to its lower pH. Conversely, the vanillin-containing coating (at 0.3% w/w) emerged as the most effective in terms of sensory quality after 2 weeks of storage [95]. This research underscores the importance of considering various factors that could influence food quality beyond just antimicrobial activity.

It is noteworthy that antimicrobial functionality can also be achieved by incorporating cationic polysaccharides, such as chitosan and cationic starch [400].

Edible alginate-based films and coatings offer an opportunity to fortify food with nutritional additives, thereby enhancing people's health. For instance, Tapia et al. [399] showcased the effectiveness of alginate coatings containing antioxidants like *N*-acetylcysteine, AA, and CA. These coatings were applied to high-moisture fresh-cut fruits such as apple and papaya, facilitating the growth of *Bifidobacterium lactis* Bb-12. This research paves the way for the development of probiotic fresh-cut fruit products, presenting new avenues for innovation in the food industry.

Incorporating certain functional ingredients into alginate films can enable them to serve as visual indicators of food freshness, which falls into the concept of intelligent food packaging. For instance, Santos et al. [48] demonstrated that alginate films loaded with 40% *Clitoria ternatea* extract not only displayed antibacterial properties against *E. coli* but also exhibited significant colorimetric capabilities. These films could change color at different pH levels (pink-green), in the presence of ammonia gas (blue-green), and during the sterilization process (blue-yellow). When the film loaded with 40% *Clitoria ternatea* extract was utilized to monitor the freshness of milk and meat products (e.g., shrimp and pork), its blue color transitioned to purple and green, respectively. Similarly, Guo et al. [162] reported alginate films formulated with beetroot extract exhibited not only antioxidant properties but also underwent discoloration when the TVB-N level surpassed 8.0 mg and 100 g during pork storage at 4 and 20 °C, respectively.

It is crucial to acknowledge that for applications like food packaging, mechanical and barrier properties are essential considerations. However, the incorporation of functional ingredients, as discussed in **Section 2.4.5** , can potentially impact these properties. Fortunately, ingredients such as sunflower oil [96], OO [52], and garlic oil [72], have been demonstrated to reduce WVP, which is advantageous for food packaging applications. The effects of different additives on alginate film properties are listed in Table 2.

Mohammed et al. [155] have shown a biodegradable formulation based on alginate, with starch and CMC as minor components, along with glycerol and PEG plasticizers. The composite films exhibited extremely low OP, good WVP and a high YM. Additionally, alginate composite films demonstrated superior OP, higher WVP, and comparable material properties compared to commercial HDPE, PET, and PLA. Therefore, this film shows great promise as an alternative for food packaging in low-moisture environments.

Producing biopolymer multilayer films, like gelatin/alginate, through a layer-by-layer process has proven to be an effective approach for overcoming the limitations of individual biopolymers and addressing the challenge of forming insoluble PECs especially related to food packaging [158].

In addition to films and coatings, alginate exhibits potential for use in other food-related products. Liu et al. [111] showcased alginate-based drinking straws prepared using the DDA method, which displayed outstanding hygroscopicity, even when exposed to hot water up to 85°C, as well as impressive mechanical properties. These properties surpass those of PLA and paper straws.

5.5. Agricultural applications

Alginate has also garnered significant interest in the field of agriculture, particularly as biodegradable mulching films. For example, Zhao et al. [47] developed a mulch film using kelp as the raw material. They discovered that the film, crosslinked simultaneously with 2% $CaCl_2$ and 1% HCl, exhibited superior physical properties compared to using either $CaCl_2$ or HCl alone, or using them sequentially for crosslinking. Liling et al. [62] demonstrated that crosslinked dried cast alginate films exhibited high TS, low WVP, and high light transmittance, making them well-suited for use as agricultural mulching films. The film crosslinked with 2% $CaCl_2$ for 2 min showed optimal performance.

Santos et al. [69] demonstrated the potential application of alginate and alginate/konjac glucomannan films enriched with sugarcane vinasse as nutrients for agricultural purposes such as mulching, seedling bags, and seed tapes. Su et al. [301] showcased that PVA films incorporated with alginate and quaternary lignin exhibited significantly improved mechanical properties, water-holding capacity, UV resistance, and degradability, while reducing the cost of PVA films, making them suitable for agricultural applications. Specifically, with optimal addition amounts, the WVP of the film was 109.2 g·m^{-2}·day^{-1}, the water evaporation rate after covering the soil with the mulch film was 500 g·m^{-2}·day^{-1}, and degradability reached 55% after 50 days. Additionally, the visible light transmission rate was only 20%.

Han et al. [53] introduced alginate/cellulose fiber films featuring a dual network, comprising the alginate network crosslinked by $CaCO_3$/GDL and a network formed by mechanical entanglement and hydrogen bonds between cellulose fibers. The films exhibited optimal mechanical strength, WVP, and biodegradability. Notably, the TS of the film reinforced with cellulose fibers at a content of 7.7% was approximately ten times that without the fibers, reaching 85 MPa. Wang et al. [68] devised a high-barrier composite mulch film comprising a base cast film made from alginate, alkali lignin, and tunicate CNCs crosslinked with $CaCl_2$ using the immersion method. Additionally, low-energy kaolin was sprayed onto the film surface with water-borne polyurethane (WPU) as a binder. This composite film demonstrated satisfactory mechanical properties, high UV resistance, excellent hydrophobicity, water vapor barrier, and water retention capability. It also displayed notable flame retardancy, self-extinguishing within 7 s of open flame ignition.

Sprayable alginate coatings for agricultural applications are intriguing due to their ease of application and potential to address the weak mechanical properties of freestanding films [141,401]. Immirzi et al. [163] formulated alginate-based coatings incorporating HEC and poly-3-glycerol to enhance the elasticity of alginate to coating development. Biodegradation tests showed that the alginate multiphase systems experienced a 65% biodegradation rate after 6 months in soil. However, the mechanical performance of these coatings needed to be

further improved, especially to enable their use in open fields, where they may be exposed to hail and rain. Merino et al. [150] showcased the positive impact of an alginate-based spray formulation containing 1% seaweed, *Undaria pinnatifida*, on the growth and physiological parameters of tomato plants. The sprayed mulch film led to enhanced tomato plant aptitude, reduced soil temperature, and increased microorganisms such as fungi and actinomycetes in the substrate, consequently reducing the need for fertilizers and mitigating water pollution.

One potential issue associated with alginate mulch films or coatings used in agriculture could be their rapid degradation, which may affect their service life [68]. However, it is worth noting that they do not require recycling, meaning they will not contribute to environmental pollution.

5.6. Other applications

Cathell and Schauer [56] demonstrated that the combination of alginate's metal ion binding ability with its structural coloration enables the use of alginate thin films for color-based optical sensing of metal ions in aqueous solutions. Further investigation revealed that changes in film thickness predominantly influence the shift in reflected film color for certain ions like Cr(III) and Cr(VI). Conversely, for ions such as Pb(II), alterations in film refractive index significantly impact the reflectance properties of the films.

Moreover, alginate-based materials have found applications in flame retardancy [402–404] and sensing [56,405]. These applications typically rely on alginate's excellent film-forming characteristics and enhanced functionality achieved through hybridization with inorganic materials.

6. Conclusions

Alginate-based multiphase systems hold significant promise as solid materials for various applications, such as food packaging, mulching films, and separation membranes. This potential is due to their excellent qualities, including renewability, biodegradability, and hydrophilicity. However, like other polysaccharides, alginate faces limitations such as weak mechanical properties, poor water and thermal resistances, and limited processability, which have hindered its industrial applications. Consequently, numerous efforts have been recently developed to address these limitations. However, conventional ionic crosslinking stands out as the most common and convenient method to enhance the water resistance and mechanical properties of alginate-based materials. However, the development of multiphase systems must be considered as one of the easiest and most cost-effective approaches to improving alginate's performance. Over past decades, different multiphase systems, including plasticized alginate, blends, and different types of (nano) composites, have been examined.

Alginate-based blends often incorporate various polysaccharides and proteins due to their widespread availability, biodegradability, and excellent compatibility with alginate. Additionally, certain hydrophilic fossil-based polymers, such as PVA, have been utilized in alginate-based blends. These blends effectively amalgamate the properties of the constituent polymers, resulting in a synergistic effect that can lead to significantly enhanced properties, such as enhanced water resistance and mechanical properties.

In alginate-based composites, cellulose nanoparticles and nanoclays are frequently employed as common fillers due to their widespread availability, cost-effectiveness, and high aspect ratio. The incorporation of nanofillers typically results in enhancements across various properties of alginate-based composites, including mechanical, thermal, barrier, and water resistance properties. These improvements are primarily attributed to the uniform dispersion of fillers within the alginate matrix and the formation of strong bonds at the alginate-filler interface.

With tailored structures and enticing characteristics, alginate-based multiphasic bulk materials show promise across diverse applications such as membrane separation, controlled release, wound healing, tissue engineering, food packaging, agriculture, and beyond.

7. Future perspectives

While significant progress has been achieved, there remains ample opportunities for future research aimed at developing new engineering techniques for crafting alginate materials and creating novel alginate multiphase systems with enhanced performance to bolster competitiveness.

Currently, our understanding of the intricate relationship between structure, processing, and properties in various alginate-based material systems must be completed. Thorough exploration is needed to comprehensively elucidate the influence of various factors and parameters. Additionally, a deeper understanding of how alginate and other polymers impact each other's chain crosslinking and aggregation is essential. Also, while there is a widespread assumption of high affinity between alginate and other hydrophilic polymers, a meticulous study of their true compatibility is vital, as it fundamentally determines material properties.

Furthermore, we must explore how to harness the structural features and properties inherent to biopolymers for the creation of robust and functional materials. In this context, particular emphasis should be placed on researching and developing cost-effective processes for creating bulk polyelectrolyte-complexed chitosan/alginate materials. These materials hold the potential to achieve significantly enhanced properties, such as mechanical strength, stability, and barrier properties.

Considering alginate's distinctive ability for ionic crosslinking using multivalent cations, it is worth focusing on developing novel, cost-effective processes for precisely controlled ionic crosslinking, allowing the production of alginate materials with well-defined structures and desired properties. Also, exploring the utilization of this ionic crosslinking characteristic to create alginate-based hybridized materials with IPN structures or cage structures holds promise for property enhancement.

Most previous research has relied on solvent casting, which poses significant limitations, particularly for blends involving non-water-soluble polymers. Solution casting is known to suffer from inefficiency and challenges in scaling up for industrial applications. Moreover, this method consumes and releases substantial amounts of solvents. Conversely, thermomechanical processing, which aligns better with industrial practices and involves minimal solvent usage, holds greater promise, although there have been limited reports in this area [129–132]. This paves the way for the wider adoption of alginate-based materials.

Last but not the least, there is a pressing need for further research in this field to harness alginate as a valuable blue carbon resource cost-effectively, while also achieving defined chemical structures and molar mass, aligning with application requirements and reducing environmental impact.

CRediT authorship contribution statement

Chengcheng Gao: Conceptualization, Visualization, Writing – original draft. **Luc Avérous:** Conceptualization, Funding acquisition, Project administration, Supervision, Validation, Writing – original draft, Writing – review & editing. **Fengwei Xie:** Conceptualization, Visualization, Validation, Writing – review & editing.

Declaration of Competing Interest

The authors declare the following financial interests/personal relationships which may be considered as potential competing interests: Luc Averous reports financial support and article publishing charges were provided by the University of Strasbourg. If there are other authors, they declare that they have no known competing financial

interests or personal relationships that could have appeared to influence the work reported in this paper.

Data Availability

No data was used for the research described in the article.

Acknowledgement

References

[1] P. Gacesa, Carbohydr. Polym. 8 (1988) 161–182.
[2] J.-W. Rhim, LWT - Food Sci. Technol. 37 (2004) 323–330.
[3] Z. Wysokinska, Fibres Text. East. Eur. 18 (2010) 7–13.
[4] H. Bojorges, A. López-Rubio, A. Martínez-Abad, M.J. Fabra, Trends Food Sci. Technol. 140 (2023) 104142.
[5] S.N. Pawar, K.J. Edgar, Biomaterials 33 (2012) 3279–3305.
[6] J.-S. Yang, Y.-J. Xie, W. He, Carbohydr. Polym. 84 (2011) 33–39.
[7] N.T.T. Uyen, Z.A.A. Hamid, N.X.T. Tram, N. Ahmad, Int. J. Biol. Macromol. 153 (2020) 1035–1046.
[8] S.H. Ching, N. Bansal, B. Bhandari, Crit. Rev. Food Sci. Nutr. 57 (2017) 1133–1152.
[9] L. Agüero, D. Zaldivar-Silva, L. Peña, M.L. Dias, Carbohydr. Polym. 168 (2017) 32–43.
[10] J.P. Paques, E. van der Linden, C.J.M. van Rijn, L.M.C. Sagis, Adv. Colloid Interface Sci. 209 (2014) 163–171.
[11] X. Zhang, X. Wang, W. Fan, Y. Liu, Q. Wang, L. Weng, Polymers 14 (2022).
[12] K. Zdiri, A. Cayla, A. Elamri, A. Erard, F. Salaun, J. Funct. Biomater. 13 (2022).
[13] P. Rastogi, B. Kandasubramanian, Biofabrication 11 (2019) 042001.
[14] K. Varaprasad, T. Jayaramudu, V. Kanikireddy, C. Toro, E.R. Sadiku, Carbohydr. Polym. 236 (2020) 116025.
[15] A.C. Hernández-González, L. Téllez-Jurado, L.M. Rodríguez-Lorenzo, Carbohydr. Polym. 229 (2020) 115514.
[16] J. Venkatesan, I. Bhatnagar, P. Manivasagan, K.-H. Kang, S.-K. Kim, Int. J. Biol. Macromol. 72 (2015) 269–281.
[17] M. Farokhi, F. Jonidi Shariatzadeh, A. Solouk, H. Mirzadeh, Int. J. Polym. Mater. Polym. Biomater. 69 (2020) 230–247.
[18] X. Gao, C. Guo, J. Hao, Z. Zhao, H. Long, M. Li, Int. J. Biol. Macromol. 164 (2020) 4423–4434.
[19] B. Wang, Y. Wan, Y. Zheng, X. Lee, T. Liu, Z. Yu, J. Huang, Y.S. Ok, J. Chen, B. Gao, Crit. Rev. Environ. Sci. Technol. 49 (2019) 318–356.
[20] A. Kumar, A. Sood, S.S. Han, Carbohydr. Polym. 277 (2022) 118881.
[21] K.I. Draget, 29 - Alginates, in: G.O. Phillips, P.A. Williams (Eds.), Handbook of Hydrocolloids, (Second Edn), Woodhead Publishing, 2009, pp. 807–828.
[22] E.A. Titlyanov, T.V. Titlyanova, X. Li, H. Huang, Chapter 2 - Marine plants of coral reefs, in: E.A. Titlyanov, T.V. Titlyanova, X. Li, H. Huang (Eds.), Coral Reef Marine Plants of Hainan Island, Academic Press, 2017, pp. 5–39.
[23] A.R. Nesic, S.I. Seslija, 19 - The influence of nanofillers on physical–chemical properties of polysaccharide-based film intended for food packaging, in: A. M. Grumezescu (Ed.), Food Packaging, Academic Press, 2017, pp. 637–697.
[24] I.D. Hay, Z.U. Rehman, M.F. Moradali, Y. Wang, B.H.A. Rehm, Microb. Biotechnol. 6 (2013) 637–650.
[25] S. Saji, A. Hebden, P. Goswami, C. Du, Sustainability 14 (2022) 5181.
[26] M. Beata Łabowska, I. Michalak, J. Detyna, Open Chem. 17 (2019) 738–762.
[27] C. Peteiro, Alginate production from marine macroalgae, with emphasis on kelp farming, in: B.H.A. Rehm, M.F. Moradali (Eds.), Alginates and Their Biomedical Applications, Springer Singapore, Singapore, 2018, pp. 27–66.
[28] K.Y. Lee, D.J. Mooney, Prog. Polym. Sci. 37 (2012) 106–126.
[29] G.T. Grant, E.R. Morris, D.A. Rees, P.J.C. Smith, D. Thom, FEBS Lett. 32 (1973) 195–198.
[30] V. Jost, K. Kobsik, M. Schmid, K. Noller, Carbohydr. Polym. 110 (2014) 309–319.
[31] H. Ertesvåg, S. Valla, Polym. Degrad. Stab. 59 (1998) 85–91.
[32] M. Rinaudo, Polym. Int. 57 (2008) 397–430.
[33] J. McLachlan, Phycologia 31 (1992) 365–367.
[34] A. Haug, B. Larsen, O. Smidsrød, Carbohydr. Res. 32 (1974) 217–225.
[35] Y. Qin, Polym. Int. 57 (2008) 171–180.
[36] M.Y. Khotimchenko, V.V. Kovalev, R.Y. Khotimchenko, Method of obtaining quick-dissolving sodium alginate, Russia Patent (2015) RU2540946C1.
[37] S.N. Pawar, K.J. Edgar, Biomacromolecules 12 (2011) 4095–4103.
[38] D. Bi, X. Yang, L. Yao, Z. Hu, H. Li, X. Xu, J. Lu, Mar. Drugs 20 (2022) 564.
[39] P. Umaraw, A.K. Verma, Crit. Rev. Food Sci. Nutr. 57 (2017) 1270–1279.
[40] A. Maizura, A. Fazilah, M.H. Norziah, A.A. Karim, J. Food Sci. 72 (2007) C324–C330.
[41] Ý.A. Mørch, I. Donati, B.L. Strand, G. Skjåk-Bræk, Biomacromolecules 7 (2006) 1471–1480.
[42] P. Sikorski, F. Mo, G. Skjåk-Bræk, B.T. Stokke, Biomacromolecules 8 (2007) 2098–2103.
[43] H. Kawarada, A. Hirai, H. Odani, T. Lida, A. Nakajima, Polym. Bull. 24 (1990) 551–557.
[44] Y. Fang, S. Al-Assaf, G.O. Phillips, K. Nishinari, T. Funami, P.A. Williams, L. Li, J. Phys. Chem. B 111 (2007) 2456–2462.
[45] L. Li, Y. Fang, R. Vreeker, I. Appelqvist, E. Mendes, Biomacromolecules 8 (2007) 464–468.
[46] M. George, T.E. Abraham, J. Control. Release 114 (2006) 1–14.
[47] Y. Zhao, J. Qiu, J. Xu, X. Gao, X. Fu, Algal Res. 26 (2017) 74–83.
[48] L.G. Santos, G.F. Alves-Silva, V.G. Martins, Int. J. Biol. Macromol. 220 (2022) 866–877.
[49] R. Puscaselu, G. Gutt, S. Amariei, Coatings 9 (2019) 360.
[50] G. Skjåk-Bræk, H. Grasdalen, O. Smidsrød, Carbohydr. Polym. 10 (1989) 31–54.
[51] K. Ingar Draget, K. Østgaard, O. Smidsrød, Carbohydr. Polym. 14 (1990) 159–178.
[52] S. Benavides, R. Villalobos-Carvajal, J.E. Reyes, J. Food Eng. 110 (2012) 232–239.
[53] Q. Han, Y. Wang, H. Wang, T. Zhou, Z. Song, D. Yu, X. Liu, W. Liu, S. Ge, ACS Sustainable, Chem. Eng. 12 (2024) 2120–2129.
[54] J. Jang, Y.-J. Seol, H.J. Kim, J. Kundu, S.W. Kim, D.-W. Cho, J. Mech. Behav. Biomed. Mater. 37 (2014) 69–77.
[55] E. Papajová, M. Bujdoš, D. Chorvát, M. Stach, I. Lacík, Carbohydr. Polym. 90 (2012) 472–482.
[56] M.D. Cathell, C.L. Schauer, Biomacromolecules 8 (2007) 33–41.
[57] M.S. Abdel Aziz, H.E. Salama, M.W. Sabaa, LWT - Food Sci. Technol. 96 (2018) 455–460.
[58] Y.J. Crossingham, P.G. Kerr, R.A. Kennedy, Int. J. Pharm. 473 (2014) 259–269.
[59] H.Y. Lee, L.W. Chan, A.V. Dolzhenko, P.W.S. Heng, J. Microencapsul. 23 (2006) 912–927.
[60] G.I. Olivas, G.V. Barbosa-Cánovas, LWT - Food Sci. Technol. 41 (2008) 359–366.
[61] A.C.K. Bierhalz, M.A. da Silva, M.E.M. Braga, H.J.C. Sousa, T.G. Kieckbusch, LWT - Food Sci. Technol. 57 (2014) 494–501.
[62] G. Liling, Z. Di, X. Jiachao, G. Xin, F. Xiaoting, Z. Qing, Carbohydr. Polym. 136 (2016) 259–265.
[63] M.J. Costa, A.M. Marques, L.M. Pastrana, J.A. Teixeira, S.M. Sillankorva, M. A. Cerqueira, Food Hydrocoll. 81 (2018) 442–448.
[64] J.L. Drury, R.G. Dennis, D.J. Mooney, Biomaterials 25 (2004) 3187–3199.
[65] Y. Fan, Y. Xu, D. Wang, L. Zhang, J. Sun, L. Sun, B. Zhang, Postharvest Biol. Technol. 53 (2009) 84–90.
[66] A.C.K. Bierhalz, M.A. da Silva, T.G. Kieckbusch, J. Food Eng. 110 (2012) 18–25.
[67] Z. Dong, Q. Wang, Y. Du, J. Membr. Sci. 280 (2006) 37–44.
[68] S. Wang, X. Li, Q. Li, Z. Sun, M. Qin, Int. J. Biol. Macromol. 262 (2024) 129588.
[69] N.L. Santos, Gd.O. Ragazzo, B.C. Cerri, M.R. Soares, T.G. Kieckbusch, M.A. da Silva, Int. J. Biol. Macromol. 165 (2020) 1717–1726.
[70] R.Y.M. Huang, R. Pal, G.Y. Moon, J. Membr. Sci. 160 (1999) 101–113.
[71] G.F. Caetano, M.A.C. Frade, T.A.M. Andrade, M.N. Leite, C.Z. Bueno, Â. M. Moraes, J.T. Ribeiro-Paes, J. Biomed. Mater. Res. Part B: Appl. Biomater. 103 (2015) 1013–1022.
[72] M.S. Abdel Aziz, H.E. Salama, Int. J. Biol. Macromol. 190 (2021) 837–844.
[73] R. Priyadarshi, H.-J. Kim, J.-W. Rhim, Food Hydrocoll. 110 (2021) 106155.
[74] Q. Dai, X. Huang, R. Jia, Y. Fang, Z. Qin, J. Food Eng. 330 (2022) 111106.
[75] S.N. Mousavi, H. Daneshvar, M.S. Seyed Dorraji, Z. Ghasempour, V. Panahi-Azar, A. Ehsani, Mater. Chem. Phys. 267 (2021) 124583.
[76] M. Cheng, J. Wang, R. Zhang, R. Kong, W. Lu, X. Wang, Int. J. Biol. Macromol. 141 (2019) 259–267.
[77] J.A. Sirviö, A. Kolehmainen, H. Liimatainen, J. Niinimäki, O.E.O. Hormi, Food Chem. 151 (2014) 343–351.
[78] E.M. Zactiti, T.G. Kieckbusch, J. Food Eng. 77 (2006) 462–467.
[79] J. Li, J. He, Y. Huang, D. Li, X. Chen, Carbohydr. Polym. 123 (2015) 208–216.
[80] M. Soazo, G. Báez, A. Barboza, P.A. Busti, A. Rubiolo, R. Verdini, N.J. Delorenzi, Food Hydrocoll. 51 (2015) 193–199.
[81] M.A. da Silva, A.C.K. Bierhalz, T.G. Kieckbusch, Carbohydr. Polym. 77 (2009) 736–742.
[82] V. Paşcalău, V. Popescu, G.L. Popescu, M.C. Dudescu, G. Borodi, A. Dinescu, I. Perhaiţa, M. Paul, J. Alloy. Compd. 536 (2012) S418–S423.
[83] M.A. da Silva, B.T. Iamanaka, M.H. Taniwaki, T.G. Kieckbusch, Packag. Technol. Sci. 26 (2013) 479–492.
[84] Z. Zheng, J. Qi, L. Hu, D. Ouyang, H. Wang, Q. Sun, L. Lin, L. You, B. Tang, Biomater. Adv. 134 (2022) 112560.
[85] Z. Bagher, A. Ehterami, M.H. Safdel, H. Khastar, H. Semiari, A. Asefnejad, S. M. Davachi, M. Mirzaii, M. Salehi, J. Drug Deliv. Sci. Technol. 55 (2020) 101379.
[86] A. Ehterami, M. Salehi, S. Farzamfar, A. Vaez, S. Ghorbani, J. Ai, H. Sahrapeyma, J. Drug Deliv. Sci. Technol. 51 (2019) 204–213.
[87] G. Theocharidis, S. Rahmani, S. Lee, Z. Li, A. Lobao, K. Kounas, X.-L. Katopodi, P. Wang, S. Moon, I.S. Vlachos, M. Niewczas, D. Mooney, A. Veves, Biomaterials 288 (2022) 121692.
[88] X. Zhao, L. Liu, T. An, M. Xian, J.A. Luckanagul, Z. Su, Y. Lin, Q. Wang, Acta Biomater. 104 (2020) 85–94.
[89] Z. Li, H.R. Ramay, K.D. Hauch, D. Xiao, M. Zhang, Biomaterials 26 (2005) 3919–3928.
[90] S. Yousefiasl, H. Manoochehri, P. Makvandi, A. Afshar, E. Salahinejad, P. Khosraviyan, M. Saidijam, S. Soleimani Asl, E. Sharifi, J. Nanostructure Chem. 13 (2023) 389–403.
[91] H. Afjoul, A. Shamloo, A. Kamali, Mater. Sci. Eng.: C 113 (2020) 110957.
[92] P.J. Zapata, F. Guillén, D. Martínez-Romero, S. Castillo, D. Valero, M. Serrano, J. Sci. Food Agric. 88 (2008) 1287–1293.
[93] F. Lu, D. Liu, X. Ye, Y. Wei, F. Liu, J. Sci. Food Agric. 89 (2009) 848–854.
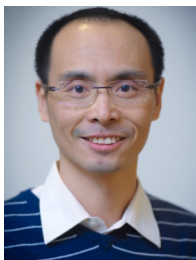[94] T. Senturk Parreidt, M. Schmid, K. Müller, J. Food Sci. 83 (2018) 929–936.

[95] M.A. Rojas-Graü, R.M. Raybaudi-Massilia, R.C. Soliva-Fortuny, R.J. Avena-Bustillos, T.H. McHugh, O. Martín-Belloso, Postharvest Biol. Technol. 45 (2007) 254–264.

[96] M.A. Rojas-Graü, M.S. Tapia, F.J. Rodríguez, A.J. Carmona, O. Martin-Belloso, Food Hydrocoll. 21 (2007) 118–127.

[97] R.D. Andrade, O. Skurtys, F.A. Osorio, Compr. Rev. Food Sci. Food Saf. 11 (2012) 323–337.

[98] H. Arnon-Rips, E. Poverenov, Trends Food Sci. Technol. 75 (2018) 81–92.

[99] R.E. Sipahi, M.E. Castell-Perez, R.G. Moreira, C. Gomes, A. Castillo, LWT - Food Sci. Technol. 51 (2013) 9–15.

[100] N. Mantilla, M.E. Castell-Perez, C. Gomes, R.G. Moreira, LWT - Food Sci. Technol. 51 (2013) 37–43.

[101] E. Poverenov, S. Danino, B. Horev, R. Granit, Y. Vinokur, V. Rodov, Food Bioprocess Technol. 7 (2014) 1424–1432.

[102] J. Moreira, A.C. Vale, N.M. Alves, J. Mater. Chem. B 9 (2021) 3778–3799.

[103] J. Zhao, Y. Zhu, G. He, R. Xing, F. Pan, Z. Jiang, P. Zhang, X. Cao, B. Wang, ACS Appl. Mater. Interfaces 8 (2016) 2097–2103.

[104] B. Marcos, P. Gou, J. Arnau, J. Comaposada, LWT - Food Sci. Technol. 74 (2016) 271–279.

[105] M. Röhrl, R.L. Timmins, D. Ghosh, D.D. Schuchardt, S. Rosenfeldt, S. Nürmberger, U. Bölz, S. Agarwal, J. Breu, J. Appl. Polym. Sci. 140 (2023) e54418.

[106] X. Zheng, Y. Zhang, L. Zou, Y. Wang, X. Zhou, L. Yao, Z. Wang, C. Li, Y. Qiu, Colloids Surf. B Biointerfaces 193 (2020) 111127.

[107] Q. Wang, X. Hu, Y. Du, J.F. Kennedy, Carbohydr. Polym. 82 (2010) 842–847.

[108] W.-F. Lai, E. Huang, K.-H. Lui, Asian J. Pharm. Sci. 16 (2021) 77–85.

[109] E. Diep, J.D. Schiffman, Biomacromolecules 24 (2023) 2908–2917.

[110] C.C. Piras, D.K. Smith, J. Mater. Chem. B 8 (2020) 8171–8188.

[111] Y. Liu, T. Wei, W. Xie, Y. Yuan, Y. Wang, Y. Qin, M. Ma, M. Li, F. Xie, A.C.S. Sustainable, Chem. Eng. 11 (2023) 16310–16321.

[112] A. Dodero, I. Donati, S. Scarfì, S. Mirata, S. Alberti, P. Lova, D. Comoretto, M. Alloisio, S. Vicini, M. Castellano, Mater. Sci. Eng.: C 124 (2021) 112067.

[113] A. Dodero, M. Alloisio, S. Vicini, M. Castellano, Carbohydr. Polym. 227 (2020) 115371.

[114] T.C. Mokhena, N.V. Jacobs, A.S. Luyt, Cellulose 25 (2018) 417–427.

[115] M.E. Talukder, M.N. Pervez, W. Jianming, Z. Gao, G.K. Stylios, M.M. Hassan, H. Song, V. Naddeo, J. Environ. Chem. Eng. 9 (2021) 106693.

[116] F. Xie, Chapter 4 - 3D printing of biopolymer-based hydrogels, in: M. Mehrpouya, H. Vahabi (Eds.), Additive Manufacturing of Biopolymers, Elsevier, 2023, pp. 65–100.

[117] N. Li, D. Qiao, S. Zhao, Q. Lin, B. Zhang, F. Xie, Mater. Today Chem. 20 (2021) 100459.

[118] C.M. Cleetus, F. Alvarez Primo, G. Fregoso, N. Lalitha Raveendran, J.C. Noveron, C.T. Spencer, C.V. Ramana, B. Joddar, Int. J. Nanomed. 15 (2020) 5097–5111.

[119] S. Im, G. Choe, J.M. Seok, S.J. Yeo, J.H. Lee, W.D. Kim, J.Y. Lee, S.A. Park, Int. J. Biol. Macromol. 205 (2022) 520–529.

[120] T. Kreller, T. Distler, S. Heid, S. Gerth, R. Detsch, A.R. Boccaccini, Mater. Des. 208 (2021) 109877.

[121] J. Lee, J. Hong, W. Kim, G.H. Kim, Carbohydr. Polym. 250 (2020) 116914.

[122] D. Chawla, T. Kaur, A. Joshi, N. Singh, Int. J. Biol. Macromol. 144 (2020) 560–567.

[123] A. Serafin, C. Murphy, M.C. Rubio, M.N. Collins, Mater. Sci. Eng. C 122 (2021) 111927.

[124] X. Yang, Z. Lu, H. Wu, W. Li, L. Zheng, J. Zhao, Mater. Sci. Eng. C 83 (2018) 195–201.

[125] S.D. Dutta, J. Hexiu, D.K. Patel, K. Ganguly, K.-T. Lim, Int. J. Biol. Macromol. 167 (2021) 644–658.

[126] D. Kang, Z. Liu, C. Qian, J. Huang, Y. Zhou, X. Mao, Q. Qu, B. Liu, J. Wang, Z. Hu, Y. Miao, Acta Biomater. 165 (2023) 19–30.

[127] A.B. Kakarla, I. Kong, I. Turek, C. Kong, H. Irving, Mater. Des. 213 (2022) 110362.

[128] A. Iglesias-Mejuto, C.A. García-González, Mater. Sci. Eng. C 131 (2021) 112525.

[129] P. Chen, F. Xie, F. Tang, T. McNally, Carbohydr. Polym. 253 (2021) 117231.

[130] P. Chen, F. Xie, F. Tang, T. McNally, ACS Appl. Polym. Mater. 2 (2020) 2957–2966.

[131] C. Gao, E. Pollet, L. Avérous, Carbohydr. Polym. 157 (2017) 669–676.

[132] C. Gao, E. Pollet, L. Avérous, Food Hydrocoll. 63 (2017) 414–420.

[133] V. Jost, M. Reinelt, J. Appl. Polym. Sci. 135 (2018) 45754.

[134] R. Russo, M. Malinconico, G. Santagata, Biomacromolecules 8 (2007) 3193–3197.

[135] C.K. Kuo, P.X. Ma, Biomaterials 22 (2001) 511–521.

[136] X. Zhang, K. Wang, J. Hu, Y. Zhang, Y. Dai, F. Xia, J. Mater. Chem. A 8 (2020) 25390–25401.

[137] N. Gao, Y. Zhang, Z. Yang, L. Xu, K. Zhao, Q. Xin, J. Gao, J. Shi, J. Zhong, H. Wang, Chin. Chem. Lett. 35 (2024) 108820.

[138] Vr.F. Duvivier-Kali, A. Omer, R.J. Parent, J.J. O'Neil, G.C. Weir, Diabetes 50 (2001) 1698–1705.

[139] J. Tan, Y. Luo, Y. Guo, Y. Zhou, X. Liao, D. Li, X. Lai, Y. Liu, Int. J. Biol. Macromol. 239 (2023) 124275.

[140] L. Aguero, S. Alpdagtas, E. Ilhan, D. Zaldivar-Silva, O. Gunduz, Eur. Polym. J. 160 (2021) 110807.

[141] M. Avella, E.D. Pace, B. Immirzi, G. Impallomeni, M. Malinconico, G. Santagata, Carbohydr. Polym. 69 (2007) 503–511.

[142] M.D. De'Nobili, L.M. Curto, J.M. Delfino, M. Soria, E.N. Fissore, A.M. Rojas, Int. J. Pharm. 450 (2013) 95–103.

[143] P. Sriamornsak, R.A. Kennedy, Int. J. Pharm. 358 (2008) 205–213.

[144] E. Tavassoli-Kafrani, H. Shekarchizadeh, M. Masoudpour-Behabadi, Carbohydr. Polym. 137 (2016) 360–374.

[145] W.H.N.S. Ashikin, T.W. Wong, C.L. Law, Carbohydr. Polym. 81 (2010) 104–113.

[146] G.A. Paula, N.M.B. Benevides, A.P. Cunha, A.V. de Oliveira, A.M.B. Pinto, J.P.S. Morais, H.M.C. Azeredo, Food Hydrocoll. 47 (2015) 140–145.

[147] T. Pongjanyakul, S. Puttipipatkhachorn, Int. J. Pharm. 333 (2007) 34–44.

[148] I. Liakos, L. Rizzello, I.S. Bayer, P.P. Pompa, R. Cingolani, A. Athanassiou, Carbohydr. Polym. 92 (2013) 176–183.

[149] S.D. Pasini Cabello, S. Mollá, N.A. Ochoa, J. Marchese, E. Giménez, V. Compañ, J. Power Sources 265 (2014) 345–355.

[150] D. Merino, M.F. Salcedo, A.Y. Mansilla, C.A. Casalongué, V.A. Alvarez, Waste Biomass Valoriz. 12 (2021) 6035–6043.

[151] K. Saravanakumar, A. Sathiyaseelan, A.V.A. Mariadoss, H. Xiaowen, M.-H. Wang, Int. J. Biol. Macromol. 153 (2020) 207–214.

[152] J.Gd Oliveira Filho, J.M. Rodrigues, A.C.F. Valadares, A.Bd Almeida, T.Md Lima, K.P. Takeuchi, C.C.F. Alves, H.Ad.F. Sousa, E.Rd Silva, F.H. Dyszy, M.B. Egea, Food Hydrocoll. 92 (2019) 267–275.

[153] A. Khan, R. Priyadarshi, T. Bhattacharya, J.-W. Rhim, Food Bioprocess Technol. 16 (2023) 2001–2015.

[154] N. Shaari, S.K. Kamarudin, Polym. Test. 81 (2020) 106183.

[155] A. Mohammed, A. Gaduan, P. Chaitram, A. Pooran, K.-Y. Lee, K. Ward, Food Hydrocoll. 135 (2023) 108192.

[156] W.Y. Tong, A.R. Ahmad Rafiee, C.R. Leong, W.-N. Tan, D.J. Dailin, Z.M. Almarhoon, M. Shelkh, A. Nawaz, L.F. Chuah, Chemosphere 336 (2023) 139212.

[157] Y. Li, J. Lu, X. Tian, Z. Xu, L. Huang, H. Xiao, X. Ren, Q. Kong, Int. J. Biol. Macromol. 193 (2021) 2093–2102.

[158] P. Shan, K. Wang, F. Yu, L. Yi, L. Sun, H. Li, Colloids Surf. A Physicochem. Eng. Asp. 662 (2023) 131013.

[159] N. Sharmin, I. Sone, J.L. Walsh, M. Sivertsvik, E.N. Fernández, Food Packag. Shelf Life 29 (2021) 100733.

[160] Y. Zhang, J. Man, J. Li, Z. Xing, B. Zhao, M. Ji, H. Xia, J. Li, Int. J. Biol. Macromol. 218 (2022) 519–532.

[161] J. Kurczewska, M. Ratajczak, M. Gajecka, Appl. Clay Sci. 214 (2021) 106270.

[162] Q. Guo, Y. Yuan, M. He, X. Zhang, L. Li, Y. Zhang, B. Li, Food Chem. 415 (2023) 135799.

[163] B. Immirzi, G. Santagata, G. Vox, E. Schettini, Biosyst. Eng. 102 (2009) 461–472.

[164] T.M.M. Swamy, B. Ramaraj, Siddaramaiah, J. Macromol. Sci., Part A 47 (2010) 877–881.

[165] Y. Pranoto, V.M. Salokhe, S.K. Rakshit, Food Res. Int. 38 (2005) 267–272.

[166] M.A. Rojas-Graü, R.J. Avena-Bustillos, C. Olsen, M. Friedman, P.R. Henika, O. Martín-Belloso, Z. Pan, T.H. McHugh, J. Food Eng. 81 (2007) 634–641.

[167] Q. Xiao, Q. Tong, Y. Zhou, F. Deng, Carbohydr. Polym. 130 (2015) 49–56.

[168] L.Z. Wang, L. Liu, J. Holmes, J.F. Kerry, J.P. Kerry, Int. J. Food Sci. Technol. 42 (2007) 1128–1138.

[169] C. Mellinas, A. Valdes, M. Ramos, N. Burgos, Md.C. Garrigos, A. Jimenez, J. Appl. Polym. Sci. 133 (2016) 42631.

[170] H. Pan, X. Xu, B. Jiang, J. Chen, Z. Jin, Food Hydrocoll. 52 (2016) 393–402.

[171] T. Budtova, P. Navard, Cellulose 23 (2016) 5–55.

[172] A. Pinkert, K.N. Marsh, S. Pang, M.P. Staiger, Chem. Rev. 109 (2009) 6712–6728.

[173] S.D. Zhu, Y.X. Wu, Q.M. Chen, Z.N. Yu, C.W. Wang, S.W. Jin, Y.G. Ding, G. Wu, Green. Chem. 8 (2006) 325–327.

[174] L.N. Zhang, D.C. Zhou, H. Wang, S.Y. Cheng, J. Membr. Sci. 124 (1997) 195–201.

[175] J.P. Zhou, L.N. Zhang, J. Polym. Sci. Part B Polym. Phys. 39 (2001) 451–458.

[176] L.N. Zhang, J.P. Zhou, D.C. Zhou, Y.R. Tang, J. Membr. Sci. 162 (1999) 103–109.

[177] G. Yang, L. Zhang, T. Peng, W. Zhong, J. Membr. Sci. 175 (2000) 53–60.

[178] M. Phisalaphong, T. Suwanmajo, P. Tammarate, J. Appl. Polym. Sci. 107 (2008) 3419–3424.

[179] B.V.K. Naidu, K. Sairam, K. Raju, T.M. Aminabhavi, Carbohydr. Polym. 61 (2005) 52–60.

[180] B.V.K. Naidu, K. Rao, T.M. Aminabhavi, J. Membr. Sci. 260 (2005) 131–141.

[181] S. Kalyani, B. Smitha, S. Sridhar, A. Krishnaiah, Carbohydr. Polym. 64 (2006) 425–432.

[182] R. Russo, M. Abbate, M. Malinconico, G. Santagata, Carbohydr. Polym. 82 (2010) 1061–1067.

[183] S.M. Ibrahim, K.M. El Salmawi, J. Polym. Environ. 21 (2013) 520–527.

[184] H.F. Zobel, Starch-Starke 40 (1988) 44–50.

[185] H. Liu, L. Yu, F. Xie, L. Chen, Carbohydr. Polym. 65 (2006) 357–363.

[186] F. Xie, L. Yu, B. Su, P. Liu, J. Wang, H. Liu, L. Chen, J. Cereal Sci. 49 (2009) 371–377.

[187] M. Schirmer, A. Höchstötter, M. Jekle, E. Arendt, T. Becker, Food Hydrocoll. 32 (2013) 52–63.

[188] P. Liu, F. Xie, M. Li, X. Liu, L. Yu, P.J. Halley, L. Chen, Carbohydr. Polym. 85 (2011) 180–187.

[189] P. Chen, L. Yu, G.P. Simon, X. Liu, K. Dean, L. Chen, Carbohydr. Polym. 83 (2011) 1975–1983.

[190] Q. Yan, J. Zhang, H. Dong, H. Hou, P. Guo, J. Appl. Polym. Sci. 127 (2013) 1951–1958.

[191] O.V. Lopez, M.D. Ninago, M.M.Soledad Lencina, M.A. Garcia, N.A. Andreucetti, A.E. Ciolino, M.A. Villar, Carbohydr. Polym. 126 (2015) 83–90.

[192] A. Cordoba, N. Cuellar, M. Gonzalez, J. Medina, Carbohydr. Polym. 73 (2008) 409–416.

[193] R.C.R. Souza, C.T. Andrade, J. Appl. Polym. Sci. 81 (2001) 412–420.

[194] G. Lozano-Vazquez, C. Lobato-Calleros, H. Escalona-Buendia, G. Chavez, J. Alvarez-Ramirez, E.J. Vernon-Carter, Food Hydrocoll. 48 (2015) 301–311.

[195] C.K.S. Pillai, W. Paul, C.P. Sharma, Prog. Polym. Sci. 34 (2009) 641–678.

[196] P. Sahariah, M. Másson, Biomacromolecules 18 (2017) 3846–3868.

[197] S.J. Lee, K. Park, Y.-K. Oh, S.-H. Kwon, S. Her, I.-S. Kim, K. Choi, S.J. Lee, H. Kim, S.G. Lee, K. Kim, I.C. Kwon, Biomaterials 30 (2009) 2929–2939.
[198] L. Dong, B. Deng, L. Ding, Q. Cheng, Y. Yang, Y. Du, Polym. Korea 38 (2014) 557–565.
[199] X. Li, H. Xie, J. Lin, W. Xie, X. Ma, Polym. Degrad. Stab. 94 (2009) 1–6.
[200] C. Jiang, Z. Wang, X. Zhang, X. Zhu, J. Nie, G. Ma, RSC Adv. 4 (2014) 41551–41560.
[201] M. Agostini de Moraes, D.S. Cocenza, F. da Cruz Vasconcellos, L.F. Fraceto, M. M. Beppu, J. Environ. Manag. 131 (2013) 222–227.
[202] X.-L. Yan, E. Khor, L.-Y. Lim, J. Biomed. Mater. Res. 58 (2001) 358–365.
[203] O. Gaserod, O. Smidsrod, G. Skjak-Braek, Biomaterials 19 (1998) 1815–1825.
[204] L. Becheran-Maron, C. Peniche, W. Arguelles-Monal, Int. J. Biol. Macromol. 34 (2004) 127–133.
[205] H.V. Saether, H.K. Holme, G. Maurstald, O. Smidsrod, B.T. Stokke, Carbohydr. Polym. 74 (2008) 813–821.
[206] D. Kulig, E. Brychcy, N. Ulbin-Figlewicz, A. Zimoch, K. Marycz, A. Jarmoluk, Przemysl Chem. 92 (2013) 1163–1168.
[207] X. Meng, F. Tian, J. Yang, C.-N. He, N. Xing, F. Li, J. Mater. Sci. Mater. Med. 21 (2010) 1751–1759.
[208] P. Treenate, P. Monvisade, M. Yamaguchi, J. Polym. Res. 21 (2014).
[209] S. Tang, J. Yang, L. Lin, K. Peng, Y. Chen, S. Jin, W. Yao, Chem. Eng. J. 393 (2020) 124728.
[210] J. Zhao, Y. Chen, Y. Yao, Z.-R. Tong, P.-W. Li, Z.-M. Yang, S.-H. Jin, J. Power Sources 378 (2018) 603–609.
[211] Y. Chen, X. Yan, J. Zhao, H. Feng, P. Li, Z. Tong, Z. Yang, S. Li, J. Yang, S. Jin, Carbohydr. Polym. 191 (2018) 8–16.
[212] X.L. Yan, E. Khor, L.Y. Lim, Chem. Pharm. Bull. 48 (2000) 941–946.
[213] P. Treenate, P. Monvisade, M. Yamaguchi, MATEC Web of Conferences 30 (2015) 02006.
[214] L. Ma, W. Yu, X. Ma, J. Appl. Polym. Sci. 106 (2007) 394–399.
[215] R.M. Gilhotra, D.N. Mishra, Pharmazie 63 (2008) 576–579.
[216] A.S. Reddy, S. Kalyani, N.S. Kumar, V.M. Boddu, A. Krishnaiah, Polym. Bull. 61 (2008) 779–790.
[217] K. Tian, C. Xie, X. Xia, Colloids Surf. B-Biointerfaces 109 (2013) 82–89.
[218] F. Maggi, S. Ciccarelli, M. Diociaiuti, S. Casciardi, G. Masci, Biomacromolecules 12 (2011) 3499–3507.
[219] M.G. Carneiro-da-Cunha, M.A. Cerqueira, B.W.S. Souza, S. Carvalhoc, M.A. C. Quintas, J.A. Teixeira, A.A. Vicente, Carbohydr. Polym. 82 (2010) 153–159.
[220] K. Manabe, K.-H. Kyung, S. Shiratori, ACS Appl. Mater. Interfaces 7 (2015) 4763–4771.
[221] K.I. Shingel, Carbohydr. Res. 339 (2004) 447–460.
[222] K. Nishinari, K. Kohyama, P.A. Williams, G.O. Phillips, W. Burchard, K. Ogino, Macromolecules 24 (1991) 5590–5593.
[223] S. Farris, I.U. Unalan, L. Introzzi, J.Maria Fuentes-Alventosa, C.A. Cozzolino, J. Appl. Polym. Sci. 131 (2014) 40539.
[224] Q. Xiao, Q. Tong, Food Res. Int. 54 (2013) 1605–1612.
[225] P. Prasad, G.S. Guru, H.R. Shivakumar, K.S. Rai, J. Polym. Environ. 20 (2012) 887–893.
[226] Q. Xiao, L.-T. Lim, Q. Tong, Carbohydr. Polym. 87 (2012) 227–234.
[227] Q. Xiao, Q. Tong, L.-T. Lim, Carbohydr. Polym. 87 (2012) 1689–1695.
[228] X. Wang, Q. Chen, X. Lü, Food Hydrocoll. 38 (2014) 129–137.
[229] G. Mao, D. Wu, C. Wei, W. Tao, X. Ye, R.J. Linhardt, C. Orfila, S. Chen, Trends Food Sci. Technol. 94 (2019) 65–78.
[230] S. Roy, R. Priyadarshi, Ł. Łopusiewicz, D. Biswas, V. Chandel, J.-W. Rhim, Int. J. Biol. Macromol. 239 (2023) 124248.
[231] W.G.T. Willats, L. McCartney, W. Mackie, J.P. Knox, Plant Mol. Biol. 47 (2001) 9–27.
[232] S. Yadav, P.K. Yadav, D. Yadav, K.D.S. Yadav, Process Biochem. 44 (2009) 1–10.
[233] P.J. Perez Espitia, W.-X. Du, Rd.J. Avena-Bustillos, Nd.F. Ferreira Soares, T. H. McHugh, Food Hydrocoll. 35 (2014) 287–296.
[234] C.K. Siew, P.A. Williams, N.W.G. Young, Biomacromolecules 6 (2005) 963–969.
[235] R.M. Gohil, J. Appl. Polym. Sci. 120 (2011) 2324–2336.
[236] L. Cao, W. Lu, A. Mata, K. Nishinari, Y. Fang, Carbohydr. Polym. 242 (2020) 116389.
[237] A.C.Krause Bierhalz, M.A. da Silva, T.G. Kieckbusch, J. Food Eng. 110 (2012) 18–25.
[238] P. Sriamornsak, R.A. Kennedy, Int. J. Pharm. 323 (2006) 72–80.
[239] P. Walkenstrom, S. Kidman, A.M. Hermansson, P.B. Rasmussen, L. Hoegh, Food Hydrocoll. 17 (2003) 593–603.
[240] S. Galus, A. Lenart, J. Food Eng. 115 (2013) 459–465.
[241] V.L. Campo, D.F. Kawano, D.Bd Silva, I. Carvalho, Carbohydr. Polym. 77 (2009) 167–180.
[242] F. Liu, P. Hou, H. Zhang, Q. Tang, C. Xue, R.W. Li, Compr. Rev. Food Sci. Food Saf. 20 (2021) 3918–3936.
[243] L.C. Geonzon, F.B.A. Descallar, L. Du, R.G. Bacabac, S. Matsukawa, Food Hydrocoll. 108 (2020) 106039.
[244] A.V. Briones, W.O. Ambal, R.R. Estrella, R. Pangilinan, C.J. De Vera, R.L. Pacis, N. Rodriguez, M.A. Villanueva, Mar. Biotechnol. 6 (2004) 148–151.
[245] J.B. Xu, J.P. Bartley, R.A. Johnson, J. Membr. Sci. 218 (2003) 131–146.
[246] P. Kaewprachu, K. Osako, S. Benjakul, W. Tongdeesoontorn, S. Rawdkuen, Packag. Technol. Sci. 29 (2016) 77–90.
[247] R.R. Koshy, S.K. Mary, S. Thomas, L.A. Pothan, Food Hydrocoll. 50 (2015) 174–192.
[248] L. Yang, J. Guo, Y. Yu, Q. An, L. Wang, S. Li, X. Huang, S. Mu, S. Qi, Carbohydr. Polym. 142 (2016) 275–281.
[249] Y. Yang, M. Anvari, C.-H. Pan, D. Chung, Food Chem. 135 (2012) 555–561.
[250] H. Zhang, G. Mittal, Environ. Prog. Sustain. Energy 29 (2010) 203–220.
[251] S.L. Turgeon, M. Beaulieu, C. Schmitt, C. Sanchez, Curr. Opin. Colloid Interface Sci. 8 (2003) 401–414.
[252] V.Y. Grinberg, V.B. Tolstoguzov, Food Hydrocoll. 11 (1997) 145–158.
[253] J.L. Doublier, C. Garnier, D. Renard, C. Sanchez, Curr. Opin. Colloid Interface Sci. 5 (2000) 202–214.
[254] Y. Li, H. Jia, Q. Cheng, F. Pan, Z. Jiang, J. Membr. Sci. 375 (2011) 304–312.
[255] L. Wang, M.A.E. Auty, J.P. Kerry, J. Food Eng. 96 (2010) 199–207.
[256] B.A. Harper, S. Barbut, L.T. Lim, M.F. Marcone, Food Res. Int. 52 (2013) 452–459.
[257] Y.A. Antonov, N.P. Lashko, Y.K. Glotova, A. Malovikova, O. Markovich, Food Hydrocoll. 10 (1996) 1–9.
[258] J.T. Kim, A.N. Netravali, Compos. Sci. Technol. 71 (2011) 541–547.
[259] S.A. Fioramonti, A.A. Perez, E.Elena Aringoli, A.C. Rubiolo, L.G. Santiago, Food Hydrocoll. 35 (2014) 129–136.
[260] H. Pan, B. Jiang, J. Chen, Z. Jin, Food Chem. 151 (2014) 1–6.
[261] V.I. Polyakov, V.Y. Grinberg, V.B. Tolstoguzov, Food Hydrocoll. 11 (1997) 171–180.
[262] C.G. de Kruif, F. Weinbreck, R. de Vries, Curr. Opin. Colloid Interface Sci. 9 (2004) 340–349.
[263] J.L. Mession, A. Assifaoui, C. Lafarge, R. Saurel, P. Cayot, Food Hydrocoll. 28 (2012) 333–343.
[264] K.J. Klemmer, L. Waldner, A. Stone, N.H. Low, M.T. Nickerson, Food Chem. 130 (2012) 710–715.
[265] H. Zheng, Z. Zhou, Y. Chen, J. Huang, F. Xiong, J. Appl. Polym. Sci. 106 (2007) 1034–1041.
[266] P. Gupta, K.K. Nayak, J. Appl. Biomater. Funct. Mater. 13 (2015) E332–E339.
[267] J. Sun, W. Xiao, Y. Tang, K. Li, H. Fan, Soft Matter 8 (2012) 2398–2404.
[268] E. Chiellini, A. Corti, S. D'Antone, R. Solaro, Prog. Polym. Sci. 28 (2003) 963–1014.
[269] Q. Chen, S. Cabanas-Polo, O.-M. Goudouri, A.R. Boccaccini, Mater. Sci. Eng. C. Mater. Biol. Appl. 40 (2014) 55–64.
[270] F. Xie, B. Zhang, D.K. Wang, Chapter 7 - Starch thermal processing: Technologies at laboratory and semi-industrial scales, in: M.A. Villar, S.E. Barbosa, M.A. García, L.A. Castillo, O.V. López (Eds.), Starch-Based Materials in Food Packaging, Academic Press, 2017, pp. 187–227.
[271] K.M. Zia, F. Zia, M. Zuber, S. Rehman, M.N. Ahmad, Int. J. Biol. Macromol. 79 (2015) 377–387.
[272] N. Eghbalifam, M. Frounchi, S. Dadbin, Int. J. Biol. Macromol. 80 (2015) 170–176.
[273] J.O. Kim, J.Y. Choi, J.K. Park, J.H. Kim, S.G. Jin, S.W. Chang, D.X. Li, M.-R. Hwang, J.S. Woo, J.-A. Kim, W.S. Lyoo, C.S. Yong, H.-G. Choi, Biol. Pharm. Bull. 31 (2008) 2277–2282.
[274] J.O. Kim, J.K. Park, J.H. Kim, S.G. Jin, C.S. Yong, D.X. Li, J.Y. Choi, J.S. Woo, B. K. Yoo, W.S. Lyoo, J.-A. Kim, H.-G. Choi, Int. J. Pharm. 359 (2008) 79–86.
[275] S.B. Kuila, S.K. Ray, Carbohydr. Polym. 101 (2014) 1154–1165.
[276] R. Russo, M. Malinconico, L. Petti, G. Romano, J. Polym. Sci. Part B Polym. Phys. 43 (2005) 1205–1213.
[277] R. Russo, A. Giuliani, B. Immirzi, M. Malinconico, G. Romano, Macromol. Symp. 218 (2004) 241–250.
[278] S. Hua, H. Ma, X. Li, H. Yang, A. Wang, Int. J. Biol. Macromol. 46 (2010) 517–523.
[279] L. Xie, M. Jiang, X. Dong, X. Bai, J. Tong, J. Zhou, J. Appl. Polym. Sci. 124 (2012) 823–831.
[280] S. Kahya, E.K. Solak, O. Sanli, Vacuum 84 (2010) 1092–1102.
[281] Y.Q. Dong, L. Zhang, J.N. Shen, M.Y. Song, H.L. Chen, Desalination 193 (2006) 202–210.
[282] R.V. Kulkarni, V. Sreedhar, S. Mutalik, C.M. Setty, B. Sa, Int. J. Biol. Macromol. 47 (2010) 520–527.
[283] T. Sheela, R.F. Bhajantri, V. Ravindrachary, S.G. Rathod, P.K. Pujari, B. Poojary, R. Somashekar, Radiat. Phys. Chem. 103 (2014) 45–52.
[284] C. Amri, M. Mudasir, D. Siswanta, R. Roto, Int. J. Biol. Macromol. 82 (2016) 48–53.
[285] R.J. Moon, A. Martini, J. Nairn, J. Simonsen, J. Youngblood, Chem. Soc. Rev. 40 (2011) 3941–3994.
[286] R. Rusli, S.J. Eichhorn, Appl. Phys. Lett. 93 (2008) 033111.
[287] I. Siro, D. Plackett, Cellulose 17 (2010) 459–494.
[288] S. Kalia, A. Dufresne, B.M. Cherian, B.S. Kaith, L. Averous, J. Njuguna, E. Nassiopoulos, Int. J. Polym. Sci. 2011 (2011) 837875.
[289] S. Kalia, L. Averous, J. Njuguna, A. Dufresne, B.M. Cherian, Int. J. Polym. Sci. 2011 (2011) 2341–2348.
[290] J. Shojaeiarani, D.S. Bajwa, S. Chanda, Compos. Part C Open Access 5 (2021) 100164.
[291] F. Xie, E. Pollet, P.J. Halley, L. Avérous, Prog. Polym. Sci. 38 (2013) 1590–1628.
[292] F. Xie, L. Avérous, P.J. Halley, P. Liu, 4 - Mechanical performance of starch-based biocomposites, in: M. Misra, J.K. Pandey, A.K. Mohanty (Eds.), Biocomposites, Woodhead Publishing, 2015, pp. 53–92.
[293] I. Šimkovic, Carbohydr. Polym. 95 (2013) 697–715.
[294] P. Chen, F. Xie, F. Tang, T. McNally, Funct. Compos. Mater. 2 (2021) 14.
[295] P. Chen, F. Xie, F. Tang, T. McNally, Polymers 13 (2021) 571.
[296] Q. Chen, U. Perez de Larraya, N. Garmendia, M. Lasheras-Zubiate, L. Cordero-Arias, S. Virtanen, A.R. Soccancini, Colloids Surf. B-Biointerfaces 118 (2014) 41–48.
[297] N. Kanjanamosit, C. Muangnapoh, M. Phisalaphong, J. Appl. Polym. Sci. 115 (2010) 1581–1588.
[298] T. Suratago, S. Taokaew, N. Kanjanamosit, K. Kanjanaprapakul, V. Burapatana, M. Phisalaphong, J. Ind. Eng. Chem. 32 (2015) 305–312.

[299] H.M.C. Azeredo, K.W.E. Miranda, M.F. Rosa, D.M. Nascimento, M.R. de Moura, LWT - Food Sci. Technol. 46 (2012) 294–297.
[300] W. Helbert, J.Y. Cavaille, A. Dufresne, Polym. Compos. 17 (1996) 604–611.
[301] W. Su, Z. Yang, H. Wang, J. Fang, C. Li, G. Lyu, H. Li, A.C.S. Sustainable, Chem. Eng. 10 (2022) 11800–11814.
[302] T. Huq, S. Salmieri, A. Khan, R.A. Khan, C. Le Tien, B. Riedl, C. Fraschini, J. Bouchard, J. Uribe-Calderon, M.R. Kamal, M. Lacroix, Carbohydr. Polym. 90 (2012) 1757–1763.
[303] X. Cao, Y. Chen, P.R. Chang, A.D. Muir, G. Falk, Express Polym. Lett. 2 (2008) 502–510.
[304] M. Alboofetileh, M. Rezaei, H. Hosseini, M. Abdollahi, J. Food Eng. 117 (2013) 26–33.
[305] M. Mariano, N. El Kissi, A. Dufresne, J. Polym. Sci. Part B Polym. Phys. 52 (2014) 791–806.
[306] A. Dufresne, M.R. Vignon, Macromolecules 31 (1998) 2693–2696.
[307] B. Deepa, E. Abraham, L.A. Pothan, N. Cordeiro, M. Faria, S. Thomas, Materials 9 (2016) 50.
[308] M. Abdollahi, M. Alboofetileh, R. Behrooz, M. Rezaei, R. Miraki, Int. J. Biol. Macromol. 54 (2013) 166–173.
[309] M. Abdollahi, M. Alboofetileh, M. Rezaei, R. Behrooz, Food Hydrocoll. 32 (2013) 416–424.
[310] W. Shao, H. Liu, X. Liu, S. Wang, J. Wu, R. Zhang, H. Min, M. Huang, Carbohydr. Polym. 132 (2015) 351–358.
[311] L. Avérous, E. Pollet, Environmental Silicate Nano-biocomposites, Springer, London, 2012, p. 447.
[312] L. Averous, E. Pollet, Mrs Bull. 36 (2011) 703–710.
[313] E. Pollet, L. Averous, Recent results in nano-biocomposites based on montmorillonites, in: V. Mittal (Ed.), Advances in Polymer Nanocomposite Technology, Nova Science Publishers, Inc, New York, 2010, pp. 315–354.
[314] S. Pavlidou, C.D. Papaspyrides, Prog. Polym. Sci. 33 (2008) 1119–1198.
[315] S.S. Ray, M. Okamoto, Prog. Polym. Sci. 28 (2003) 1539–1641.
[316] A.C.S. Alcantara, M. Darder, P. Aranda, A. Ayral, E. Ruiz-Hitzky, J. Appl. Polym. Sci. 133 (2016) 54–59.
[317] E. Ruiz-Hitzky, M. Darder, F.M. Fernandes, B. Wicklein, A.C.S. Alcantara, P. Aranda, Prog. Polym. Sci. 38 (2013) 1392–1414.
[318] F. Tezcan, E. Gunister, G. Ozen, F.B. Erim, Int. J. Biol. Macromol. 50 (2012) 1165–1168.
[319] M. Alboofetileh, M. Rezaei, H. Hosseini, M. Abdollahi, J. Food Process. Preserv. 38 (2014) 1622–1631.
[320] N. Golafshan, R. Rezahasani, M. Tarkesh Esfahani, M. Kharaziha, S.N. Khorasani, Carbohydr. Polym. 176 (2017) 392–401.
[321] T. Pongjanyakul, A. Priprem, S. Puttipipatkhachorn, J. Control. Release 107 (2005) 343–356.
[322] B. Benli, F. Boylu, M.F. Can, F. Karakas, K. Cinku, G. Ersever, J. Appl. Polym. Sci. 122 (2011) 19–28.
[323] D.F. Xie, V.P. Martino, P. Sangwan, C. Way, G.A. Cash, E. Pollet, K.M. Dean, P. J. Halley, L. Avérous, Polymer 54 (2013) 3654–3662.
[324] A. Sorrentino, G. Gorrasi, V. Vittoria, Trends Food Sci. Technol. 18 (2007) 84–95.
[325] T. Pongjanyakul, Int. J. Pharm. 365 (2009) 100–108.
[326] T. Pongjanyakul, S. Puttipipatkhachorn, Int. J. Pharm. 346 (2008) 1–9.
[327] J.-W. Rhim, Carbohydr. Polym. 86 (2011) 691–699.
[328] T. Pongjanyakul, H. Suksri, Colloids Surf. B Biointerfaces 74 (2009) 103–113.
[329] H.-B. Chen, Y.-Z. Wang, M. Sanchez-Soto, D.A. Schiraldi, Polymer 53 (2012) 5825–5831.
[330] S.D. Bhat, T.M. Aminabhavi, Sep. Purif. Technol. 51 (2006) 85–94.
[331] P. Dubois, M. Alexandre, Adv. Eng. Mater. 8 (2006) 147–154.
[332] W. Li, X. Li, Y. Chen, X. Li, H. Deng, T. Wang, R. Huang, G. Fan, Carbohydr. Polym. 92 (2013) 2232–2238.
[333] A.C.S. Alcantara, M. Darder, P. Aranda, E. Ruiz-Hitzky, Appl. Clay Sci. 96 (2014) 2–8.
[334] T. Pongjanyakul, H. Suksri, Carbohydr. Polym. 80 (2010) 1018–1027.
[335] M.F. Abou Taleb, D.E. Hegazy, S.A. Ismail, Carbohydr. Polym. 87 (2012) 2263–2269.
[336] E. Bilotti, R. Zhang, H. Deng, F. Quero, H.R. Fischer, T. Peijs, Compos. Sci. Technol. 69 (2009) 2587–2595.
[337] P. Chen, F. Xie, F. Tang, T. McNally, Int. J. Biol. Macromol. 163 (2020) 683–693.
[338] P. Chen, F. Xie, F. Tang, T. McNally, Int. J. Biol. Macromol. 158 (2020) 420–429.
[339] K. Vilcinskas, B. Norder, K. Goubitz, F.M. Mulder, G.J.M. Koper, S.J. Picken, Macromolecules 48 (2015) 8323–8330.
[340] L. Valentini, N. Rescignano, D. Puglia, M. Cardinali, J. Kenny, Eur. J. Inorg. Chem. (2015) 1192–1197.
[341] M. Ionita, M.A. Pandele, H. Iovu, Carbohydr. Polym. 94 (2013) 339–344.
[342] D.P. Suhas, A.V. Raghu, H.M. Jeong, T.M. Aminabhavi, RSC Adv. 3 (2013) 17120–17130.
[343] K. Cao, Z. Jiang, J. Zhao, C. Zhao, C. Gao, F. Pan, B. Wang, X. Cao, J. Yang, J. Membr. Sci. 469 (2014) 272–283.
[344] H. Zheng, J. Yang, S. Han, J. Appl. Polym. Sci. 33 (2016) 43616.
[345] K. Chen, B. Shi, Y. Yue, J. Qi, L. Guo, ACS Nano 9 (2015) 8165–8175.
[346] X. Hu, S. Rajendran, Y. Yao, Z. Liu, K. Gopalsamy, L. Peng, C. Gao, Nano Res. 9 (2016) 735–744.
[347] Y. Shi, S. Jiang, K. Zhou, C. Bao, B. Yu, X. Qian, B. Wang, N. Hong, P. Wen, Z. Gui, Y. Hu, R.K.K. Yuen, ACS Appl. Mater. Interfaces 6 (2014) 429–437.
[348] L. Liu, Y. Shi, B. Yu, Q. Tai, B. Wang, X. Feng, H. Liu, P. Wen, B. Yuan, Y. Hu, RSC Adv. 5 (2015) 11761–11765.
[349] M. Yang, Y. Xia, Y. Wang, X. Zhao, Z. Xue, F. Quan, C. Geng, Z. Zhao, J. Appl. Polym. Sci. 133 (2016) 43489.
[350] Y. Tal, J. van Rijn, A. Nussinovitch, Appl. Microbiol. Biotechnol. 51 (1999) 773–779.
[351] A. Lopez-Cordoba, L. Deladino, M. Martino, Carbohydr. Polym. 99 (2014) 150–157.
[352] A. Lopez-Cordoba, L. Deladino, M. Martino, LWT - Food Sci. Technol. 59 (2014) 641–648.
[353] M. Bogun, A. Lacz, J. Therm. Anal. Calorim. 106 (2011) 953–963.
[354] M. Agostini de Moraes, D.S. Cocenza, F. da Cruz Vasconcellos, L.F. Fraceto, M. M. Beppu, J. Environ. Manag. 131 (2013) 222–227.
[355] F. Liu, Z. Zhou, Y. Tu, J. Chen, F. Zhang, S. Tian, Z. Ren, J. Water Process Eng. 49 (2022) 103124.
[356] Q. Li, Y. Li, X. Ma, Q. Du, K. Sui, D. Wang, C. Wang, H. Li, Y. Xia, Chem. Eng. J. 316 (2017) 623–630.
[357] S. Kalyani, B. Smitha, S. Sridhar, A. Krishnaiah, Desalination 229 (2008) 68–81.
[358] S.D. Bhat, T.M. Aminabhavi, Sep. Purif. Rev. 36 (2007) 203–229.
[359] C. Bai, L. Wang, Z. Zhu, Int. J. Biol. Macromol. 147 (2020) 898–910.
[360] F. Ugur Nigiz, Desalination 485 (2020) 114465.
[361] J. Yu, Y. Wang, Y. He, Y. Gao, R. Hou, J. Ma, L. Zhang, X. Guo, L. Chen, Sep. Purif. Technol. 276 (2021) 119348.
[362] G. Jie, Z. Kongyin, Z. Xinxin, C. Zhijiang, C. Min, C. Tian, W. Junfu, Mater. Lett. 157 (2015) 112–115.
[363] W.Z. Durrani, A. Nasrullah, A.S. Khan, T.M. Fagieh, E.M. Bakhsh, K. Akhtar, S. B. Khan, I.U. Din, M.A. Khan, A. Bokhari, Chemosphere 302 (2022) 134793.
[364] N. Ullah, Z. Ali, S. Ullah, A.S. Khan, B. Adalat, A. Nasrullah, M. Alsaadi, Z. Ahmad, Chemosphere 309 (2022) 136623.
[365] R. Xing, F. Pan, J. Zhao, K. Cao, C. Gao, S. Yang, G. Liu, H. Wu, Z. Jiang, RSC Adv. 6 (2016) 14381–14392.
[366] S. Kahya, O. Şanlı, Desalin. Water Treat. 52 (2014) 3517–3525.
[367] M.G. Mali, G.S. Gokavi, J. Polym. Res. 19 (2012) 9976.
[368] A.I. Kuzminova, M.E. Dmitrenko, D.Y. Poloneeva, A.A. Selyutin, A.S. Mazur, A. V. Emeline, V.Y. Mikhailovskii, N.D. Solovyev, S.S. Ermakov, A.V. Penkova, J. Membr. Sci. 626 (2021) 119194.
[369] E.K. Solak, S. Kahya, O. Şanlı, Desalin. Water Treat. 31 (2011) 291–295.
[370] U.S. Toti, T.M. Aminabhavi, J. Membr. Sci. 228 (2004) 199–208.
[371] N. Shaari, S.K. Kamarudin, J. Power Sources 289 (2015) 71–80.
[372] B. Smitha, S. Sridhar, A.A. Khan, Eur. Polym. J. 41 (2005) 1859–1866.
[373] A. Permatasari, M. Mara Ikhsan, D. Henkensmeier, Y. Kwon, J. Ind. Eng. Chem. 122 (2023) 264–273.
[374] J. Wang, Z. Zhang, J. Zhu, M. Tian, S. Zheng, F. Wang, X. Wang, L. Wang, Nat. Commun. 11 (2020) 3540.
[375] N. Gao, W. Xie, L. Xu, Q. Xin, J. Gao, J. Shi, J. Zhong, W. Shi, H. Wang, K. Zhao, L. Lin, Int. J. Biol. Macromol. 253 (2023) 126367.
[376] J. Shi, Z. Zhang, W. Qi, S. Cao, Int. J. Biol. Macromol. 50 (2012) 747–753.
[377] L.-F. Wang, J.-W. Rhim, Int. J. Biol. Macromol. 80 (2015) 460–468.
[378] M.S. Abdel Aziz, H.E. Salama, Int. J. Biol. Macromol. 212 (2022) 294–302.
[379] S.A. Shah, S. Sohail, S. Khan, M.U. Minhas, M. de Matas, V. Sikstone, Z. Hussain, M. Abbasi, M. Kousar, Int. J. Biol. Macromol. 139 (2019) 975–993.
[380] W.-R. Lee, J.-H. Park, K.-H. Kim, S.-J. Kim, D.-H. Park, M.-H. Chae, S.-H. Suh, S.-W. Jeong, K.-K. Park, Wound Repair Regen. 17 (2009) 505–510.
[381] J.W. Doyle, T.P. Roth, R.M. Smith, Y.-Q. Li, R.M. Dunn, J. Biomed. Mater. Res. 32 (1996) 561–568.
[382] A.R. Abbasi, M. Sohail, M.U. Minhas, T. Khaliq, M. Kousar, S. Khan, Z. Hussain, A. Munir, Int. J. Biol. Macromol. 155 (2020) 751–765.
[383] T. Wang, W. Yi, Y. Zhang, H. Wu, H. Fan, J. Zhao, S. Wang, Colloids Surf. B Biointerfaces 222 (2023) 113096.
[384] R.N.F. Moreira Filho, N.F. Vasconcelos, F.K. Andrade, Md.F. Rosa, R.S. Vieira, Colloids Surf. B Biointerfaces 194 (2020) 111222.
[385] J. Zhang, C. Hurren, Z. Lu, D. Wang, Int. J. Biol. Macromol. 222 (2022) 1723–1733.
[386] L. Wang, E. Khor, A. Wee, L.Y. Lim, J. Biomed. Mater. Res. 63 (2002) 610–618.
[387] O. Catanzano, V. D'Esposito, S. Acierno, M.R. Ambrosio, C. De Caro, C. Avagliano, P. Russo, R. Russo, A. Miro, F. Ungaro, A. Calignano, P. Formisano, F. Quaglia, Carbohydr. Polym. 131 (2015) 407–414.
[388] A. Serafin, M. Culebras, M.N. Collins, Int. J. Biol. Macromol. 233 (2023) 123438.
[389] W.-Y. Zhao, Q.-Q. Fang, X.-F. Wang, X.-W. Wang, T. Zhang, B.-H. Shi, B. Zheng, D.-D. Zhang, Y.-Y. Hu, L. Ma, W.-Q. Tan, Wound Repair Regen. 28 (2020) 326–337.
[390] Y. Ueyama, K. Ishikawa, T. Mano, T. Koyama, H. Nagatsuka, K. Suzuki, K. Ryoke, Biomaterials 23 (2002) 2027–2033.
[391] K. Ishikawa, Y. Ueyama, T. Mano, T. Koyama, K. Suzuki, T. Matsumura, J. Biomed. Mater. Res. 47 (1999) 111–115.
[392] J.F.A. Valente, T.A.M. Valente, P. Alves, P. Ferreira, A. Silva, I.J. Correia, Mater. Sci. Eng. C 32 (2012) 2596–2603.
[393] L. Wang, R.M. Shelton, P.R. Cooper, M. Lawson, J.T. Triffitt, J.E. Barralet, Biomaterials 24 (2003) 3475–3481.
[394] L. Benedini, J. Laiuppa, G. Santillán, M. Baldini, P. Messina, Mater. Sci. Eng. C. 115 (2020) 111101.
[395] I. Ielo, G. Calabrese, G. De Luca, S. Conoci, Int. J. Mol. Sci. 23 (2022) 9721.
[396] J.L. Aparicio-Collado, N. García-San-Martín, J. Molina-Mateo, C. Torregrosa Cabanilles, V. Donderis Quiles, A. Serrano-Aroca, R. Sabater i Serra, Colloids Surf. B Biointerfaces 214 (2022) 112455.
[397] A.C.K. Bierhalz, M.A. da Silva, H.C. de Sousa, M.E.M. Braga, T.G. Kieckbusch, J. Supercrit. Fluids 76 (2013) 74–82.
[398] Z. Riahi, R. Priyadarshi, J.-W. Rhim, E. Lotfali, R. Bagheri, G. Pircheraghi, Colloids Surf. B Biointerfaces 215 (2022) 112519.

[399] M.S. Tapia, M.A. Rojas-Graü, F.J. Rodríguez, J. Ramírez, A. Carmona, O. Martin-Belloso, J. Food Sci. 72 (2007) E190–E196.

[400] F. Şen, İ. Uzunsoy, E. Baştürk, M.V. Kahraman, Carbohydr. Polym. 170 (2017) 264–270.

[401] R. Adhikari, K.L. Bristow, P.S. Casey, G. Freischmidt, J.W. Hornbuckle, B. Adhikari, Agric. Water Manag. 169 (2016) 1–13.

[402] Y. Liu, J.-C. Zhao, C.-J. Zhang, Y. Guo, L. Cui, P. Zhu, D.-Y. Wang, RSC Adv. 5 (2015) 64125–64137.

[403] Y. Liu, C.-J. Zhang, J.-C. Zhao, Y. Guo, P. Zhu, D.-Y. Wang, Carbohydr. Polym. 139 (2016) 106–114.

[404] Y. Liu, J.-C. Zhao, C.-J. Zhang, Y. Guo, P. Zhu, D.-Y. Wang, J. Mater. Sci. 51 (2016) 1052–1065.

[405] B. Ibarlucea, A. Pérez Roig, D. Belyaev, L. Baraban, G. Cuniberti, Microchim. Acta 187 (2020) 520.

Dr Chengcheng Gao is an associate professor of Nanjing University of Finance and Economics in Nanjing, China. She received her doctor degree from South China University of Technology in 2015. She was a post-doctoral fellow at the University of Strasburg during 2015–2016, and then joined Nanjing University of Finance and Economics. Her current research interests include developing polysaccharide-based materials through extrusion processing, active edible coating for food preservation, and polysaccharide-based particles through electrostatic interaction, Schiff base reaction, Maillard reaction, etc. for controlled release of active molecules, simulating solid fat, and stabilizing oil/water systems. She has published more than 20 research papers as the first author or corresponding author and two patents, and managed one national research project and two provincial-level research projects.

Pr. Fengwei (David) Xie is a professor at the University of Bath, UK. His previous career experience includes serving as a senior lecturer (equivalent to associate professorship) at Newcastle University (UK) and holding a Marie Curie Fellowship at the University of Warwick (UK). Before moving to the UK, he worked as a postdoctoral research fellow/research fellow at the University of Guelph (Canada) and The University of Queensland (Australia). Besides, he had visiting research experiences at the Université de Strasbourg (France) and the California Institute of Technology (USA). Specializing in polymer engineering and science, Dr. Xie's research is dedicated to the world of biopolymers, encompassing polysaccharides and proteins for both material and food applications. His areas of expertise encompass the modification, processing, and characterization of biopolymers, as well as the design of biopolymer-based materials and composites tailored for specific applications. In recent years, Dr. Xie has secured a highly prestigious EPSRC Fellowship, along with two Marie Curie Fellowships, all in the UK. Cumulatively, his research funding spans various sources worldwide, encompassing Australia, China, the EU, and the UK. His research has led to over 180 refereed journal articles with more than 10,000 citations (Google Scholar), 1 monograph, and 8 book chapters. He serves as an esteemed editorial board member for reputable journals like *Carbohydrate Polymers* and *Polymers*.

Pr. Luc Avérous from the University of Strasbourg (France) is a Group (BioTeam) Leader, Head of Polymer Research Department at ICPEES (UMR CNRS), Head of Joint Research Lab and former Lab Director. He became a Full Professor at ECPM (European School of Chemistry, Polymers and Materials Science) in 2003. During the last 30 years, his research activities have been focused on (bio)synthesis, formulation, characterization, and process of polymers. His major projects have dealt with biobased, sustainable and/or biodegradable polymers for environmental & biomedical applications. As a leading international expert in these fields, he has developed strong collaborations with several foreign labs (Australia, Latin America, Canada, and EU) and major companies. He is involved in different national and international projects. He serves as a member of research advisory boards for companies. He is regularly invited to co-organize conferences, to chair symposia, and to give plenary or keynote lectures. He is a member of several Journals' editorial boards and international panels. He is a referee for journals, books, international institutions, and projects. He is named among the World's Top 1% Scientists. He has co-edited 4 books. He has published 40 book chapters and more than 200 articles with impact factors, with about 20,000 citations (Scopus database).